Temporal and thermal stability of stacks of amorphous silicon and silicon nitride for surface passivation of silicon solar cells

Ida Margrete Hasle

Norwegian University of Life Sciences
Department of Mathematical Sciences and Technology
Master Thesis 30 credits 2013

Preface

This master thesis in physics concludes my studies of Teacher Education in Natural Sciences at Norwegian University of Life Sciences (UMB), Department of Mathematical Sciences and Technology (IMT). The work was carried out at the Department for Solar Energy at the Institute for Energy Technology (IFE), in the spring of 2013 and has been funded by the Research Council of Norway through the project "Thin and highly efficient silicon-based solar cells incorporating nanostructures", NFR Project No. 181884/S1. The assignment was developed and supervised by Dr Erik Stensrud Marstein (IFE) and PhD student Halvard Haug (IFE). Dr Espen Olsen (UMB) was the responsible supervisor. I would like to thank my supervisors for the guidance, experimental training and support. I would also like to thank Halvard Haug for performing the preparation of the samples. Last I would like to thank the employees and students at the Department for Solar Energy for useful discussions, experimental training and encouragements and friends and family for the support.

Kjeller, 14.05.13

Ida Margrete Hasle

Abstract

Surface passivation is important for high efficiency solar cells. Stacks of hydrogenated amorphous silicon (a-Si:H) and hydrogenated amorphous silicon nitride (a-SiN_x:H) have been shown to provide good surface passivation. One advantage of this passivation is the low temperature deposition, which means it is energy and cost effective and does not affect the bulk lifetime of the wafer. In previous studies the stacks have been found to provide better passivation than single layers of a-Si:H or a-SiN_x:H. Layers of a-Si:H capped with a-SiN_x:H are more stable than single layers of a-Si:H, both with respect to time and temperature.

In this study 10 *n*-type and 15 *p*-type wafers were deposited symmetrically on both sides with single layers of a-Si:H, a-SiN_x:H or stacks of these two materials, with varying film thicknesses, by plasma enhanced chemical vapour deposition (PECVD). Effective lifetimes were measured using the quasi steady state photoconductance (QSSPC) method and photoluminescence (PL) imaging. The stacks investigated were found to provide very good surface passivation as deposited. The best effective lifetime measured on the *n*-type samples one day after deposition was 12.5 ms for an excess carrier concentration of 10^{15} cm^{-3}. The upper limit of the surface recombination velocity (SRV) was calculated to be 1.0 cm/s for this sample. The highest effective lifetime of a passivated *p*-type wafer was measured to be 5.3 ms for an excess carrier concentration of 10^{15} cm^{-3} shortly after deposition of a single layer of 20 nm a-Si:H. The corresponding upper limit of the SRV was calculated to be 2.7 cm/s.

The passivation of the thin a-Si:H single layers were found to degrade rapidly with time. After nine weeks, the effective lifetimes of the *p*-type samples with 5, 10 and 20 nm a-Si:H films, were reduced to about 30 % of their value one day after deposition. The effective lifetimes of the *n*-type samples with 5 and 10 nm a-Si:H layers, had decreased to 25 % of their value one day after deposition. The capped a-Si:H layers showed greater temporal stability being relatively stable during the nine weeks after deposition when measurements were carried out. After nine weeks the best measured lifetime was 11.3 ms corresponding to upper limits of the SRV of 1.3 cm/s on *n*-type and 4.0 ms corresponding to an upper limit of the SRV of 3.6 cm/s on *p*-type. The thickest a-Si:H layer of 40 nm was almost as stable as the stacks. The stacks are probably more stable than the single layers because the silicon nitride prevents the hydrogen from effusing out from the interface with time.

The thermal stability of the passivation is important because of the metallisation processes of solar cells. Rapid thermal annealings (RTA) of the samples were carried out for one minute at different temperatures. A maximum effective lifetime occurred after annealing at 300-400 °C for all the samples, probably because of redistribution of hydrogen, resulting in a lower defect density at the surface and lower SRV. Rapid degradation was observed from 450 °C and after annealing at 500 °C the effective lifetimes were below 0.1 ms, probably caused by effusion of hydrogen, resulting in a higher defect density at the surface and higher SRV. A one minute annealing in belt furnace at 450 °C improved the effective lifetime of some samples and degraded others. Some samples improved during the one hour when frequent measurements were made, maybe due to the illumination. A conventional contact firing process at a peak temperature of 945 °C degrades the effective lifetime of all the investigated samples to about the same as an unpassivated sample, thus the stacks and single layers cannot withstand a firing process for metallisation with standard metal pastes.

Table of Contents

Preface I

Abstract II

List of Symbols V

List of Acronyms VII

1. Introduction 1

1.1. Thesis outline 2

2. Theory 3

2.1. Solar cells 3

2.2. Recombination and lifetime 4

2.2.1. Radiative recombination 5

2.2.2. Auger recombination 6

2.2.3. Shockley Read Hall recombination 6

2.2.4. Surface recombination 7

2.3. The effect of surface recombination on conversion efficiency 9

2.4. Surface passivation 10

2.4.1. Chemical passivation 11

2.4.2. Field effect passivation 11

2.4.3. Surface passivation from silicon nitride 12

2.4.4. Surface passivation from hydrogenated amorphous silicon 13

2.4.5. Surface passivation from a-Si:H/a-SiN_x:H stacks 13

2.5. Lifetime measurements 14

2.5.1. The quasi steady state photoconductance method 15

2.5.2. The transient photoconductance decay method 15

2.5.3. Photoluminescence imaging 15

3. Experimental 17

3.1. Instruments 17

3.1.1. PlasmaLab System 133 from Oxford Instruments 17

3.1.2. WTC-120 Photoconductance Lifetime Tester from Sinton 18

3.1.3. LIS-R1 PL imaging setup from BT Imaging 19

3.1.4. Infrared furnaces from Radiant Technology Corporation 20

3.1.5. Rapid thermal processing system AccuThermo AW610 21

3.2. The samples 22

3.2.1. Preparation of the samples 22

3.2.2. The pieces for different analysis 25

3.2.3. Thermal stability experiments ... 26
3.3. Measurements ... 27
3.3.1. Temporal stability measurements ... 27
3.3.2. Thermal stability measurements ... 28
3.3.3. Uncertainties in the effective lifetime measurements ... 29
3.3.1. Influence of the bulk lifetime on the measured effective lifetime ... 30
4. Results and discussion ... 31
4.1. Lifetimes shortly after deposition ... 31
4.1.1. The samples passivated with silicon nitride ... 33
4.1.2. The effective lifetimes of the *p*-type samples shortly after deposition ... 34
4.1.3. The effective lifetimes of the *n*-type samples shortly after deposition ... 34
4.1.4. Summary of the results from the measurements shortly after deposition ... 35
4.1.5. Discussion of passivation quality shortly after deposition ... 35
4.1.6. Replacement of the *p*-type sample with 40 nm a-Si:H ... 37
4.2. Temporal stability ... 37
4.2.1. The temporal stability of the *p*-type samples ... 38
4.2.2. The temporal stability of the *n*-type samples ... 47
4.2.3. Summary of the results from the temporal stability measurements ... 53
4.2.4. Discussion of the temporal stability ... 53
4.3. Thermal stability ... 54
4.3.1. Rapid thermal annealing at different temperatures ... 54
4.3.2. Annealing in the belt furnace at 450 °C ... 60
4.3.3. Normal firing process ... 65
4.3.4. Summary of the results from the thermal stability experiments ... 66
4.3.5. Discussion of the thermal stability ... 66
4.4. Light induced improvement of the passivation from the stacks ... 69
5. Conclusions ... 71
5.1. Passivation provided shortly after deposition ... 71
5.2. Temporal Stability ... 71
5.3. Thermal stability ... 71
5.4. Light induced improvement of the passivation from the stacks ... 72
5.5. Suggestions for further work ... 72
References ... 74
Appendix 1, PC1D model parameter settings ... 76

List of Symbols

Symbol	Description	Unit
A_n ; A_p	Auger recombination coefficient for electrons and holes	$cm^6\ s^{-1}$
B_n ; B_p	Coefficient of bimolecular capture by trap of electrons and holes	$cm^3\ s^{-1}$
B_{rad}	Radiative recombination coefficient	$cm^3\ s^{-1}$
C	Calibration constant for the photoluminescence images	cm^6
D_{it}	Density of surface states	cm^{-3}
D_n ; D_p	Diffusion coefficients for electrons and holes	$cm^2\ s^{-1}$
E_c	The lowest energy in the conduction band	eV
E_F	Fermi level	eV
E_{Fn} ; E_{Fp}	Fermi level of *n*-type and *p*-type material	eV
E_T	Energy level of trap state	eV
E_v	The highest energy in the valence band	eV
G	Generation rate	$cm^{-3}\ s^{-1}$
I_{PL}	Intensity of the photoluminescence	—
K	Coefficient of proportionality, i.e. the percentage of photoluminescence detected by the camera in the PL imaging setup	$cm^3\ s$
n	Density of electrons	cm^{-3}
n^+	Highly doped *n*-type	—
n_i	Intrinsic carrier density	cm^{-3}
n_t	Density of electrons when the Fermi level of the *n*-type material is equal to the energy level of the trap state i.e. when $E_{Fn} = E_T$	cm^{-3}
N_s	Density of traps per unit area surface	cm^{-2}
N_t	Density of states in the band gap	cm^{-3}
N_A	Density of acceptor impurity atoms	cm^{-3}
N_D	Density of donor impurity atoms	cm^{-3}
p	Density of holes	cm^{-3}
p_t	Density of holes when the Fermi level of the *p*-type material is equal to the energy level of the trap state i.e. when $E_{Fp} = E_T$	cm^{-3}
q	Elementary charge	C
R	Reflectivity	—
S	Surface recombination velocity	$cm\ s^{-1}$

S_{eff}	Effective surface recombination velocity	cm s^{-1}
S_n ; S_p	Surface recombination velocity of electrons and holes	cm s^{-1}
U	Recombination rate	cm^{-3} s^{-1}
U_{rad}	Radiative recombination rate	cm^{-3} s^{-1}
U_{SRH}	SRH recombination rate	cm^{-3} s^{-1}
V_{bi}	Built-in voltage	V
v_n, v_p	Mean thermal velocity of electrons and holes	cm s^{-1}
W	Thickness of the wafer/cell	cm
$\Delta\sigma$	Photoconductivity	S cm^{-1}
Δn	Excess charge carrier concentration	cm^{-3}
Φ_{ex}	Photon flux	cm^{-2}?
μ_n; μ_p	Mobility of electrons and holes	cm^2 V^{-1} s^{-1}
σ_n ; σ_p	Capture cross section of the for electrons and holes	cm^2
Σ	Conductivity	S cm^{-1}
σ_{dark}	Conductivity in the dark	S cm^{-1}
τ_b	Bulk lifetime	s
τ_{eff}	Effective lifetime	s
τ_s	Surface lifetime	s
$\tau_{n, Aug}$, $\tau_{p, Aug}$	Auger recombination lifetime for electrons and holes	s
$\tau_{n, rad}$ $\tau_{p, rad}$	Radiative recombination lifetime for electrons and holes	s
$\tau_{n, SRH}$; $\tau_{p, SRH}$	SRH recombination lifetime for electrons and holes	s
$\tau_{n, s}$; $\tau_{p, s}$	Surface lifetime of electrons and holes	s
τ_s	Surface lifetime	s

List of Acronyms

Acronym	Description
a-Si:H	Hydrogenated amorphous silicon
a-SiN_x:H	Hydrogenated amorphous silicon nitride
ARC	Antireflection coating
BSF	Back surface field
c-Si	Crystalline silicon
Cz	Czochralski growth method for crystalline silicon
DI	Deionised
EPBT	Energy payback time
FZ	Float Zone
NRA	Neutron reaction analysis
PECVD	Plasma enhanced chemical vapour deposition
PL	Photoluminescence
PV	Photovoltaic
QSSPC	Quasi steady state photoconductance
RF	Radio frequency
RTA	Rapid thermal annealing
RTP	Rapid thermal processing
SRH	Shockley-Read-Hall
SRV	Surface recombination velocity
UV	Ultraviolet

1. Introduction

There is a need for more environmentally friendly energy supply to meet the world's energy demand, minimize anthropogenic climate change and contribute to sustainable development. Solar energy is an ample energy resource available for humans to utilise in environmentally friendly ways.

A solar cell is a device that converts electromagnetic waves directly into electricity [1]. Photovoltaic (PV) solar cells utilise the photovoltaic effect to generate electricity [1, 2]. Thus solar cells can use the solar irradiation on earth's surface to produce relatively environmentally friendly renewable energy with no emissions during operation [2]. The most common solar cell today is the crystalline silicon solar cell [1]. Crystalline silicon, and especially monocrystalline silicon, is expensive and energy demanding to produce [2]. If the conversion efficiency is raised without raising the cost and energy demand in production, the energy pay-back time (EPBT) of the cell will be reduced and electricity generated by solar cells will get closer to grid parity [3, 4].

The efficiency of conventional silicon solar cells is limited by surface recombination [5]. Making thinner cells can reduce material consumption and lower the costs and the energy consumption of the solar cell production, but in thinner cells surface recombination losses are even more important [2, 5]. Good surface passivation is therefore needed to reduce surface recombination losses and increase the conversion efficiency of silicon solar cells.

The passivation needs to be stable with respect to time because the operation time of a solar cell should be at least 20 years. It should also be stable with respect to temperature because firing of the cells in the metallisation process, the conventional way of making contacts by screen printing pastes, is carried out at high temperatures, typically 900 °C for a few seconds or 400-500 °C for a few minutes [6]. The passivation also needs to be stable with respect to illumination, as the cells will be illuminated during operation. Therefore investigations of the stability of the passivation layers are important.

In this thesis, temporal and thermal stability of passivation by layered stacks have been investigated. The double layer stack consisting of hydrogenated amorphous silicon nitride (a-SiN_x:H) and hydrogenated amorphous silicon (a-Si:H) have been shown to create good surface passivation [7-9]. Such stacks with different film thicknesses have been deposited on both sides of both *n*- and *p*-type polished float zone (FZ) monocrystalline silicon wafers. The varying film thicknesses of both a-Si:H and a-SiN_x:H have been investigated with respect to passivation quality as deposited and the stability of the passivation with respect to time and temperature.

The effective minority charge carrier lifetimes of the samples have been measured using quasi steady state photoconductance (QSSPC) and photoluminescence (PL) imaging. Assuming infinite bulk lifetime the upper limit of the surface recombination velocities (SRV) for each passivated wafer has been calculated to compare the passivation quality. The stability of the passivation provided by the

stack has been investigated by comparing the effective lifetimes measured regularly for the first two months after deposition. The optimal film thicknesses with respect to time were then determined.

The stability of the passivation of the different stacks with respect to temperature was investigated measuring lifetime before and after rapid thermal annealing (RTA) at different temperatures, before and after one minute annealing in a belt furnace at 450 °C and before and after a firing process normally used for metallization by screen printed pastes. Optimal film thicknesses with respect to the thermal stability were determined and the results were analysed to evaluate the time and temperature range in which a metallization process can be applied.

1.1. Thesis outline

In Chapter 2 the relevant theory of solar cells, recombination in general and surface recombination in particular, effect of the SRV on the efficiency and surface passivation is presented. Then a short summary of some of the relevant research already carried out in the field of passivation from a-Si:H, a-SiN_x:H and a-Si:H/a-SiN_x:H stack is given. Chapter *3 Experimental* describes the samples used, how the measurements were made and the setup and operation of the instruments used. The next chapter summarizes the results and important findings and discusses possible interpretations using the theory and what have been found earlier. The last chapter states the conclusions reached based on the obtained results and their interpretation as well as suggestions for further work for investigation of the passivation provided by a-Si:H/a-SiN_x:H stacks.

2. Theory

This chapter first presents relevant theory on solar cells, recombination in general and surface recombination in particular, the effect of the surface recombination on the conversion efficiency of a cell and surface passivation. Then a short summary of some of the relevant research already carried out in the field of passivation from a-Si:H, a-SiN_x:H and a-Si:H/a-SiN_x:H stack is given focusing especially on temporal and thermal stability.

2.1. Solar cells

Thorough descriptions of the physics of solar cells are found in several textbooks, including Nelson's *The Physics of Solar Cells* and Green's *Solar Cells*. [1, 10]

A solar cell usually consists of *n*- and *p*-type semiconductors [2]. Many different semiconductors and doping impurities can be used in solar cell devices. Most used is the crystalline silicon solar cell with a *p*-type base, lightly doped with boron (B) and an *n*-type emitter heavily doped with phosphorous (P) [2].

The Fermi level of intrinsic silicon is in the middle of the band gap between the valence band and the conduction band [11]. The band gap of silicon is 1.12 eV at 300 K [1]. For intrinsic silicon at low temperatures, the valence band is almost full and the conduction band is almost empty [11]. This means there are almost no charge carriers available [11]. When silicon is doped to become *p*-type using boron (B), the Fermi level is shifted towards the valence band [11]. The boron introduces allowed states just above the valence band [11]. These introduced states are empty at ground state and filled at room temperature, because very little energy is needed to excite electrons from the valence band to the introduced allowed state [11]. When silicon is doped to become *n*-type using phosphorous (P), the Fermi level is shifted towards the conduction band [11]. This happens because the phosphorous introduces allowed states just below to the conduction band [11]. These states are filled at ground state and empty at room temperature, because very little energy is needed to excite electrons from the introduced allowed state into the conduction band [11]. The energy bands and Fermi levels of intrinsic, *n*-type and *p*-type silicon are illustrated in Figure 1.

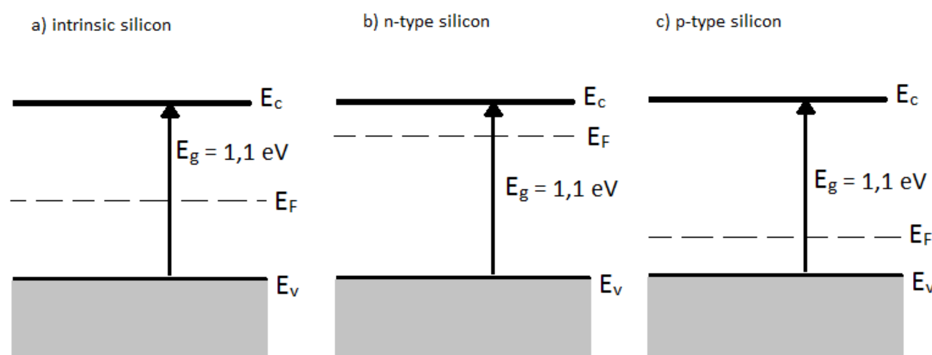

Figure 1 Illustration of the energy bands and Fermi levels of intrinsic, *n*-type and *p*-type silicon.

In the *pn*-junction the energy bands have shifted for the Fermi level to be equal throughout the entire material in equilibrium [11]. This is illustrated in Figure 2. This shift of energy bands gives rise to the asymmetry of a solar cell, the built-in voltage, V_{bi} [1]. The built in voltage is needed to separate the charge carriers generated by the incoming light [1]. The generated electrons will drift down the slope in the conduction band to the *n*-type material, while the holes will drift up the slope in the valence band to the *p*-type material [1]. Both the electron and hole drift currents contribute to the net current generated by an illuminated solar cell [1].

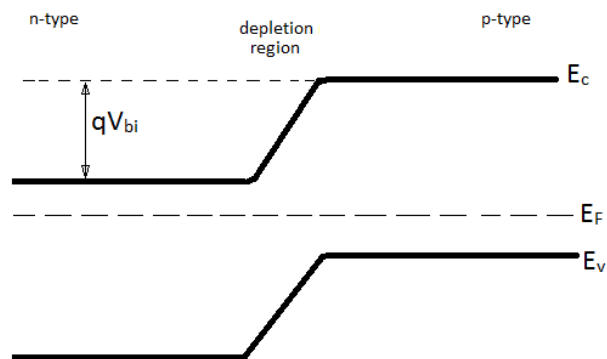

Figure 2 Schematic band gap diagram of a *pn*-junction. The energy bands have shifted for the Fermi level to be equal throughout the entire material.

2.2. Recombination and lifetime

Recombination is relaxation of an exited electron from the conduction band to the valence band. Recombination may occur through three different recombination processes. These recombination processes are called radiative recombination, Auger recombination and Shockley Read Hall recombination. The lifetime is the average time before an exited electron relaxes from the conduction band to the valence band, i.e. before an excess minority carrier recombines [12].

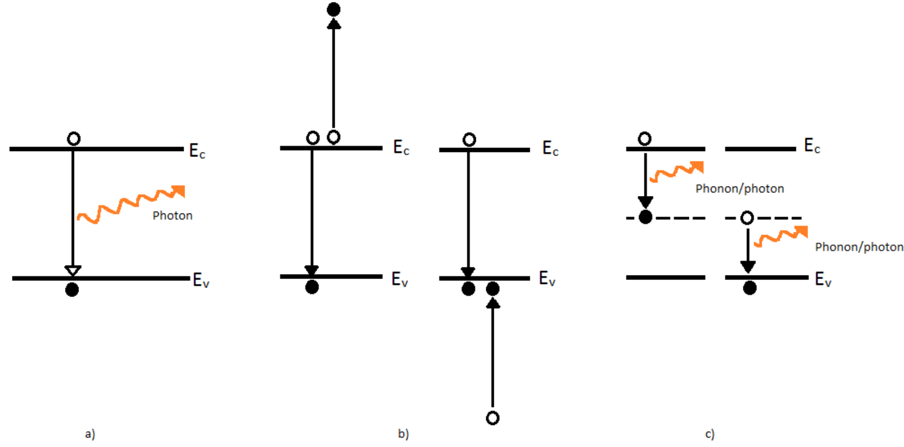

Figure 3 Illustration of recombination processes: a) radiative recombination, b) Auger recombination and c) two-step SRH recombination through a defect state introduced close to the middle of the band gap. The electrons are drawn as black dots where they are situated at the end of the process. The holes left behind by the electron are drawn as white dots. The orange arrows are illustrating the photons/phonons emitted in the processes. E_v denotes the upper edge of the valence band and E_c denotes the lower edge of the conduction band.

2.2.1. Radiative recombination

Radiative or band-to-band recombination is a process where an electron in the conduction band relaxes down to the valence band emitting a photon [1]. This process is illustrated by Figure 3 a. The radiative recombination rate is higher in direct band materials than in indirect band materials [1]. In indirect band materials, the radiative recombination process is less likely than in direct band materials, because it involves a phonon as well as a photon [1, 10]. The radiative recombination rate U_{rad} depends on the density of electrons in the conduction band n and the density of holes in the valence band p and is given by Equation (1)

$$U_{rad} = B_{rad}(np - {n_i}^2) \quad (1)$$

where n_i is the intrinsic carrier density and B_{rad} is the material specific radiative recombination coefficient [1]. The recombination coefficient for silicon is $B_{rad} = 2\cdot 10^{-5}$ cm^3/s [1, 10]. In moderately doped material the approximation that the concentration of minority carriers in equilibrium is a lot smaller than the excess carrier concentration, which again is a lot smaller than the majority charge carrier concentration can be used. The radiative lifetimes of electrons and holes in moderately doped materials at low injection are then given by Equation (2) and (3), respectively

$$\tau_{n,rad} = \frac{1}{B_{rad}N_A} \quad (2)$$

$$\tau_{p,rad} = \frac{1}{B_{rad}N_D} \quad (3)$$

where N_A and N_D are the density of acceptor and donor impurity atoms, respectively [1].

2.2.2. Auger recombination

In Auger recombination an electron in the conduction band interacts with another electron in the same band, and then relaxes down to the valence band [1]. The relaxing electron transfers its excess energy as kinetic energy to the other electron in the interaction [1]. The exited electron then loses its gained kinetic energy by thermalisation [1]. The Auger recombination process, shown in Figure 3 b, may also occur analogous to the process described above as a hole in the valence band interacting with another hole in the same band [10]. The rate of Auger recombination depends strongly on the density of electrons in the conduction band, and the density of holes in the valence band, i.e. the doping levels and the excess carrier concentration [1]. Therefore Auger recombination is the dominating recombination process at high excess carrier concentration [13]. The Auger lifetimes of electrons and holes in moderately doped materials at low injection are given by Equation (4) and (5), respectively

$$\tau_{n,Aug} = \frac{1}{A_n {N_A}^2} \quad (4)$$

$$\tau_{p,Aug} = \frac{1}{A_p {N_D}^2} \quad (5)$$

where A_n and A_p are the Auger recombination coefficients for electrons and holes [1]. Auger recombination is the dominant loss mechanism in pure silicon, especially for doping levels greater than 10^{17} cm^{-3} [1, 10].

2.2.3. Shockley Read Hall recombination

The Shockley Read Hall (SRH) recombination process occurs through defect states in the band gap [10]. Defects or impurities in a material may introduce allowed states in the energy gap, thus the rate of SRH recombination depends on density of such states which again depends on the material quality [10]. The defect states function as trapping states or recombination centres, depending on their position in the energy gap [1]. Equation (6) shows the expression for the SRH recombination rate through a single state close to the middle of the band gap.

$$U_{SRH} = \frac{np - {n_i}^2}{\tau_{n,SRH}(p + p_t) + \tau_{p,SRH}(n + n_t)} \quad (6)$$

n and p are the densities of electrons and holes, n_i is the intrinsic carrier density [1]. p_t is the density of holes when the Fermi level of the p-type material is equal to the energy level of the trap state, i.e.

when E_{Fp} = E_T *[1].* n_t is the density of electrons when the Fermi level of the *n*-type material is equal to the energy level of the trap state i.e. when E_{Fn} = E_T [1].

$\tau_{n,SRH}$ and $\tau_{p,SRH}$ are the SRH lifetimes of electrons and holes, respectively and are given by

$$\tau_{n,SRH} = \frac{1}{B_n N_t} \tag{7}$$

$$\tau_{p,SRH} = \frac{1}{B_p N_t} \tag{8}$$

in moderately doped materials at low injection, where N_t is the density of states in the band gap and B_n and B_p are the coefficients of bimolecular capture by trap of electrons and holes, respectively. The coefficients of bimolecular capture by trap are expressed by Equation (9) and (10)

$$B_n = v_n \sigma_n \tag{9}$$

$$B_p = v_p \sigma_p \tag{10}$$

where v_n and v_p are the mean thermal velocities of electrons and holes and σ_n and σ_p are the capture cross sections of the trap for electrons and holes [1].

2.2.4. Surface recombination

For high lifetime material, recombination through defect states is especially important at the surfaces where the number of crystal defects and extrinsic impurities are the greatest [1]. At the surface, the periodic nature of the crystal structure ends [14]. Therefore the density of dangling or broken bonds is high at an untreated surface. The concentration of contamination from the production of the wafer is also highest at the surface as this is in contact with the surroundings [1]. This results in a high density of surface states [1]. Dangling bonds at a silicon surface are illustrated in Figure 4 a and states introduced in the band gap at the surface of a crystalline silicon wafer are illustrated in Figure 4 b.

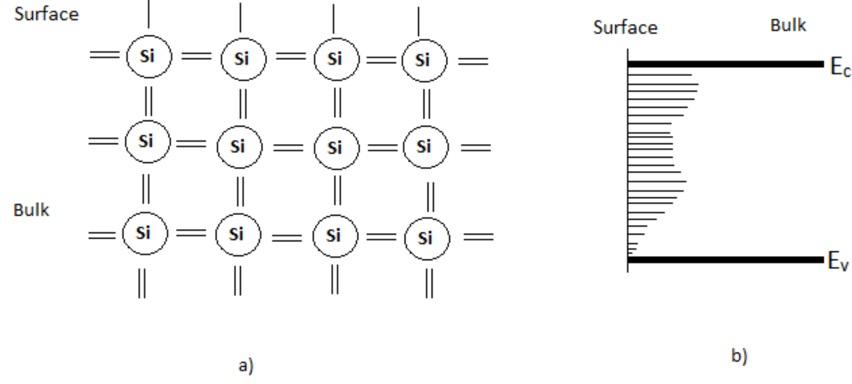

Figure 4 a) Two dimensional illustration of the dangling bonds at the surface of crystalline silicon. b) Schematic band diagram of allowed states in the band gap at an untreated surface of silicon. The states in the band gap are introduced by dangling bonds and other defects and impurities [10].

2.2.4.1. Surface recombination velocity

The surface recombination velocity (SRV) is a measure of the rate of recombination at the surface with the units cm/s [1]. The SRV depends on the density of localized states at the surface [1]. Surface recombination velocity *S* is defined by Equation (11) and (12) for electrons and holes, respectively

$$S_n = B_n N_s \quad (11)$$

$$S_p = B_p N_s \quad (12)$$

where N_s is the trap density per unit area of surface and B_n and B_p defined by Equation (9)(10) and stated above [1]. The surface recombination is quite analogous to the rate of SRH recombination.

For surfaces with equal SRV on the rear and front surface, the relation between the surface lifetime, τ_s, and the SRV *S* for electrons and holes, respectively, is given by Equation (13) and (14)

$$\tau_{n,s} = \frac{W}{2S_n} + \frac{1}{D_n}(\frac{W}{\pi})^2 \quad (13)$$

$$\tau_{p,s} = \frac{W}{2S_p} + \frac{1}{D_p}(\frac{W}{\pi})^2 \quad (14)$$

where *W* is the thickness of the wafer [15, 16]. For high values of SRV the second term of the equation dominates and the exact value of the SRV will have very little influence on the surface lifetime. Hence the thickness and the diffusion coefficient are the main parameters affecting the surface lifetimes for high values of SRV. For a given thickness only the diffusion coefficient limits the surface recombination. The diffusion coefficient is greater when the bulk lifetime is higher, thus surface recombination is more limiting in high bulk lifetime materials. For low values of SRV, the diffusion of carriers to the surface does not limit the surface recombination. Hence the relations

between SRV S and surface lifetime τ_s given above can be simplified to Equation (15) and (16) for low values of SRV

$$\tau_{n,s} = \frac{W}{2S_n} \tag{15}$$

$$\tau_{p,s} = \frac{W}{2S_p} \tag{16}$$

Thus the relation between SRV S and effective lifetime τ_{eff} for low values of SRV and equal SRV on both surfaces is given by Equation (17) [17]

$$\frac{1}{\tau_{eff}} = \frac{1}{\tau_b} + \frac{1}{\tau_s} = \frac{1}{\tau_b} + 2\frac{S}{W} \tag{17}$$

where τ_b is the bulk lifetime and τ_s is the surface lifetime.

2.3. The effect of surface recombination on conversion efficiency

For high quality material with high bulk lifetime it is necessary to reduce the SRV to achieve solar cells with high conversion efficiencies [17]. Simulations of how the SRV affects the cell conversion efficiency were carried out in PC1D, a one dimensional simulation program for crystalline semiconductor devices, available for free from the University of New South Wales [18, 19]. The PC1D software solves the nonlinear equations for charge carrier transport in these devices, and can thus be used to calculate current, voltage and power generated by a solar cell when the parameters of the device are set [19]. In the simulations, the front and rear side SRVs were set to be equal. The SRVs were varied from 1 to 10^8 cm/s. The simulations were carried out for two different thicknesses, 50 and 200 µm, keeping all the other parameters in the model constant. A table showing the other parameter settings in the simulation is given in Appendix 1. The results are plotted in Figure 5.

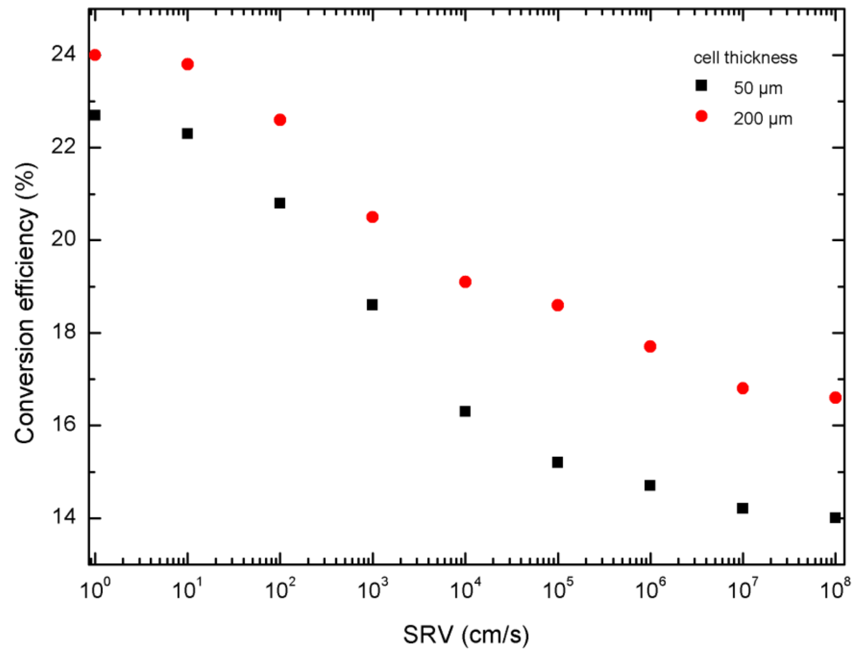

Figure 5 The simulated efficiency of a PC1D model for different values of SRV for two different cell thicknesses; 50 and 200 µm.

The conversion efficiency of a solar cell decreases with increasing SRV. For the cell with a thickness of 50 µm, the simulated efficiency decreases almost 40 relative per cent, from 22.7 % to 14.0 %, for an increase of the SRV from 1 to 10^8 cm/s. Most of this efficiency decrease occurs in the range of SRVs from 10 to 10^4 cm/s. For the cell with a thickness of 200 µm, the simulated efficiency decreases about 30 relative per cent, from 24.0 % to 16.6 %, for an increase of the SRVs from 1 to 10^8 cm/s. The decrease of the efficiency is most rapid in the range of SRVs from 10^2 to 10^4 cm/s. For the 200 µm cell the total decrease of conversion efficiency is smaller than for the 50 µm cell, which means losses due to high SRV is even more important for thinner cells. Still, for the 200 µm cell, a conversion efficiency loss of more than 7 absolute per cent is a considerable loss. This needs to be greatly reduced to achieve high conversion efficiencies.

2.4. Surface passivation

The surfaces of silicon wafers for solar cells are passivated to reduce the surface recombination, which can be minimised either by reducing the density of surface states or by reducing the concentration of free electrons or holes at the surface [17]. Reducing the density of surface states is referred to as chemical passivation [20]. Reducing the concentration of free electrons or holes at the surface is referred to as field effect passivation [17, 20]. Silicon oxide (SiO_2), hydrogenated silicon nitride (a-SiN_x:H), hydrogenated amorphous silicon (a-Si:H) and aluminium oxide (AlO_x) are some examples of grown or deposited layers used to passivate the surfaces of silicon for solar cells. A region of highly doped silicon at the rear surface, inducing a back surface field (BSF), can also be used for passivation of silicon solar cells. Some of these passivation techniques will be discussed in more detail in Section 2.4.3-2.4.5.

2.4.1. Chemical passivation

Chemical passivation is reducing the surface recombination through saturation of dangling and other recombination active bonds and thus reduction of the surface state density (D_{it}) [20, 21]. This can be achieved by depositing or growing a film that binds to the silicon at the surface, thus reducing the number of recombination active surface states. Such films may be a-Si:H [20]. The energy state of the covalent Si-H bond lies within the band of already allowed energy states for silicon [17]. For example, the number of recombination active states will be reduced if the dangling bonds of the silicon surface are bound to hydrogen atoms. An annealing for the right time and temperature usually improves the passivation. The annealing functions as an activation where the heating of the wafer with a layer of for example a-Si:H, causes the hydrogen to redistribute saturating more bonds at the a-Si:H/c-Si interface and restructuring of other recombination active bonds [22]. However, the hydrogen will be released with time, and the efficiency of the chemical passivation from saturation of dangling bonds with hydrogen will diminish.

2.4.2. Field effect passivation

The goal of field effect passivation is to reduce the concentration of either free electrons or holes at the surface to minimise the surface recombination [20, 23]. An electric field, repelling one type of charge carriers and attracting the other type, is created for example by an applied voltage layer or by a dielectric material with fixed charges close to the surface [20]. Depending on the amount of fixed charge or applied voltage and the doping polarity and doping level three different conditions may arise, called accumulation, inversion or depletion conditions. When a thin film of a-SiN_x:H is deposited on a silicon wafer, fixed positive charges will be present in the a-SiN_x:H-layer close to the c-Si/a-SiN_x:H-interface. The positive fixed charge at the c-Si/a-SiN_x:H interface will repel holes and attract electrons. This creates either a depletion layer or an inversion layer close to the interface in *p*-type silicon depending on the amount of fixed charge present and the doping level. In *n*-type silicon an accumulation layer is created close to a c-Si/a-SiN_x:H interface.

The inversion condition close to the interface in *p*-type material is created by either a high positive applied voltage or a high concentration of positive charges. The majority charge carriers are repelled and the minority carriers are attracted, thus the concentration of majority carriers is reduced and the concentration of minority carriers is greatly increased. This results in less surface recombination. Inversion is illustrated in Figure 6. Since the concentration of majority carriers is reduced and the concentration of minority carriers is greatly increased, the Fermi level will be closer to the conduction band. This causes the bands to bend downwards at the surface. When the bands are bent enough, i.e. the electron density at the surface is high enough for the intrinsic energy level to be below the Fermi level, this layer becomes *n*-type [14]. A band diagram of inversion in *p*-type silicon is shown in Figure 7 b.

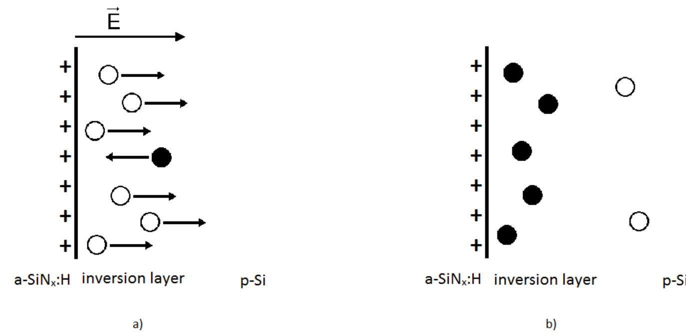

Figure 6 Illustration of field effect passivation from a layer of a-SiN_x:H at the surface of a *p*-type silicon wafer. The electric field induced by the fixed positive charges are causing the electrons to move towards the interface and the holes to move away from the interface. This is shown in a). The resulting inversion layer is shown in b).

For moderate positive charges on a *p*-type wafer the majority carriers, the holes, are repelled and the minority carriers, the electrons, are attracted. This induces a depletion layer close to the interface in the silicon [14]. In Figure 7 a the depletion condition is illustrated with a band diagram. Because the concentration of electrons and holes are similar, depletion gives high surface recombination and is not desirable for passivation purposes.

The positive fixed charges close to the Si/a-SiN_x:H interface on an *n*-type wafer causes accumulation conditions. The minority charge carriers, the holes, are repelled and this reduces the concentration of minority carriers at the interface. The majority charge carriers, the electrons, are attracted and the concentration is increased at the interface. This reduces the surface recombination. The electrons accumulate close to the surface, causing the Fermi level to shift towards the conduction band and hence the band to bend downwards. This layer therefore becomes more *n*-type, i.e. an n^+ region [14]. Accumulation is illustrated by a band diagram in Figure 7 c.

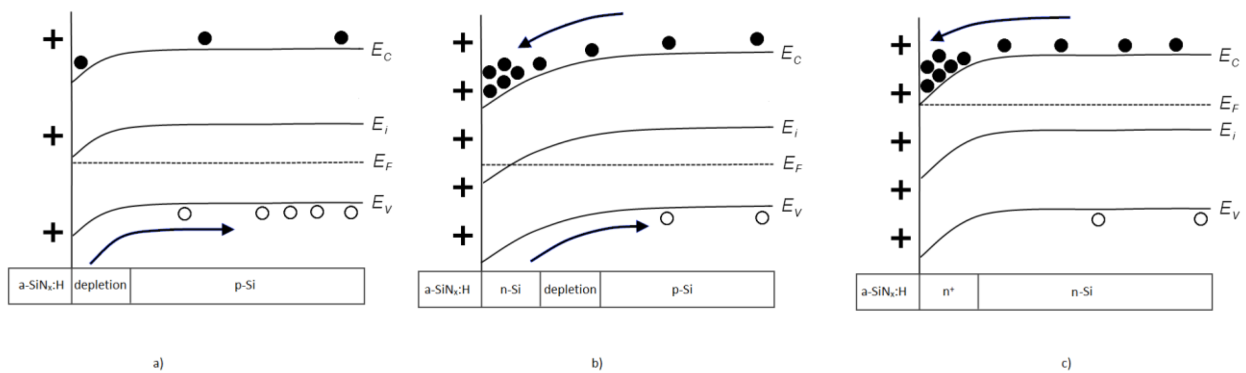

Figure 7 Band diagram of doped silicon wafers with a passivation layer of a-SiNx:H with positive fixed charges close to the interface. a) *p*-type silicon in depletion, b) *p*-type silicon in inversion c) *n*-type silicon in accumulation. The figure is taken from Helland [23] and modified.

2.4.3. Surface passivation from silicon nitride

Surface passivation by hydrogenated amorphous silicon nitride deposited by plasma enhanced chemical vapour deposition (PECVD) does not require high temperature processing [17]. Deposition

can be carried out at 200-400 °C [6]. Silicon nitride can act as both a passivation layer and antireflection coating (ARC) [17] For silicon the ARC should have a refractive index of around 2 [1, 3, 17]. The optimal thickness of an ARC with a refractive index of 2 is one eights of the designer wavelength [3]. The designer wavelength is usually 600 nm, which gives an ideal thickness of 75 nm [3]. The refractive index of amorphous silicon nitride is determined by process conditions, but is in the range around 2. Therefore silicon nitride is suitable as ARC for silicon [1, 17]. A layer of a-SiN_x:H on silicon provides both chemical and field effect passivation [24]. The field effect passivation is provided by the positive charges present in the silicon nitride layer close to the crystalline silicon/silicon nitride interface [17]. The passivation provided by silicon nitride is more stable than the one from a-Si:H, but the chemical passivation provided by silicon nitride is not as good as the one from a-Si:H. The values of S_{eff} for surfaces passivated with SiN_x:H are very low [21, 25]. Lelièvre et al. measured SRVs of 4 cm/s on *n*-type and 14 cm/s on *p*-type in a study of the passivation quality of hydrogenated silicon nitride [21]. Lauinger et al. measured SRVs of 4 cm/s on *p*-type silicon wafers in a study of passivation of *p*-type wafers with silicon nitride [26].

2.4.4. Surface passivation from hydrogenated amorphous silicon

Hydrogenated amorphous silicon, a-Si:H, provides very good passivation of silicon surfaces [27, 28]. The passivation is mainly chemical passivation [29]. Since the band gap of hydrogenated amorphous silicon is wider than that of the crystalline silicon, the number of recombination active states can be reduced by hydrogenation at the a-Si:H/c-Si interface [29]. The passivation quality has a low thermal and temporal stability [28]. The hydrogen is released fast when fired at high temperatures because hydrogen effuses from the passivation layer [28]. De wolf et al. found that light degrades a-Si:H/c-Si interfaces of [100] oriented samples [27].

Because amorphous silicon absorbs light above 1.7 eV the a-Si:H film should be as thin as possible when used as passivation on the front side of a cell, in order to absorb as little as possible of the incoming light [6]. For the front side a thin layer of 10 nm has been found to be close to the optimal with respect to passivation and minimal absorption [6]. The thermal degradation of the passivation quality depends on the thickness of the a-Si:H layer [28]. Li and Wenham found that the lifetime of the samples with the thinner a-Si:H layers degrade much faster than thicker when annealed at temperatures above 250°C [28]. Gatz et al. states that thin layers of a-Si:H are not thermally stable above 400 °C [6].

2.4.5. Surface passivation from a-Si:H/a-SiN_x:H stacks

Stacks of a-Si:H and a-SiN_x:H provide very good passivation quality that is relatively stable with respect to time and temperature [6-8]. Such stacks are a promising alternative for surface passivation of silicon wafers for solar cells [9]. The stack provides better passivation than single layers of a-Si:H and a-SiN_x:H.

The passivation quality of an a-SiN_x:H layer can be improved by inserting an a-Si:H layer between the silicon nitride and the crystalline silicon [8]. When a layer of hydrogenated amorphous silicon is added in this way, the number of nitrogen dangling bonds at the interface may be reduced [8].

The thermal stability of a-Si:H can be improved by capping the a-Si:H layer with a layer of a-SiN_x:H [6]. Hydrogenated amorphous silicon without capping degrades at temperatures above 300 °C, whereas hydrogenated amorphous silicon with a capping of hydrogenated silicon nitride degrades at 500 °C [6]. Heating causes hydrogen to be released from the a-Si:H film by effusion [30]. The thermal stability of the stacks also depend of the deposition temperature of the layers. Gatz et al. found for example that stacks where the a-SiN_x:H layer is deposited at 400 °C is more stable that when the a-SiN_x:H layer is deposited at 300 °C [6].

Tucci and Serenelli states that the passivation mechanism of an amorphous silicon/silicon nitride stack is a superficial field effect induced by the charge of hydrogen ions in the stack [9]. Because the hydrogen is involved in the passivation, one will see metastability effects [9]. Exposure to UV-light can, for example, break the bonds between silicon and hydrogen [9]. Tucci and Serenelli found that specific annealing procedures can improve the metastability of the passivation quality with respect to UV-light exposure [9].

2.5. Lifetime measurements

The effective minority charge carriers lifetime of a sample can be calculated for different excess carrier concentrations using the quasi steady state photoconductance (QSSPC) method for short lifetimes and the transient photoconductance decay method for longer lifetimes [31]. The effective lifetime is calculated via the measured photoconductance [31]. The effective lifetime τ_{eff} can be written as

$$\tau_{eff} = \frac{\Delta n}{G - \frac{d}{dt}\Delta n} \tag{18}$$

where G is the generation rate [32]. The photoconductivity $\Delta\sigma$ of a sample is related to the excess carrier concentration Δn through Equation (19) [16, 31]

$$\Delta n = \frac{\Delta\sigma(t)}{q(\mu_n + \mu_p)W} \tag{19}$$

where W is the thickness of the sample, q is the elementary charge and μ_n and μ_p are the mobilities of electrons and holes, respectively. $\Delta\sigma$ is the conductivity due to the excess charge carrier density

$$\Delta\sigma = \sigma - \sigma_{dark} \tag{20}$$

where σ_{dark} is the conductance of the sample in the dark.

2.5.1. The quasi steady state photoconductance method

For steady state the excess carrier concentration is nearly constant, thus $\frac{d}{dt}\Delta n$ is close to zero reducing the expression in Equation (18) to [32]

$$\tau_{eff} = \frac{\Delta n}{G} \quad (21)$$

Steady state is achieved by subjecting the sample to a long, slowly decaying pulse of light [31]. The pulse must decay at least 10 times slower than the carrier lifetime for the excess charge carriers to be close to quasi steady state and the QSSPC method to be valid [31].

2.5.2. The transient photoconductance decay method

For transient mode the generation rate *G* is close to zero reducing Equation (18) to [32]

$$\tau_{eff} = \frac{-\Delta n}{\frac{d}{dt}\Delta n} \quad (22)$$

In the transient photoconductance decay method the light pulse used should be short compared to the lifetime. In transient mode the conductivity is measured after the flash has finished [31]. From the measured conductivity the excess carrier concentration is calculated and then the derivative of the excess carrier concentration with respect to time can be determined and used in Equation (22) to calculate the lifetime [31]. For this method to be valid, the lifetime should be much longer than the flash [31].

2.5.3. Photoluminescence imaging

The intensity of the photoluminescence from a sample detected by a camera is proportional to the rate of radiative recombination U_{rad} in the sample [33]. An expression relating the rate of radiative recombination and the concentration of holes and electrons is given by Equation (1) stated above in section 2.2.1.

For a *p*-type material the relation between the intensity of the photoluminescence I_{PL} and the excess carrier density is given by [33]

$$I_{PL} = k\, U_{rad} = k\, B_{rad}\, \Delta n\, (N_A + \Delta n) \quad (23)$$

where N_A is the doping concentration and k is a coefficient of proportionality which depends on the percentage of photoluminescence detected by the camera. This relation is valid when the density of electrons in equilibrium is much smaller than both the doping concentration and the excess carrier concentration and therefore can be neglected. The radiative recombination coefficient is independent of the excess carrier concentration for excess carrier concentrations $\Delta n < 10^{15}$ cm^{-3} [1, 33].

Thus Equation (23) can be written as the relation in Equation (24)

$$I_{PL}(\Delta n) = CN_A\Delta n + C\Delta n^2 \tag{24}$$

where C is the calibration constant, a combined constant of the camera dependent constant k and the sample dependent constant B_{rad}.

This means that measuring the excess carrier density and the intensity of photoluminescence under the same conditions and using the same setup gives enough information to determine the calibration constant C for those particular measurement conditions [33].

Equation (18) can be used to calculate the effective lifetime from the excess carrier concentration Δn and the generation rate G. The generation rate can be calculated form the equation

$$G = \Phi_{ex}(1 - R)\frac{1}{W} \tag{25}$$

where R is the reflectivity from the front side of the sample, Φ_{ex} is the photon flux and W is the thickness of the sample [33]. This relation is an approximation based on the assumption that all the incoming photons that are not reflected are absorbed by the sample. This assumption is valid because the photons have very high energies compared to the band gap of silicon and the penetration depth is therefore short.

3. Experimental

This chapter first presents the instruments used. The relevant parameters of the samples and the preparation and thermal processing of these are then given. The last part of this chapter concerns the effective lifetime measurements of the samples.

3.1. Instruments

This section presents the instruments used for preparation of the samples, the effective lifetime measurements and the thermal processing.

3.1.1. PlasmaLab System 133 from Oxford Instruments

The PlasmaLab System 133 from Oxford Instruments was used for plasma enhanced chemical vapour deposition (PECVD) of the a-Si:H and a-SiN_x:H films. This is a direct high frequency plasma deposition reactor using a radio frequency of 13.56 MHz. A schematic illustration of the PECVD chamber is shown in Figure 8.

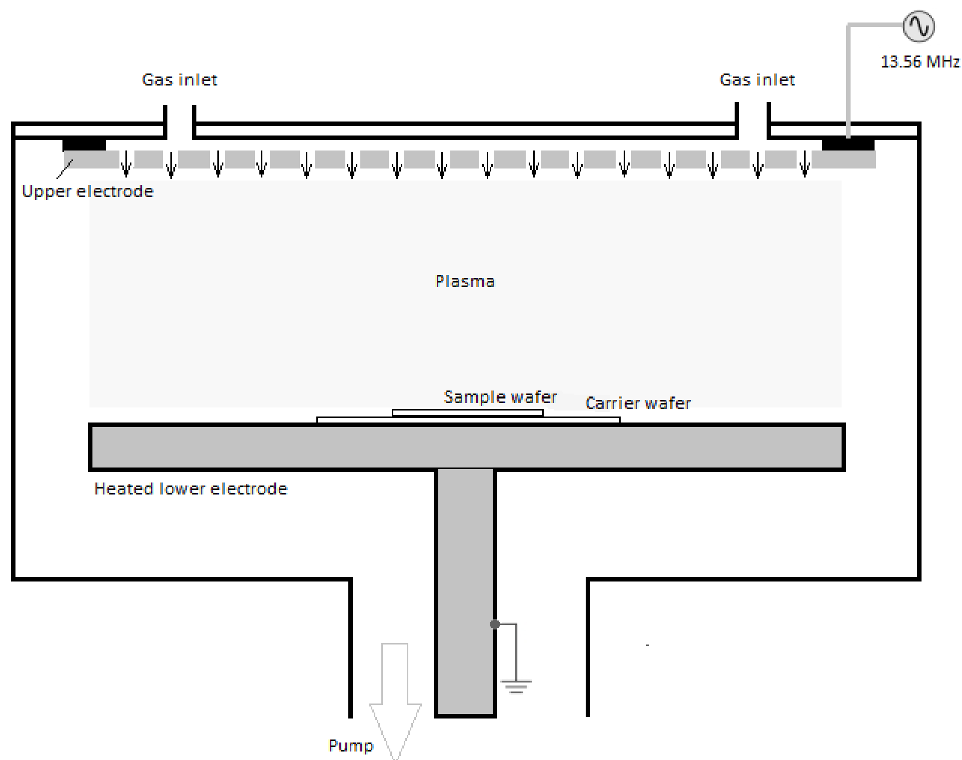

Figure 8 Schematic illustration of the plasma enhanced chemical vapour deposition (PECVD) chamber.

The process gases used are fed into the chamber through the upper electrode, ionized by the radio frequency (RF) radiation and plasma is created of the gases. The sample is placed on the lower electrode in the chamber. A vacuum pump keeps the chamber at low pressure.

3.1.2. WTC-120 Photoconductance Lifetime Tester from Sinton

The *Photoconductance Lifetime Tester* from Sinton was used to calculate the effective lifetime of a sample for different excess carrier concentrations using the quasi steady state photoconductance (QSSPC) method for short lifetimes and the transient photoconductance decay method for longer lifetimes [31]. The effective lifetime is calculated via the measured photoconductance [31].

3.1.2.1. The quasi steady state photoconductance method

To achieve quasi steady state, the pulse must decay at least 10 times slower than the carrier lifetime. The flash of Sinton's WCT-120 Photoconductance lifetime tester is 2 ms when set for measurements in quasi steady state mode [31]. This means that the QSSPC method should only be used for lifetimes below 200 µs [31].

3.1.2.2. Transient photoconductance decay method

The flash of Sinton's WCT-120 Photoconductance lifetime tester is 10-20 µs in transient mode [31]. In transient mode the conductivity is measured after the flash has finished [31]. For the transient photoconductance decay method to be valid, the lifetime should be much longer than the flash, i.e. longer than 100 µs [31].

3.1.2.3. The instrument setup

The sample is placed on an inductive coil connected to an RF bridge. The diameter of the coil is about 2 cm. This coil and bridge is used to measure the conductivity of the sample before and during the flash. The light intensity of the flash is measured simultaneously by the reference photodiode. The calculation of the generation rate is based on an estimate of the proportion of the light absorbed in the sample which again is based on the optical constant inserted in the accompanying software. A schematic representation of the setup is shown in Figure 9.

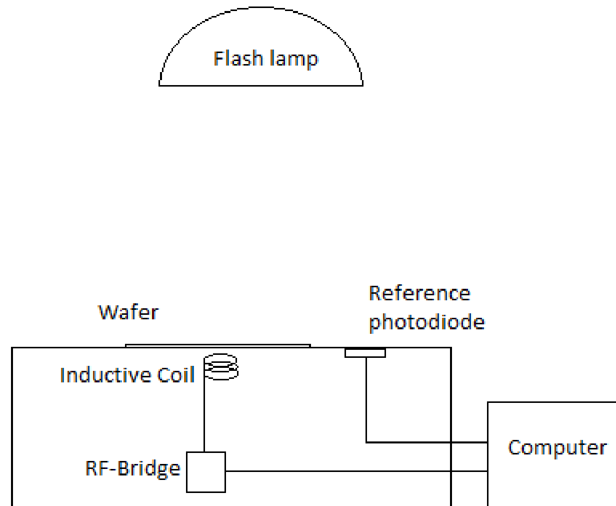

Figure 9 Schematic representation of the QSSPC setup.

3.1.3. LIS-R1 PL imaging setup from BT Imaging

Lifetime measurements were carried out using LIS-R1 PL imaging setup from BT Imaging. Figure 10 shows a schematic representation of the photoluminescence setup. The excitation laser radiates photons of wavelength λ = 808 nm. The photons excite electrons in the wafer. When the electron-hole pairs recombine radiatively, light is emitted. The emitted light is detected by the camera placed above the sample. The calibration constant is determined from an independent measurement using the QSSPC method as described in section 2.5.1-2.5.3 above. The excitation laser is used to imitate a flash and the flash is set to decay at least 10 times slower than the lifetime for the measurements made for the QSSPC method to be valid. The duration of the light pulse was set to 0.2 s. This is 14 times longer than the highest lifetime. The excess carrier concentration Δn is calculated using Equation (19) with the values of the measured photoconductance inserted for $\Delta\sigma$. For the reflectance R and the thickness W the values used are those entered into the in the accompanying software from BT Imaging. Equation (21) is used to calculate the effective lifetime from the generation rate and the calculated excess carrier concentration Δn. The PL intensity of the entire wafer is calibrated to the effective lifetime using the QSSPC measurement of a reference region, just above the RF coil.

The penetration depth of photons with a wavelength of 808 nm in silicon is approximately 13 µm. The samples are almost 300 µm thick. Therefore the assumption mentioned in section 2.5.3 that all the incoming photons that are not reflected are absorbed in the sample is valid [33].

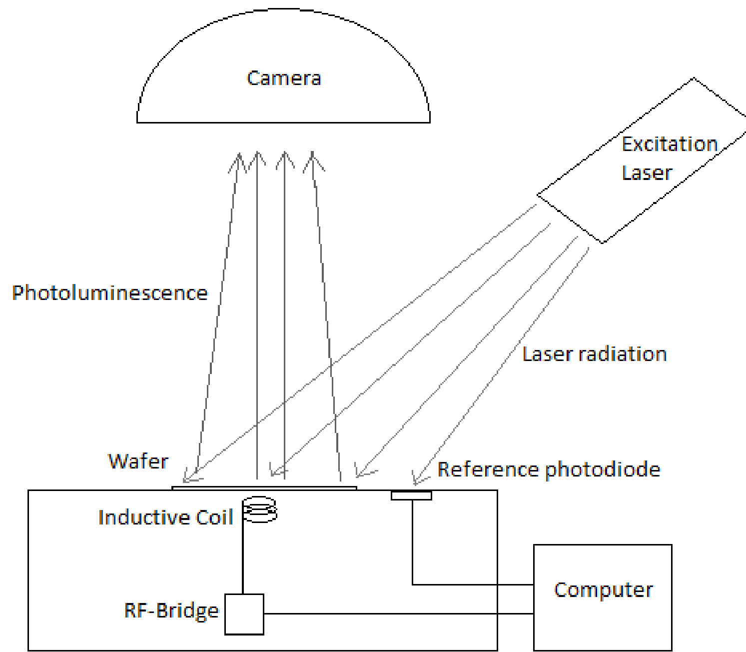

Figure 10 Schematic representation of the photoluminescence imaging setup

3.1.4. Infrared furnaces from Radiant Technology Corporation

Infrared belt furnaces from Radiant Technology Corporation (RTC) with controlled atmosphere were used for firing and annealing experiments.

The furnaces have a conveyor belt running through heating zones with a total length 76.2 cm [34]. These zones are heated by infrared heating lamps. After the heating zones there is a cooling section as shown in Figure 11 [34]. In the annealing and firing experiments carried out in this study air was used for cooling.

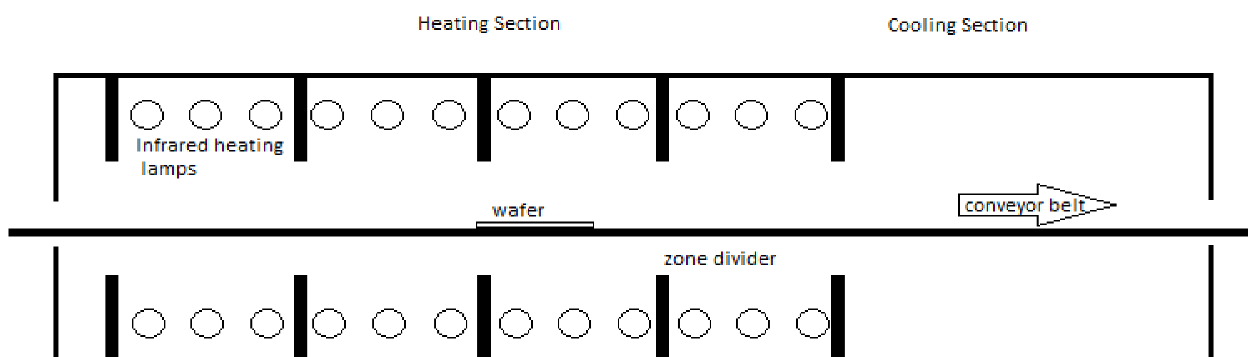

Figure 11 Schematic illustration of the belt furnace LA-309 from Radiant Technology Corporation (RTC) used in this study. The furnace has 4 heating zones [34].

The model LA-309 has four 19 cm long heating zones. This belt furnace was used for the normal firing process. The temperature of each zone is given in Table 1. The belt speed was set to 520 cm/min giving a total time of the firing process of 8.8 seconds, 2.2 seconds in each of the heating zones.

Table 1 Parameters of the firing process used in this study.

Parameter	Unit	zone 1	zone 2	zone 3	zone 4
Temperature	°C	780	825	870	945

The model LA-310 has three heating zones, the first and last are 19 cm and the second is 38 cm. This belt furnace was used for the 1 minute annealing at 450 °C. All the zones were set to 450 °C and the belt speed was set to 80 cm/min.

The samples with the same doping type and the same capping thickness were annealed or fired together. The samples were placed on a 6 inch etched multicrystalline carrier wafer on the conveyor belt during annealing or firing to avoid contamination from the belt and minimise potential scratches in the surface layers caused by the sample handling.

3.1.5. Rapid thermal processing system AccuThermo AW610

The rapid thermal processing (RTP) system AccuThermo AW610 from AllWin21 was used for annealing of the wafers at specific temperatures for 1 minute at steady state. The RTP system uses high intensity visible radiation to heat the wafers. The temperatures of the wafers were measured with a thermocouple. The thermocouple was also connected to the AccuThermo software. The model temperature was programmed in the software. The annealing temperature programs used were: ramp up to a given temperature for 20 seconds, keep the wafer at steady state at that temperature for 60 seconds, and ramp down as fast as possible. Nitrogen gas was used for cooling. The temperature was below 100 °C within 2 minute after the end of the steady state period for all the samples. The recommended steady state temperature for the system is between 150 and 1150 °C. The system was used in the range from 100 to 500 °C.

The samples were annealed four or five at a time. The 2·2 cm^2 pieces with the same capping layers were placed on a 5 inch etched monocrystalline wafer to avoid contamination of the samples during the annealing. This wafer was placed on a quartz tray that was carefully pushed into the furnace ensuring that the samples did not slide on the carrier wafer. The furnace consists of a quartz isolation tube and heating lamps both above and below the wafer as shown in Figure 12. To reduce the required number of samples, annealing of the wafers for determining thermal stability was performed consecutively at different temperatures. The ramp up rate is programmable between 10°C and 200°C per second [35]. In the annealing temperature programs used the ramp up rates were between 3.5 and 27.5 °C/s. The manual of the RTP states that the thermocouple shows the temperature with an accuracy ± 0.5 °C [35].

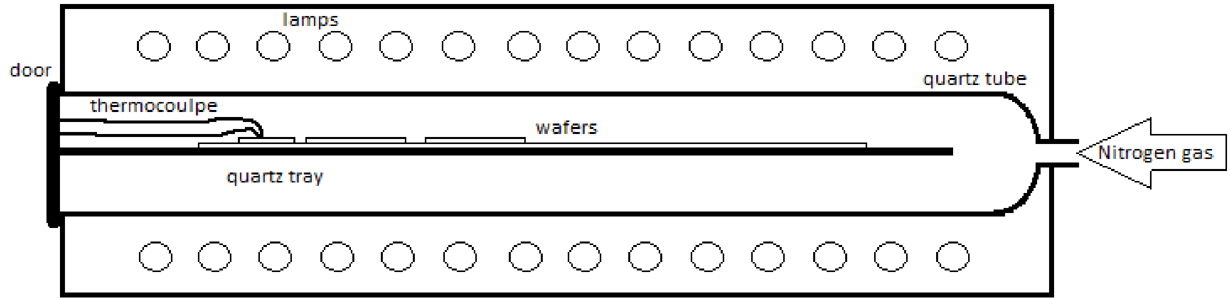

Figure 12 Schematic illustration of the rapid thermal processing (RTP) system AccuThermo AW610 [35]. To the left, attached to the door, is the thermocouple for measuring the temperature of the wafers.

3.2. The samples

The samples used in this study were 25 monocrystalline float zone (FZ) silicon wafers of *n*- and *p*-type, delivered by Topsil Semiconductor Materials A/S. The Float zone wafers were used because they have high and stable bulk lifetimes with respect to both time and temperature. The changes of the effective lifetimes can therefore be attributed to changes of the passivation quality. The orientation of both the *n*- and *p*-type wafers are <1 0 0>. The wafers were polished on both sides. Table 2 lists the relevant parameters of the wafers.

Table 2 List of sample parameters for the FZ, *n*-type wafers specified by Topsil Semiconductor Materials A/S.

Parameter	Unit	*n*-type	*p*-type
Doping type		N (Phosphorous)	P (Boron)
Wafer thickness	µm	283.9 ± 4.45	288.4 ± 0.85
Radius	mm	50	50
Resistivity	Ω cm	3.43 ± 0.11	3.21 ± 0.06
Bulk lifetime (minimum)	ms	6.225	2.551

3.2.1. Preparation of the samples

Prior to deposition, the wafers were dipped in two different 5 % HF solutions for 10 s each, rinsed in deionised (DI) water and blow dried with nitrogen gas. This was done in order remove the oxide on the surface of the wafer and to ensure a clean interface, which is required to obtain a low density of interface states. A stack of a-Si:H and a-SiN_x:H layers was then deposited equally on both surfaces in the PECVD unit. The samples were loaded onto carrier wafers which were then placed in a wafer cassette in the load lock of the PECVD setup. One *p*-type and one *n*-type wafer were deposited in a first batch to test that the PECVD was functioning properly. The rest of the *p*-type wafers were deposited in one batch and the rest of the *n*-type wafers were deposited in a different batch.

3.2.1.1. The Stacks

Passivating stacks of films of hydrogenated amorphous silicon (a-Si:H) and hydrogenated amorphous silicon nitride (a-SiN_x:H) were deposited by plasma enhanced chemical vapour deposition (PECVD) at

230 and 200 °C, respectively. Silane (SiH_4) was used at process gas for deposition of the a-Si:H films. For deposition of the a-SiN_x:H films silane (SiH_4) , ammonia (NH_3) and nitrogen (N_2) were used as process gases. The deposition parameters are given in Table 3.

Table 3 PECVD processing parameters.

Parameter	Unit*	a-Si:H layer	a-SiN_x:H capping layer
Temperature	°C	230	200
Power density	W/cm^2	9.4	46.8
Chamber pressure	mTorr	300	800
Flow rate, SiH_4	sccm	25	20
Flow rate, NH_3	sccm	-	20
Flow rate, N_2	sccm	-	980

*sccm = standard cubic centimetres per minute

The same two films were deposited on both sides of the wafers as shown in Figure 13.

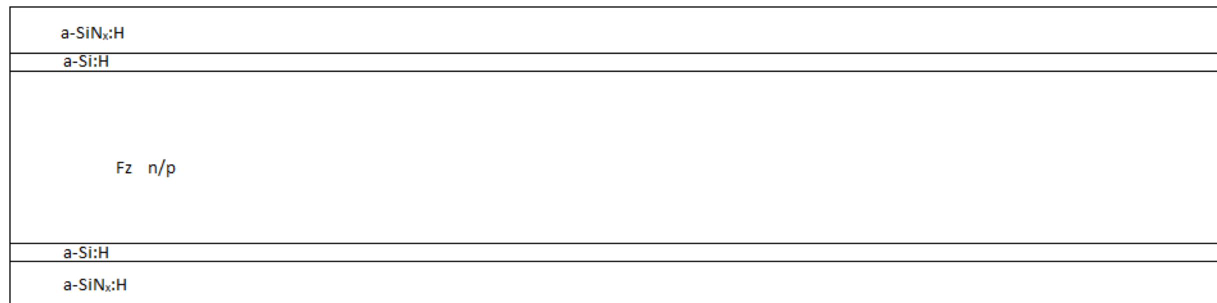

Figure 13 Schematic cross sectional view of the symmetric sample with passivating stack consisting of films of a-Si:H and a-SiN_x:H on both sides.

The PECVD chamber was preconditioned by depositing a film of a material with the same composition as the desired films before the deposition of the investigated single layers and stacks. The layer of a-Si:H was deposited on one side, then the wafers were turned carefully on the carriers and put back in the load lock and a-Si:H was deposited on the other side. A layer of a-SiN_x:H was then deposited on this side before the wafers were turned again and a-SiN_x:H was deposited on the other side.

The thickness of the film was varied by changing the deposition time. The deposition time was calculated from rates of deposition determined earlier with the same parameter settings and materials in the same chamber. The rates used for the calculations were 7.9 nm/min for a-Si:H and 19 nm/min for a-SiN_x:H. The deposition times for the layers of a-Si:H and a-SiN_x:H are listed in Table 4 and Table 5. As the film thicknesses were not measured, the thickness values given in this study are not accurate and may deviate slightly from the real values. The thinnest layers of a-Si:H have the most uncertain thicknesses, as it is not known whether the deposition rate is faster or slower in the beginning of the deposition.

Table 4 Deposition times for the a-Si:H films.

Film thickness a-Si:H	Deposition time
5 nm	38 s
10 nm	1 min 15 s
20 nm	2 min 30 s
40 nm	5 min

Table 5 Deposition times for the a-SiN_x:H films.

Film thickness a-SiN_x:H	Deposition time
100 nm	5 min 16 s
200 nm	10 min 32 s

For the 15 *p*-type wafers the thicknesses of the a-SiN_x:H layer were 0, 100 or 200 nm. The a-Si:H films were deposited with five different thicknesses from 0-40 nm. On the *n*-type wafers a a-SiN_x:H layer of 100 nm was deposited on each of the five a-Si:H thicknesses between 0 and 40 nm. One wafer with each thickness of a-Si:H was kept without a capping layer of a-SiN_x:H. The different combinations of the a-Si:H and a-SiN_x:H layers on the *p*-type and *n*-type wafers are given in Table 6 and Table 7, respectively.

Table 6 Film thicknesses of the a-Si:H and a-SiN_x:H on the *p*-type samples.

	Film thickness [nm]		Reflectance
Sample	a-Si:H	a-SiN_x:H	[%]
P1, test	40	0	36
P2	0	100	0
P3	0	200	32
P4	5	0	32.5
P5	5	100	0.5
P6	5	200	32.5
P7	10	0	33
P8	10	100	1
P9	10	200	33
P10	20	0	34
P11	20	100	2
P12	20	200	34
P13	40	0	36
P14	40	100	4
P15	40	200	36

Table 7 Film thicknesses of the a-Si:H and a-SiN_x:H on the *n*-type samples.

Sample	Film thickness [nm]		Reflectance
	a-Si:H	a-SiN_x:H	[%]
N1, test	40	0	36
N2	0	100	0
N3	5	0	32.5
N4	5	100	0.5
N5	10	0	33
N6	10	100	1
N7	20	0	34
N8	20	100	2
N9	40	0	36
N10	40	100	4

3.2.2. The pieces for different analysis

The wafers were cut into smaller pieces for different analysis and measurements as shown in Figure 14. The quarter wafer was kept as a reference sample and the half wafer was used for lifetime stability measurements with respect to time. The smaller pieces were used for thermal stability experiments. The 2·2 cm^2 pieces, denoted a, b and c, were used for annealing experiments. The 1·1 cm^2 pieces were used for tests of annealing methods and the normal firing experiments. The half waferused for the temporal stability measurements, was cut such that the QSSPC lifetime stability measurements could be continued to be carried out on the same spot as before the cutting. Depending on where the most uniform areas with the highest lifetimes were, the left side or right side was chosen for cutting into smaller pieces for thermal stability measurements. The most uniform area was cut into smaller pieces for thermal processing experiments.

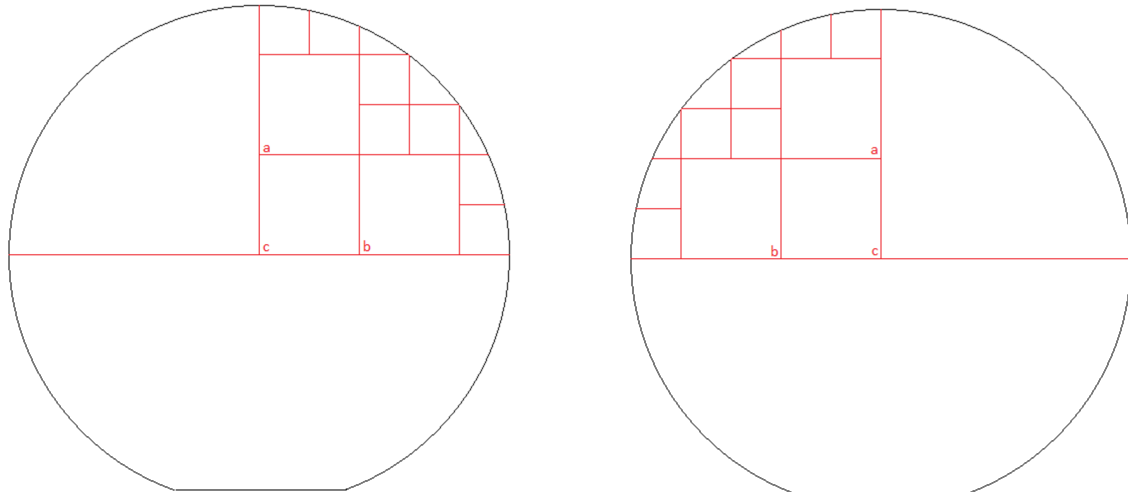

Figure 14 Illustration of the half wafer, the quarter wafer, the three 2·2 cm^2 pieces and the ten 1·1 cm^2 pieces that each sample was cut into for different experiments. The letters in the bottom right or left corner were inscribed using the laser. The primary flat is shown.

The wafers were cut using an RSM 20E class 4 laser from Rofin-Sinar. The intensity was set to a current of 38 A and frequency of 20 kHz. The line width was 0.020 mm and the speed was set to 200 mm/s. 40 repetitions of the laser were used, cutting the wafer almost all the way through and

the smaller pieces of the wafer could be broken apart very easily. One repetition of the laser was used to inscribe sample labels.

3.2.3. Thermal stability experiments

This section describes how the samples were processed thermally in the different experiments investigating their thermal stability. In the three experiments described below, all the samples with the same capping layers were processed and measured together. The reflectance of the samples affects both the thermal processing and the measurements, however the samples with the same capping layers have approximately the same reflection and can therefore be processed and measured together.

3.2.3.1. Rapid thermal annealing at different temperatures

The 2·2 cm^2 samples were annealed in a rapid thermal processing (RTP) system from for 1 minute at steady state at 100, 200, 250, 300, 350, 400, 450 and 500°C. The annealings were consecutive and lifetime measurements were carried out before the first annealing and then 6 minutes after every annealing. It was about 10 minutes between each annealing at different temperatures of the same samples. The annealing processes were carried out as described in Section 3.1.5.

3.2.3.2. Annealing in belt furnace at 450 °C

Annealing at 450 °C in a belt furnace has previously shown to improve the lifetimes of similar passivating layers. Therefore it was investigated how such an annealing affects the samples. The 2·2 cm^2 samples were annealed in were the belt furnace LA-310 at 450 °C for 1 minute. Lifetime measurements were carried out before annealing and every 3 minutes after annealing for the first half an hour, then every 5 minutes for the following half an hour and once or twice more the next hours. The lifetimes were also measured after a few days and weeks to investigate the degradation of the lifetime after annealing with respect to time. The annealing processes are described in Section 3.1.4.

3.2.3.3. Firing in belt furnace at 945 °C peak

To investigate how a conventional contact firing process would affect the passivation, 1·1 cm^2 samples of each stack and single layer were annealed in the belt furnace LA-309 at temperatures up to 945 °C for 8.8 seconds. The temperatures used are shown in Table 1. The effective lifetimes of the samples were measured before and 2 minutes after firing. The firing process is described in Section 3.1.4.

3.3. Measurements

This section describes how the measurements were carried out, the uncertainties of the measurements, assumptions made and the possible influence of the bulk lifetime on the measured effective lifetimes.

3.3.1. Temporal stability measurements

For investigation of the temporal stability of the passivation quality, the effective lifetimes were measured using the PL imaging setup described in Section 3.1.3. The effective lifetime for different excess carrier concentrations were obtained from the QSSPC measurements. The effective lifetime images were calibrated at the excess carrier concentration induced by one sun for all the samples. This excess carrier concentration is dependent on the effective lifetimes and therefore varies for the different samples.

The *p*-type samples were measured two times a day the first two days after deposition, then about every second day for the following week, and then weekly. On the *n*-type wafers 2 measurements were made on the day after deposition, 3 measurements the next day, and 1 measurement a day the following two days. The second week 3 measurements were made and then measurements were made weekly. There were some exceptions from this schedule during the 9 weeks the measurements were carried out. Two extra measurements of all the wafers were made on the same day, the day that the samples were cut into smaller pieces, two weeks after deposition. Several measurements were made on some of the wafers because these were used as reference samples for calibration of the PL images in the annealing experiments. The samples that seemed most stable were chosen for this purpose assuming that these samples would be least affected by the extra measurements. For the calibration to be as correct as possible the lifetimes of the reference wafers were also considered and the reference that had the lifetime most similar to the samples to be investigated was chosen. Between the measurements the samples were kept in a dark cupboard.

The effective lifetimes for the excess carrier concentration of 10^{15} cm^{-3} were recorded to compare the different samples. These were also used to calculate the SRVs using Equation (17). Infinite bulk lifetime was assumed to calculate the SRV. This means that the calculated SRV is an upper limit for the SRV of each wafer at an excess carrier concentration of 10^{15} cm^{-3}. The calculated SRVs were used to compare the passivation quality of the different stacks.

Since the effective lifetimes of the wafers were not uniform, the PL images were used to make sure that the QSSPC measurement was made on a relatively uniform area with high lifetimes. The images were also used to make sure that the measurements were made on the same area every time. Lastly they were used to identify any scratches occurring because of wafer handling. As these may greatly affect the passivation quality and is not the interest of the investigation, the area for QSSPC measurements was moved a little to avoid the scratches from wafer handling to exclude this effect

from the results. If it was not possible to move to avoid measuring on an area with scratches this was recorded for the analysis.

To verify one of the very high effective lifetimes measured with the PL imaging setup using the QSSPC method, the photoconductance lifetime tester described in Section 3.1.2 was used in transient mode.

3.3.2. Thermal stability measurements

The thermal stability measurements were also carried out using the PL imaging setup described in Section 3.1.3. The 2·2 cm^2 and 1·1 cm^2 samples were too small for QSSPC measurements because the sample barely covered the inductive coil, and therefore the edge effect would be considerable in the measurement. Therefore a half wafer with the same capping thickness as the samples to be measured was used for calibration of the effective lifetime images obtained from the photoluminescence measurements. The effective lifetime of the samples were then deduced from the calibrated effective lifetime images. These lifetimes are given for different excess carrier concentrations, because they are calibrated for the excess carrier concentration created by one sun illumination of the calibration wafer. The setup of the calibration wafer and the samples to be investigated, used for all the annealing and firing experiments, is shown in Figure 15.

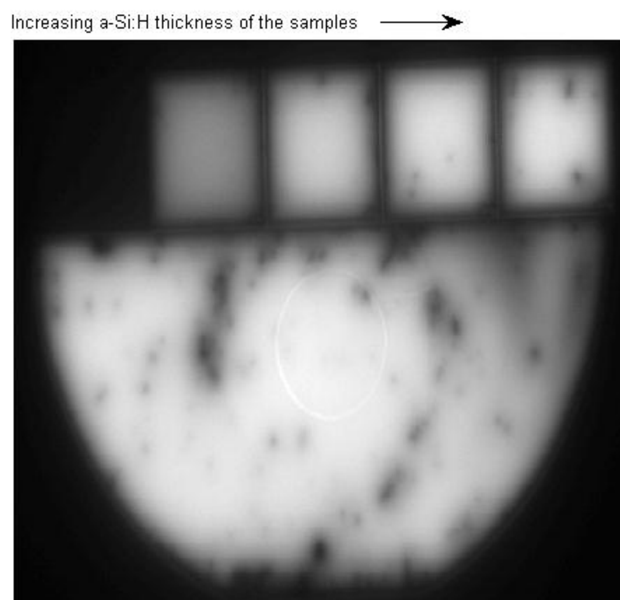

Figure 15 The measurement setup with the calibration wafer (below) and the annealed samples to be investigated (above). The samples with the thinnest a-Si:H layer are placed to the left and then the other samples are placed further to the right with increasing a-Si:H thickness.

The deduced absolute values of the effective lifetimes of these samples are therefore not perfectly comparable, but the relative behaviour of the samples after annealing can be compared.

3.3.3. Uncertainties in the effective lifetime measurements

This section describes some of the assumptions and calculations that the effective lifetime measurements are based on, and the uncertainties for the measurement itself. Problems with carrying out successive measurements to get statistics for the measured effective lifetimes are also addressed. The main uncertainties in the approach used to investigate the temporal and thermal stability are the reduced lifetimes because of damages caused by wafer handling and variation of the measured lifetimes because the position of the wafer may vary slightly from measurement to measurement.

In the software of the PL imaging setup used for both the QSSPC measurements and the measured PL images, the thickness, the resistivity and the reflection of the samples are parameters that need to be set. The resistivity and thickness were specified with low uncertainties by the supplier of the wafers. The reflections from the stacks or single layers for a wavelength of 808 nm were calculated. The a-SiN_x:H film was assumed to have a refractive index of 1.89 for a wavelength of 630 nm. This is the refractive index that has been measured on the a-SiN_x:H films deposited in the same PECVD chamber earlier with the same process parameters. Based on this previous measurement, the reflection for the 100 and 200 nm thick layers of a-SiN_x:H was simulated for the wavelength of the laser, 808 nm. These were found to be 0 and 32 % for the 100 and 200 nm a-SiN_x:H layers, respectively. The a-Si:H film was assumed to have a refractive index of 3.6 for a wavelength of 808 nm, about the same as crystalline silicon and the reflection of all the a-Si:H single layers were calculated to be 32 %. Both the reflection from the passivating stack or single layer and the absorption of the a-Si:H layer were incorporated in the reflection setting. The a-Si:H was assumed to absorb about 1 % of the incoming light per 10 nm thickness. This assumption was based on previous measurements with ellipsometry on a-Si:H layers deposited with the same parameters in the same PECVD chamber. Therefore 1 % was added to the reflection setting per 10 nm of a-Si:H film. The reflection settings used for each of the *n*- and *p*-type samples are given in the column to the right in Table 6 and Table 7, respectively.

Errors in the reflection setting will result in systematic errors. If the reflectivity setting for one stack or single layer is too high the measured effective lifetime will be too high. This effect will, however, be small. For example, if the reflectivity is set to 32 % when it is actually 30 %, the measured effective lifetime will be 3 % too high. The potential systematic error from inaccurate reflectivity settings will not affect the investigations of the trends of the stability with respect to time or temperature. On the other hand, the systematic errors will have to be taken into consideration when comparing the absolute values of the effective lifetimes of the different stacks with different reflectivity settings.

The uncertainty of the QSSPC measurements is very low. Five successive measurements were made on a representative *n*-type sample with 40 nm a-Si:H to investigate the uncertainty of the QSSPC measurement. The standard deviation of the mean of these five measurements was found to be 0.3 %. Five successive measurements were also made on the same sample, removing the sample and

placing it back in approximately the same position between each measurement. The standard deviation of the mean of these five measurements was found to be 0.4 %.

A problem with this method of making several measurements on a sample to determine the uncertainty of the measurement is that the illumination needed for the measurement might affect the passivation quality of the stack, hence also the measured value. Illumination has been shown to degrade the passivation from a-Si:H single layers [27], and in this thesis it has been observed a persistent improvement of the effective lifetime during frequent measurements. To influence the passivation quality as little as possible repeated measurements were not carried out for each measured point shown in the effective lifetime graphs in Section 4 and therefore no error bars are shown. Only one wafer with each stack has been investigated as the experiments would be too extensive and expensive if several wafers with each stack had been used, though this would have given better statistics.

3.3.1. Influence of the bulk lifetime on the measured effective lifetime

If the bulk lifetimes of the samples are very high and the wafers are otherwise similar the differences in passivation quality provided by the different stacks can be investigated by comparing the measured effective lifetimes. Thus the measurements can be used to find optimal film thicknesses with respect to passivation quality shortly after deposition and a period after deposition when the effective lifetimes have stabilised. In this study the effective lifetimes measured one day after deposition are very high. This indicates that the passivation quality as deposited is very good. The lifetimes measured after depositions are much higher than the specified minimum bulk lifetimes of the wafers. The bulk lifetime may therefore be the limiting factor for some of the samples, hence affecting the effective lifetime. Comparing the deposition quality of the different stacks is in that case not straight forward. To exclude the effect of possibly varying bulk lifetimes of the samples, the bulk lifetimes could be measured before the passivation. With a known bulk lifetime, the surface lifetime could be calculated from the effective lifetimes and these could be compared to investigate the passivation quality. Different stack could also be investigated on different pieces from the same wafers to exclude the effect of different limiting bulk lifetimes. The bulk lifetime of float zone wafers have very high temporal and thermal stability and therefore changes in the effective lifetimes can be attributed to changes in the passivation quality. Therefore, for the investigation of the thermal and temporal stability of the passivation, the effect of the possibly limiting bulk lifetime will not be a problem.

4. Results and discussion

In this chapter the results from the experiments are presented and discussed using relevant theory and findings from other studies. First there is a section on lifetimes and passivation quality shortly after deposition showing examples of PL images and QSSPC curves measured. Then the measurements of the effective lifetimes for the 9 weeks after the deposition are presented and analysed with respect to temporal stability of the different single layers and stacks. The calculated corresponding upper limits of the SRVs are also shown. The effective lifetimes after nine weeks are shown and discussed with respect to passivation quality in the next section. The results from the experiments carried out to investigate the thermal stability are given in the following sections. First the results from the rapid thermal processing at different temperatures are presented and analysed with respect to thermal stability. Then the lifetimes before and after an annealing at 450 °C and the investigation of temporal stability after the annealing are shown. The results from the firing experiments are briefly stated before the thermal stability with respect to metallisation processes commonly used in solar cell production is discussed. Lastly, results demonstrating improved measured effective lifetimes during frequent QSSPC and PL measurements are presented and discussed.

4.1. Lifetimes shortly after deposition

An example of a QSSPC curve is shown in Figure 16. The figure shows the QSSPC measurement for the *n*-type sample with 10 nm a-Si:H and 100 nm a-SiN_x:H three days after deposition.

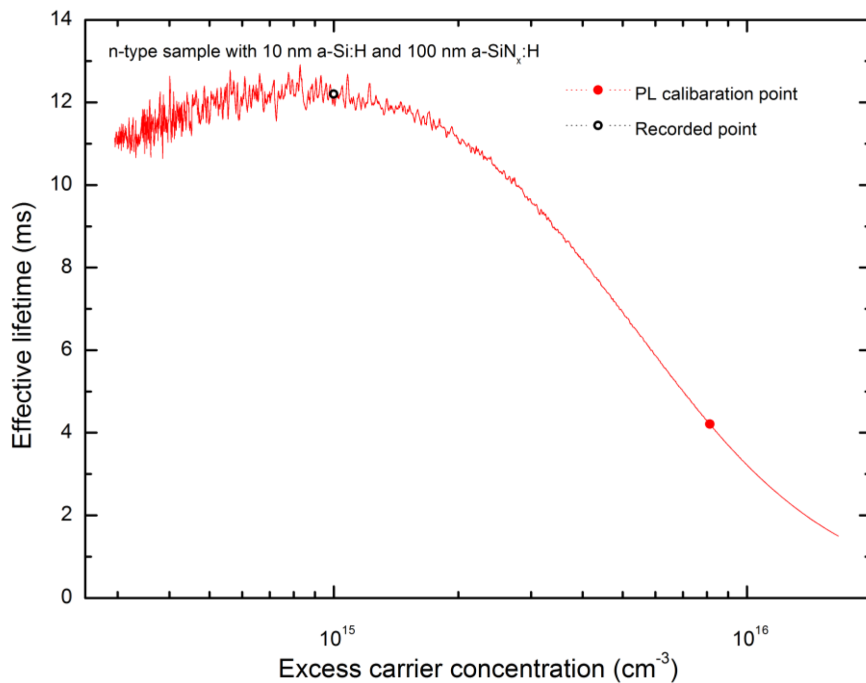

Figure 16 The measured effective lifetime for different excess carrier concentrations of one *n*-type sample. The passivation stack on the sample consists of 10 nm of a-Si:H and 100 nm of a-SiN_x:H. The measurements were carried out using the QSSPC method. The black circle shows the point recorded for comparison of the lifetimes and the red dot shows the point used for calibration of the PL image.

This is the sample with the highest measured effective lifetime of 12.2 ms for an excess carrier concentration of 10^{15} cm^{-3} three days after deposition. This point is shown in the graph by a black circle. The effective lifetime is very high and the upper limit for the corresponding SRV is 1.2 cm/s. This very low SRV indicates an excellent passivation quality.

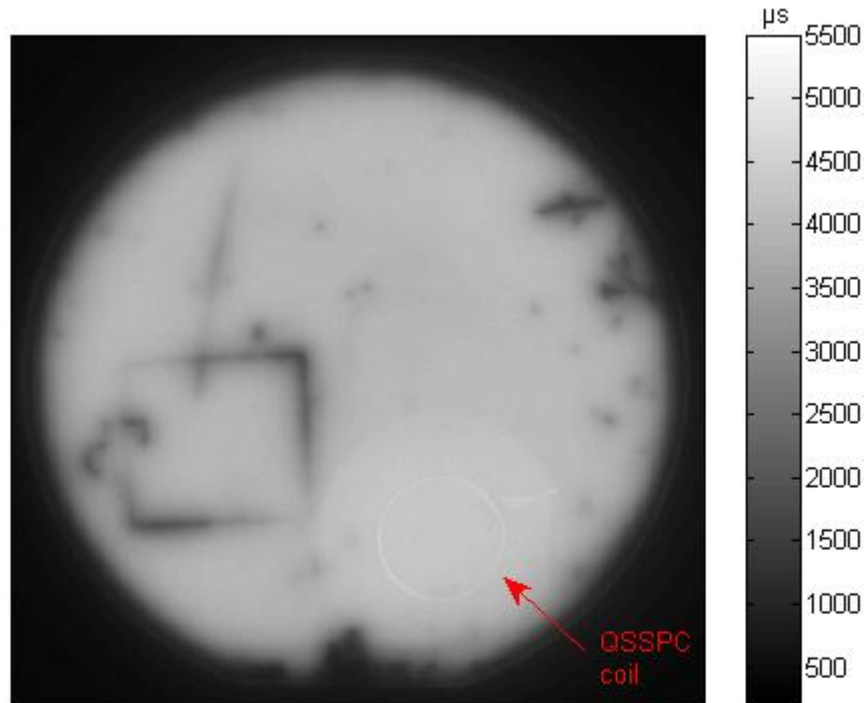

Figure 17 PL image of the *n*-type sample with 10 nm a-Si:H and 100 nm a-SiN_x:H taken three days after deposition. The scale to the right shows the effective lifetime at the excess carrier concentration of the calibration point $8 \cdot 10^{15}$ cm^{-3}. Because of the enhanced reflection caused by the QSSPC coil, its position underneath the wafer can be seen in the right bottom quadrant of the image. The coil is intentionally placed under a uniform area with high lifetimes. A square with lower lifetime can be seen to the left. This may be caused by contamination from the carrier wafers used during PECVD.

The corresponding PL image is presented in Figure 17. This PL image shows effective lifetimes a lot lower than 12.2 ms for the entire wafer. The red point in the graph in Figure 16 is the point used for calibration of the PL image. The effective lifetime for the calibration point is 4.1 ms and is given for an excess carrier concentration of $8 \cdot 10^{15}$ cm^{-3}. From the graph of the effective lifetimes versus excess carrier concentration it is clear why the calibrated effective lifetime of the PL image is a lot lower than the recorded value for the same sample. The excess carrier concentration for the recorded point, 10^{15} cm^{-3}, is approximately the value that gives the highest lifetime. For higher excess carrier concentrations the lifetime decreases rapidly. This is due to the auger recombination increasing in importance towards higher excess carrier densities [1]. Thus, for the higher excess carrier concentration used for calibration, the effective lifetime is a lot lower.

The PL image also shows how the wafer was placed during measurements to measure the area of the wafer with the most uniform and highest lifetimes. To achieve this, the wafer was placed such that this area was placed above the QSSPC coil. This particular sample shows a square pattern with lower effective lifetime than the surrounding area. Some similar patterns that do not look like typical bulk defect or scratches in the passivation layers are seen on PL images of some of the other wafers as

well. Some patterns looks like squares and some look like circle sectors, but the square showing up in the PL image shown in Figure 17 is the most distinct. The effective lifetime is probably lower due to poorer passivation in the area of the pattern. Contamination from the carrier wafer used during deposition might have caused the poorer passivation quality. The carrier wafers had been used before, for deposition of different layers on other samples. The square pattern might be the circumference of a square sample previously placed on the carrier wafer during a deposition with aluminium. If traces of aluminium are present at the interface, there will be more interface states introduced in the band gap. This will result in higher surface recombination rates. The patterns have not been observed before on wafers deposited on these carrier wafers and in this deposition chamber. The pattern might be showing up on this wafer because the passivation is very good around it. The effective lifetime of the pattern is about 2 ms or above and will therefore not be detected on samples where the highest lifetime is 2 ms for an excess carrier concentration of $8 \cdot 10^{15}$ cm^{-3}.

There is a lot more noise in the measured QSSPC curves for the samples with the highest lifetimes of 8-13 ms than for those with lower lifetimes. Therefore there is a greater uncertainty for the highest lifetimes. One reason may be that the samples were not as close to steady state during the measurement as the samples with lower lifetimes. The measurement of the samples with effective lifetime of about 12 and 8 ms were therefore verified by measurements in the photoconductance tester, described in Section 3.1.2, using transient photoconductance decay method, described in Section 3.1.2.2. The measurements in transient mode resulted in approximately the same value of about 12 and 8 ms for the two wafers.

4.1.1. The samples passivated with silicon nitride

The effective lifetimes of the samples passivated with a single layer of silicon nitride, are too low for the PL imaging setup to give a lifetime for an excess charge carrier concentration of 10^{15} cm^{-3}. This applies to both the *n*- and *p*-type samples as deposited and after annealing and firing. Therefore no data will be shown for these samples in the following sections and “all samples” refers to the samples with all the different single layers or stacks described in Table 6 and Table 7, except for the single layers of silicon nitride. A probable reason for the low passivation quality provided by the silicon nitride stack is the low deposition temperature of 200 °C. The depositon temperature affects the composition of the a-SiN_x:H, the bonds between the hydrogen, silicon and nitrogen and the amount of fixed charge in the layer. The deposition temperature of 200 °C was chosen in order to not affect the a-Si:H layer underneath. To be able to deposit the stacks and the single layers in the same batch the temperature of the silicon nitride in the stacks and in the single layers had to be the same and therefore a low temperature was used for the deposition of the single layer as well.

4.1.2. The effective lifetimes of the *p*-type samples shortly after deposition

The measured effective lifetimes of the *p*-type samples one day after deposition are shown in Figure 18. The deposition of a single layer of a-Si:H results in measured effective lifetimes between 1.4 and 5.3 ms one day after deposition for all the different thicknesses. The double passivation layers consisting of an a-Si:H/a-SiN_x:H stack, results in measured values between 1.7 and 3.6 ms and 2.4 and 4.1 ms, for the stack with 100 and 200 nm capping, respectively. This corresponds to an upper limit of the SRV of between 3 and 10 cm/s for all the samples. One day after deposition the samples with 20 nm a-Si:H give the highest measured effective lifetimes. 5 nm a-Si:H without capping results in the lowest measured effective lifetime. All the measured values and SRVs mentioned above are given for an excess carrier concentration of 10^{15} cm^{-3}. For 3 out of 4 thicknesses of the a-Si:H, the samples capped with 200 nm a-SiN_x:H results in the highest effective lifetimes.

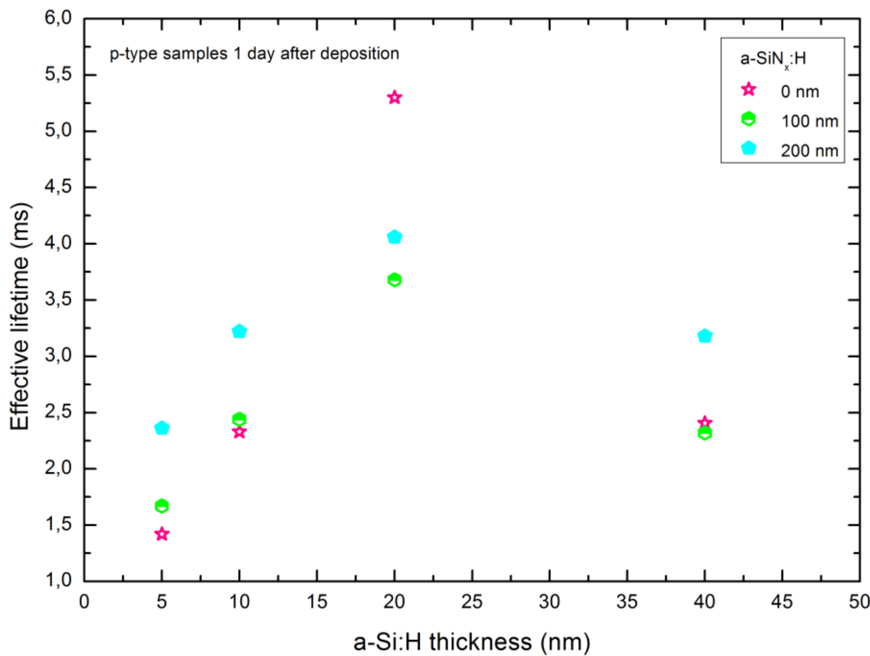

Figure 18 The effective lifetimes of the *p*-type samples one day after deposition for an excess carrier concentration of 10^{15} cm^{-3}.

One day after deposition the a-Si:H thickness of 20 nm seems to be the optimal thickness for passivation both capped and uncapped. With the exception of the sample with a single layer of a-Si:H, which results in the highest lifetime, a capping thickness of 200 nm a-SiN_x:H seems to be optimal with respect to the effective lifetime.

4.1.3. The effective lifetimes of the *n*-type samples shortly after deposition

The measured effective lifetimes of the *n*-type samples one day after deposition are plotted in Figure 19, showing values between 3.3 and 12.5 ms. The capped and uncapped samples had effective lifetimes between 4.5 and 13 ms, and between 3 and 8 ms, respectively. The thickness of the a-Si:H or a-SiN_x:H layer does not seem to influence the effective lifetime measured one day after deposition.

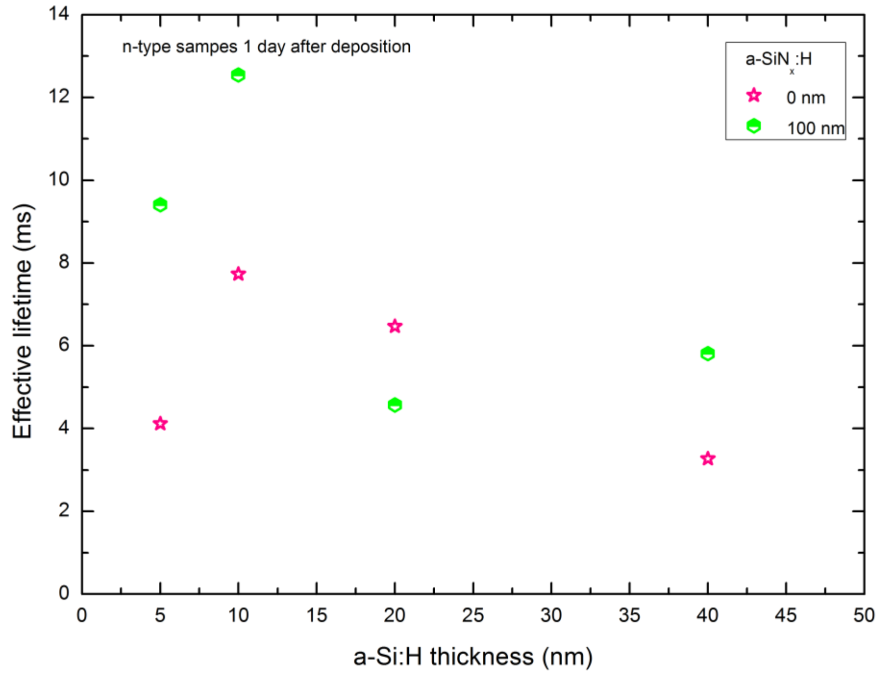

Figure 19 The measured effective lifetimes for an excess carrier consecration of 10^{15} cm^{-3} one day after deposition plotted versus the a-Si:H thickness. The graph shows all the *n*-type samples investigated.

4.1.4. Summary of the results from the measurements shortly after deposition

All the stacks and single layers investigated had high effective lifetimes, thus they provided good surface passivation resulting in low SRVs one day after deposition. Most of the stacks investigated, both on *n*- and *p*-type samples, resulted in higher effective lifetimes than the single layers. The highest effective lifetime measured one day after deposition was 12.5 ms for an excess carrier concentration of 10^{15} cm/s. This results in an upper limit for the SRV of this sample of 1.0 cm/s. This was measured on an *n*-type wafer with a stack consisting of 10 nm a-Si:H and 100 nm a-SiN_x:H. The highest effective lifetime measured for a *p*-type wafer was 5.3 ms for an excess carrier concentration of 10^{15} cm^{-3} one day after deposition of a single layer of 20 nm a-Si:H. The upper limit of the SRV of this sample was calculated to be 2.7 cm/s.

4.1.5. Discussion of passivation quality shortly after deposition

De Wolf and Kondo states that a few nanometre thin a-Si:H layer usually have more dangling bonds than thicker layers [29]. This might explain why the *p*-type sample with 5 nm of a-Si:H has a much lower effective lifetime than the samples with thicker a-Si:H layers.

For most of the a-Si:H thicknesses the capped samples have higher effective lifetimes than the uncapped samples, and the samples with 200 nm have higher effective lifetimes than the samples with 100 nm silicon nitride. The higher lifetimes may be caused by field effect passivation provided by fixed charges near the interface in the silicon nitride layer. If there are positive fixed charges in the a-SiN_x:H layer on the *n*-type samples the accumulation condition will arise providing filed effect

passivation. For field effect passivation of the *p*-type samples there will have to be enough charges present for the inversion condition to arise. In both of these cases the recombination is reduced because the number of the limiting charge carriers is further reduced by the surface field.

It is not nescessarily only the passivation provided by the a-SiN_x:H capping layer itself that improves the measured effective lifetime. The capping layer is deposited at 200 °C and 5 or 10 minutes extra at 200 °C may serve as an annealing for those samples that go through the deposition process of a capping layer. De Wolf and Kondo investigated low temperature annealing of thin a-Si:H layers on crystalline silicon [29]. Stepwise annealings for temperatures between 120 and 260 °C were carried out on crystalline silicon wafers with a few nanometre thick a-Si:H layers [29]. Annealings at all the temperatures investigated, especially temperatures from 160-200 °C were found to increase the effective lifetime of the samples [29]. The increased lifetime may be due to hydrogen diffusing to the interface during the extra period of time at 200 °C, causing a reduction in the number of recomination active surface states. Thus the a-Si:H layer would provide better passivation after the deposition of the capping layer because of the extended time at 200 °C. To exclude this potential effect from the results, all the samples could have been subjected to the same temperatures for the same lengths of time, even though they were not deposited during that time. If there is an annealing effect from 5-10 minutes at 200 °C straight after the deposition of the a-Si:H layer, then all the samples would experience this same annealing effect. The disadvantage of carrying out the depositions in this way is that it would extend the total time needed for the deposition of the stacks on a batch considerably.

Another possibility is that the silicon nitride capping improves the passivation quality by chemical passivation. Since the measurements are made one day after deposition the samples may already have degraded. As it will be shown in the chapter on temporal stability, the degradation of the a-Si:H layers was more rapid a shortly after deposition. The deposited a-SiN_x:H capping layer might have stopped a rapid degradation of the chemical passivation provided by the hydrogen in the a-Si:H layer for the first 14 hours after the deposition.

For the *p*-type samples 20 nm seems to be the optimal a-Si:H thickness for passivation one day after deposition. The two stacks and the single layer with 20 nm a-Si:H, all seem to provide the best passivation of the silicon wafers. The *n*-type samples do not show this same trend. For the *n*-type samples 10 nm seems to be the best thickness of the a-Si:H layer with respect to effective lifetime one day after deposition. In comparison Focsa et al. determined the optimal a-Si:H layer thickness for a deposition temperature of 50 °C to be 10-15 nm for an a-Si:H/a-SiN_x:H stack [36]. To determine the optimal stack or single layers shortly after deposition more samples with the same stacks should be investigated to make sure the differences in measured effective lifetimes one day after deposition is not only due to statistical dispersion. To minimise the potential effect from the bulk lifetime, different stacks could be deposited on quarter wafer samples from the same wafer.

4.1.6. Replacement of the *p*-type sample with 40 nm a-Si:H

The measured effective lifetime of the sample with 40 nm a-Si:H and no capping that was originally part of the *p*-type series was 0.1 ms one day after deposition. The lifetime of this sample one day after deposition was 4 % of the lifetime of the test sample deposited with the same passivation layer 2 days days earlier. Something probably went wrong in the process of preparing the *p*-type sample with 40 nm a-Si:H, originally part of the set of samples investigated, resulting in the unexpected low lifetime. The wafer might not have been properly cleaned before deposition, the carrier wafer might have been contaminated or something might have gone wrong in the depostition process in the plasma chamber. Because the lifetime of this wafer is considerably lower than the test sample, lifetimes reported in the litterature for similar passivation treatment and all the samples in the series of *p*-type samples studied in this thesis, this sample was replaced by the test sample mentioded above. This was done to be able to investigate a complete series of the different stacks and single layers as described in Table 6 . The sample was replaced in the series 8 days after deposition. At that time 5 measurements had been carried out on the other samples whearas only one had been made on the replacing sample.

4.2. Temporal stability

The temporal stability of the passivation is very important, the operation time of the solar cell taken into consideration. A high passivation quality shortly after deposition is promising, but will not be very useful if it degrades rapidly. Therefore the temporal stability of the single layers of amorphous silicon and the stacks of amorphous silicon and silicon nitride was investigated by lifetime measurements for the first nine weeks after deposition.

To simplify the data analysis the effective lifetimes and the calculated upper limits for the corresponding SRVs were recorded for an excess carrier concentration of 10^{15} cm^{-3}. In Figure 20, a graph showing the effective lifetimes for different excess carrier concentration one, five and 61 days after deposition is given for the *p*-type sample with 5 nm of a-Si:H and no capping layer . The graph is shown as an example to illustrate how the effective lifetime curves change with time and at the same time show the change of the recorded points which are used to compare the development of effective lifetimes of the samples.

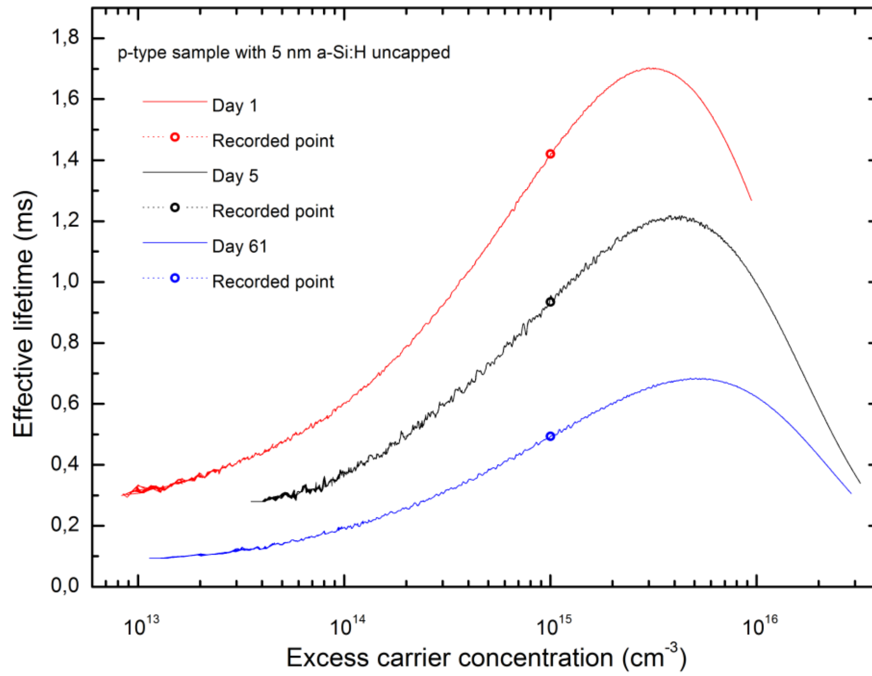

Figure 20 QSSPC measurement of the *p*-type sample with 5 nm a-Si:H one, 5 and 61 days after deposition. The recorded points for an excess carrier concentration of 10^{15} cm^{-3} are shown by circles.

4.2.1. The temporal stability of the *p*-type samples

In Figure 21 all the measured effective lifetimes of all the *p*-type samples are given. The measurements were carried out for the nine first weeks after deposition, frequently in the beginning and less frequently when the samples seemed more stable. The effective lifetimes are given for an excess carrier concentration of 10^{15} cm^{-3}. The same measured values are also shown in three different graphs; Figure 23 , Figure 25 and Figure 26, one for each capping layer thickness, to get a better overview.

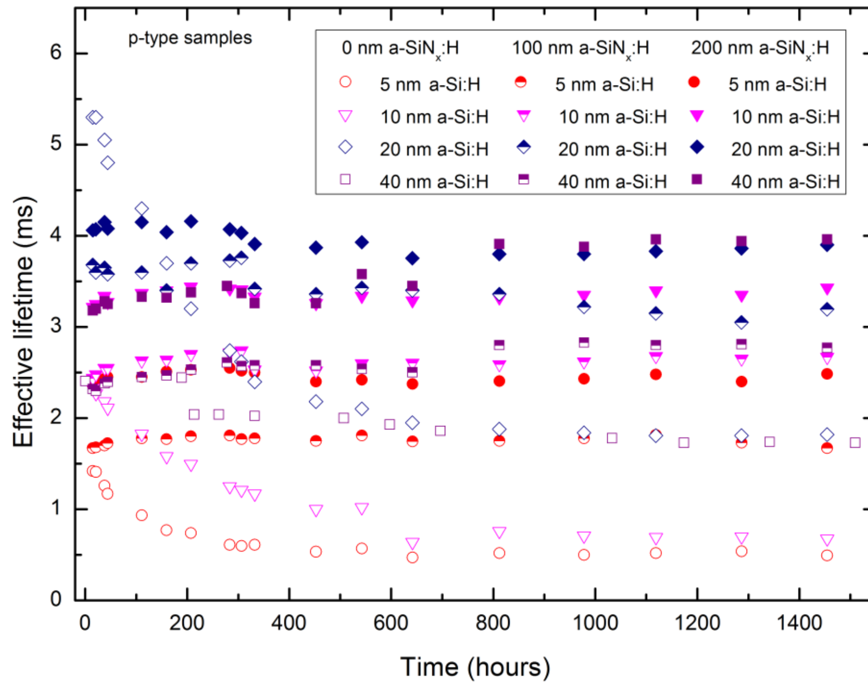

Figure 21 Effective lifetime of the *p*-type samples passivated with different stacks for an excess carrier concentration of 10^{15} cm^{-3} the first 9 weeks after deposition.

From Figure 21 it can be seen that all the capped samples are quite stable with respect to time. The uncapped samples degrade quite rapidly for the first 200 hours (8 days). The samples capped with 200 nm a-SiN$_x$:H seem to stabilise at the highest lifetimes, while the uncapped samples stabilise at lower values. For all capping thicknesses, increased a-Si:H thickness seem to result in higher stabilised effective lifetime. In Figure 22 the results from Figure 21 nomalised with respect to the measurements one day after deposition, are shown.

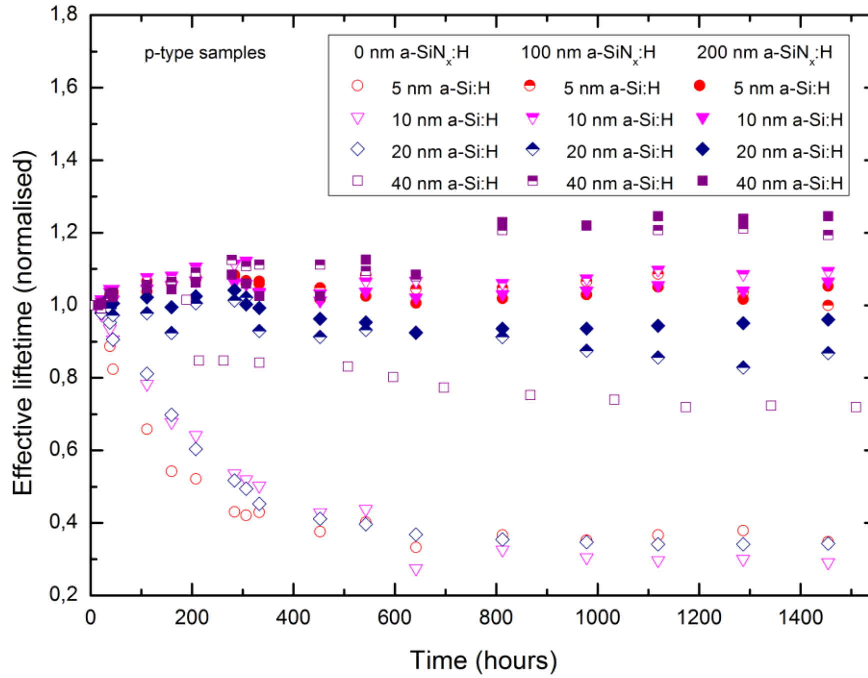

Figure 22 The normalised lifetimes of all the *p*-type samples for the first 9 weeks after deposition. The lifetimes are given for an excess carrier concentration of 10^{15} cm^{-3}.

From Figure 22 it can be seen that the capped samples either degrade very little, are stable or even improve during the nine week period after deposition. The relative degradation of the effective lifetime of the uncapped samples are quite similar except for the 40 nm sample which seems to stabilise closer to the capped samples.

4.2.1.1. Temporal stability of the uncapped p-type samples

The measured effective lifetimes of the uncapped *p*-type samples for the first 9 weeks are shown in Figure 23. The sample with a single layer consisting of 20 nm a-Si:H is degrading until 800 hours after deposition. This is the sample that has the highest lifetime one day after deposition. It seems to stabilise at the same lifetime as the sample with a 40 nm a-Si:H layer. The effective lifetime of the 5 nm a-Si:H sample degrades rapidly for the first 300 hours, then it degrades more slowly and finally seems to stabilise at 0.5 ms.

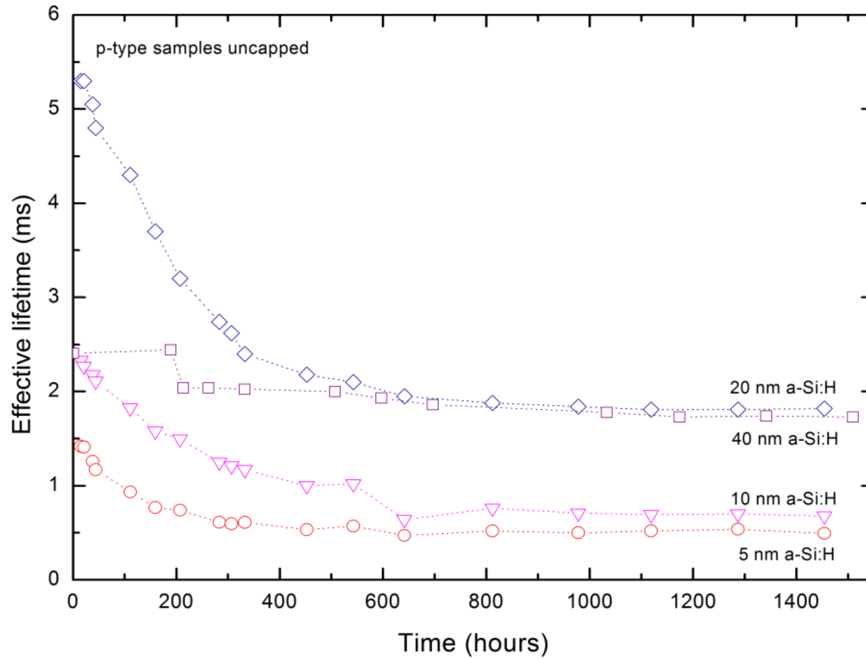

Figure 23 The measured effective lifetimes of the uncapped *p*-type samples for the 9 weeks after deposition and an excess carrier concentration of 10^{15} cm^{-3}. The dotted lines are guides to the eye.

The effective lifetime of the 10 nm a-Si:H sample seems to stabilise about 500 hours after deposition. Before the measurement 642 hours after deposition was made, this sample accidentally fell on the floor and was scratched. Afterwards the lifetime was greatly decreased. If this sample had not been scratched, it seems likely that it would have stabilised a bit higher than it did.

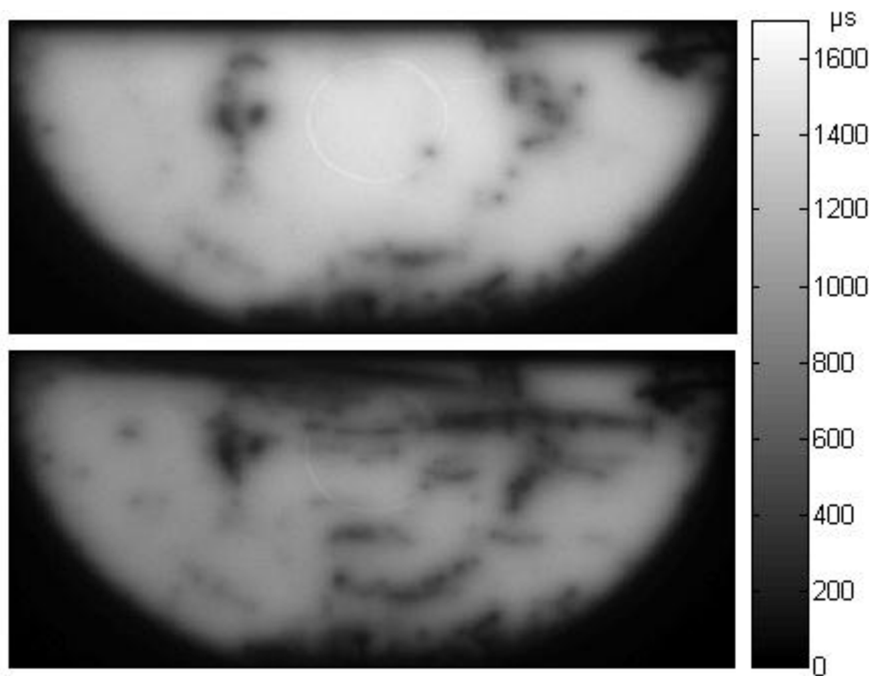

Figure 24 PL images of the wafer with 10 nm a-Si:H before and after it fell on the floor and was scratched. The scale to the right gives the effective lifetimes in μs for an excess carrier concentration of about $1.5 \cdot 10^{15}$ cm^{-3}.

Figure 24 shows the PL image of the wafer with 10 nm a-Si:H before and after it fell on the floor. The scratches may be very thin and shallow, but affects the surface recombination a lot because the passivating layer is thin, the bulk lifetime is high and therefore the diffusion length is long. The long diffusion lengths is also the reason why the image is blurred.

4.2.1.2. Temporal stability of the p-type samples with 100 nm capping

None of the *p*-type samples with 100 nm a-SiN_x:H degrade significantly. The samples with 5, 10 and 40 nm improve slightly for the first 50 (5 nm) and 300 (10 and 40 nm) hours. The measured effective lifetime of the 20 nm sample varies more than the other samples, and shows a tendency to decrease a little. The sample with 40 nm a-Si:H improves from 2.5-2.8 ms while it is used as a reference sample and frequent QSSPC and PL image measurements are carried out for an hour. In total 28 extra measurements were made on this sample between the measurement after 642 hours (27 days) and 812 hours (34 days). 13 of the measurements were carried out within one hour. The following weeks the measured effective lifetime is stable at 2.8 ms and the improvement seems to be persistent. This improvement during frequent measurements is looked into more closely in Section 4.4.

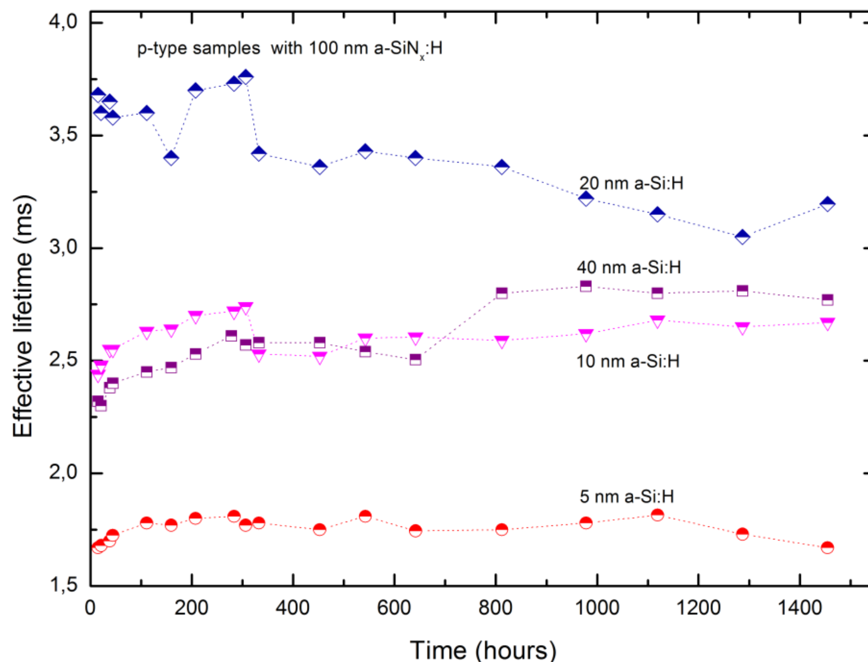

Figure 25 The measured effective lifetimes of the *p*-type samples capped with 100 nm a-SiN_x:H. The measurements carried out for the 9 weeks after deposition are shown. The effective lifetimes are given for an excess carrier concentration of 10^{15} cm^{-3}. The dotted lines are guides to the eye.

4.2.1.3. Temporal stability of the p-type samples with 200 nm capping

The measured effective lifetimes of the *p*-type samples capped with 200 nm a-SiN_x:H for the nine weeks after deposition are shown in Figure 26. The samples capped with 200 nm a-SiN_x:H show a similar behaviour to the samples capped with 100 nm. The 20 nm a-Si:H sample degrades slightly and the three other samples improves slightly within the first 300 hours. The sample with 40 nm a-Si:H

and 200 nm capping was used as a reference sample between the measurements plotted for 642 and 812 hours. The measured effective lifetime of the sample increased from 3.5 to 3.9 ms while almost 30 measurements were carried out. The improvement during frequent measurements is looked into more closely in Section 4.4.

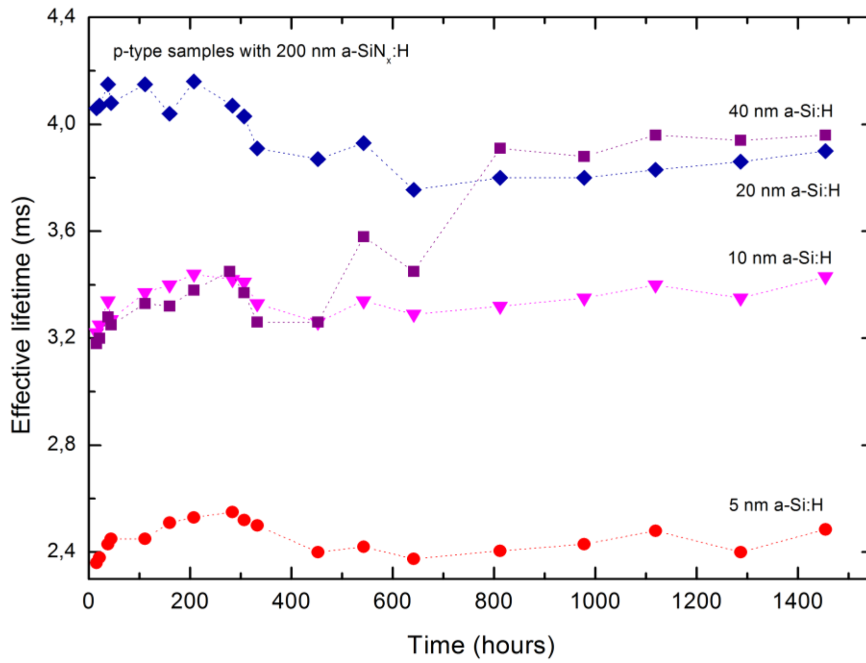

Figure 26 The measured effective lifetimes of the *p*-type samples capped with 200 nm a-SiN_x:H. Measurements carried out 9 weeks after deposition are shown. The effective lifetimes are given for an excess carrier concentration of 10^{15} cm^{-3}. The dotted lines are guides to the eye.

4.2.1.4. Effective lifetimes of the p-type samples nine weeks after deposition

The measured effective lifetimes of the *p*-type samples nine weeks after deposition versus the a-Si:H thickness are shown in Figure 27.

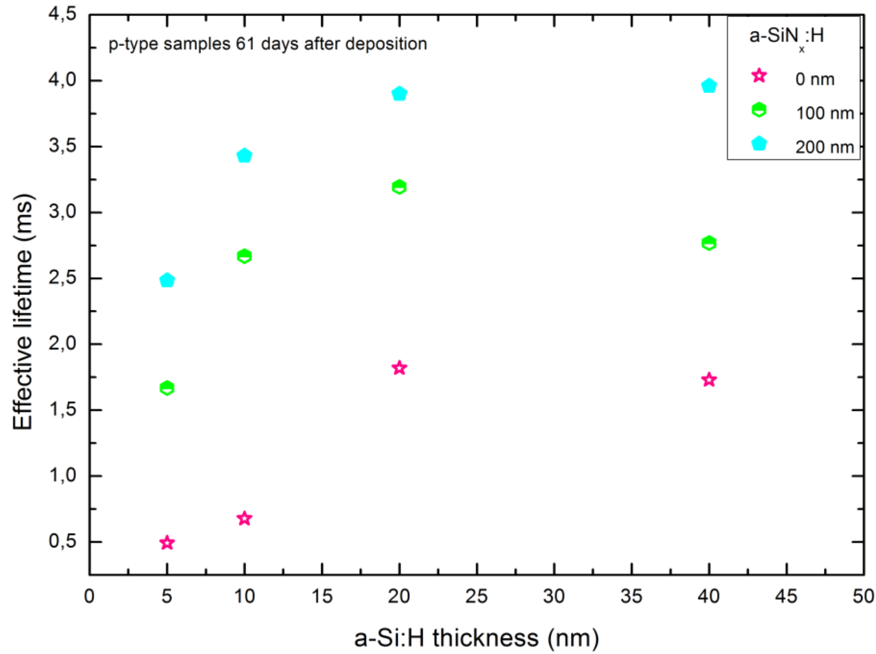

Figure 27 The effective lifetimes of the *p*-type samples 61 days after deposition. The effective lifetime is given for an excess carrier concentration of 10^{15} cm^{-3}.

61 days after the deposition the measured effective lifetimes are between 0.5 and 4.0 ms and all the samples seem to have stabilised with respect to time. These values correspond to maximum surface recombination velocities between 4 and 27 cm/s. Looking at each of the capping thicknesses separately it seems that the lifetime stabilises at higher values for thicker a-Si:H thicknesses up to 20 nm. The 20 and 40 nm a-Si:H samples stabilises at approximately the same values for each capping thickness. The thickest capping layer results in the highest measured effective lifetimes for each a-Si:H thickness after 61 days. The effective lifetimes of the 20 and 40 nm a-Si:H samples with 200 nm capping are almost 4 ms, i.e. the corresponding SRVs have an upper limit of 4 cm/s. The effective lifetimes of the 20 and 40 nm a-Si:H samples with 100 nm capping are 3.2 and 2.8 ms, respectively. The corresponding upper limit of the SRVs are 5 cm/s. The effective lifetimes of the 20 and 40 nm a-Si:H samples with no capping are about 1.75 ms, i.e. SRVs are 8 cm/s or below. These uncapped samples, with the thickest a-Si:H layers, have about the same effective lifetime as the capped sample with the lowest lifetime, the sample with 5 nm a-Si:H and 100 nm a-SiN$_x$:H. The measured values 61 days after deposition, normalised with respect to the measured values one day after deposition are plotted versus the a-SI:H thickness in Figure 28.

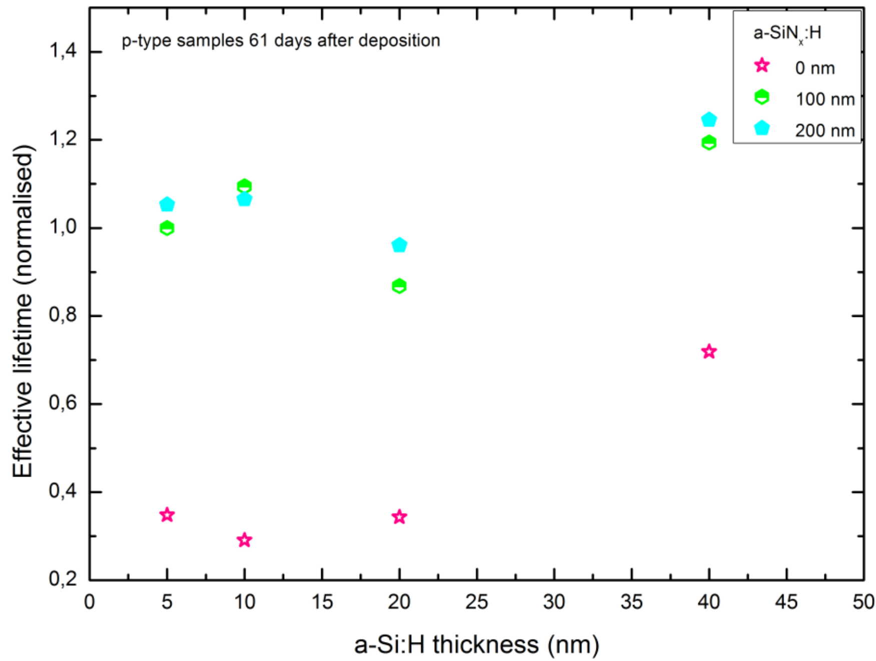

Figure 28 The normalised effective lifetimes of the *p*-type samples 61 days after deposition for an excess carrier concentration of 10^{15} cm^{-3}. The measurements 61 days after deposition are normalised with respect to the measurements one day after deposition.

The graph shows that the passivation of the uncapped 5, 10 and 20 nm a-Si:H layer degrades the most. These layers degrade to between 30 and 40 % of the effective lifetime one day efter deposition. The reason why the relative change of the uncapped 20 nm a-Si:H sample is about the same as the uncapped samples with thinner a-Si:H layersmight be that the initial lifetime is very high compared to the other samples and possibly therefore less stable than the other samples.

4.2.1.5. Surface recombination velocity of the p-type samples

The SRVs of the samples are calculated from the effective lifetimes assuming infinite bulk lifetime, thus giving an upper limit for the SRV for that particular effective lifetime. The SRVs are given for an excess carrier concentration of 10^{15} cm/s. The calculated upper limits of the SRVs for the first nine weeks after deposition are shown in Figure 29.

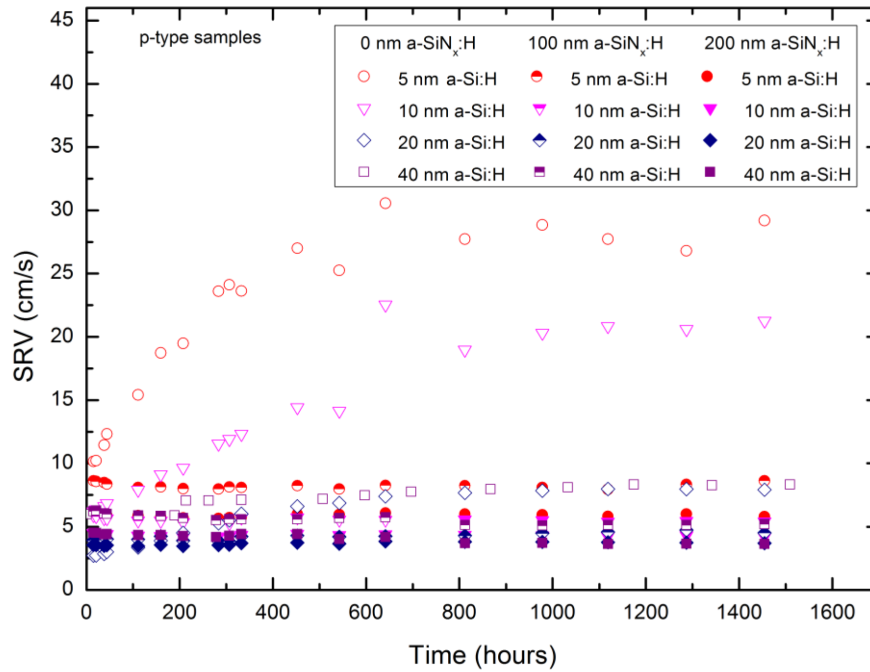

Figure 29 The surface recombination velocity (SRV) of all the *p*-type samples with different passivation layers. The SRVs for the first nine weeks are shown in the graph. The SRVs are calculated from the measured effective lifetimes assuming infinite bulk lifetime and is therefore an upper limit of the SRV.

The degradation of the passivation quality of the uncapped sample with the thinnest a-Si:H layer of 5 nm results in the upper limit for the SRV increasing from 10 to about 30 cm/s during the 25 first days after deposition. For an ideal cell as the one used in the simulations in PC1D presented in Section 2.3 and with parameter settings given in Appendix 1, this increase of the SRV corresponds to a decrease of the conversion efficiency of a cell of 0.4 absolute per cent from 23.8 to 23.4 % for a 200 µm cell and 0.6 absolute per cent from 22.3 to 21.7 % for a 50 µm cell. The bulk lifetime of the cell in the PC1D model is set to 1 ms. The bulk lifetime of the wafers used in this study are specified to be minimum 6.2 ms for *n*-type and 2.5 ms for *p*-type. For these lifetimes the conversion efficiency loss due to the increased conversion efficiency would be even higher. The passivation quality of the sample with the 20 nm a-Si:H single layer also degrades, but not as much. Some of the degradation is most likely due to scratches caused by accidentally falling on the floor. The upper limit of the SRV after 61 days is about 20 cm/s. All the other samples have an upper limit of SRVs below 10 cm/s also after 61 days. The decrease in conversion efficiency for an increased SRV from 1 to 10 is 0.2 absolute per cent from 24 to 23.8 % for a 200 µm thick cell. The decrease of the conversion efficiency for the same increase in SRV is 0.4 absolute per cent for from 22.7 to 22.3 % for a 50 µm thick cell. Thus the most stable layers can reduce the efficiency losses with 0.2 absolute per cent compared to the less stable layers.

4.2.2. The temporal stability of the *n*-type samples

The effective lifetimes of the passivated *n*-type samples were measured with the QSSPC and are given for an excess carrier concentration of 10^{15} cm^{-3}. Figure 30 shows the effective lifetimes measued within the first nine weeks after deposition.

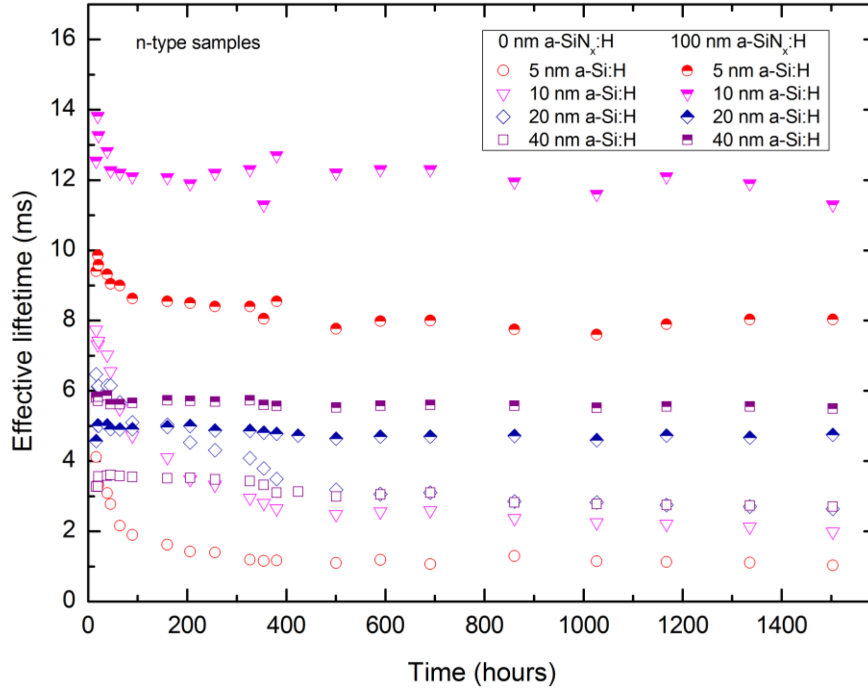

Figure 30 Effective lifetime of the *n*-type samples passivated with different stacks for an excess carrier concentration of 10^{15} cm^{-3} the first 9 weeks after deposition.

The capped samples have effective lifetimes between 4.6 and 12.5 ms as deposited. The layers with 20 and 40 nm a-Si:H are stable for the entire period of 9 weeks whereas the two capped samples with the thinnest a-Si:H layer degrade for about the first 50 hours. The first measurement of the sample with the capped 10 nm a-Si:H layer resulted in a lower lifetime than the second measurement. The QSSPC coil did not measure exactly the same area in these two measurements, which may explain why the measured effective lifetime so suddenly increases from 12.5 to 13.8 ms. Another possible reason why the recorded lifetime of this samples varies might be the noise in the QSSPC curve for the range around the excess carrier concentration that the effective lifetime is recorded for this very high lifetime sample. The uncapped samples degrade within the first 500 hours after deposition and then seem to be quite stable. They seem to stabilise at lower lifetimes with thinner a-Si:H thickness.

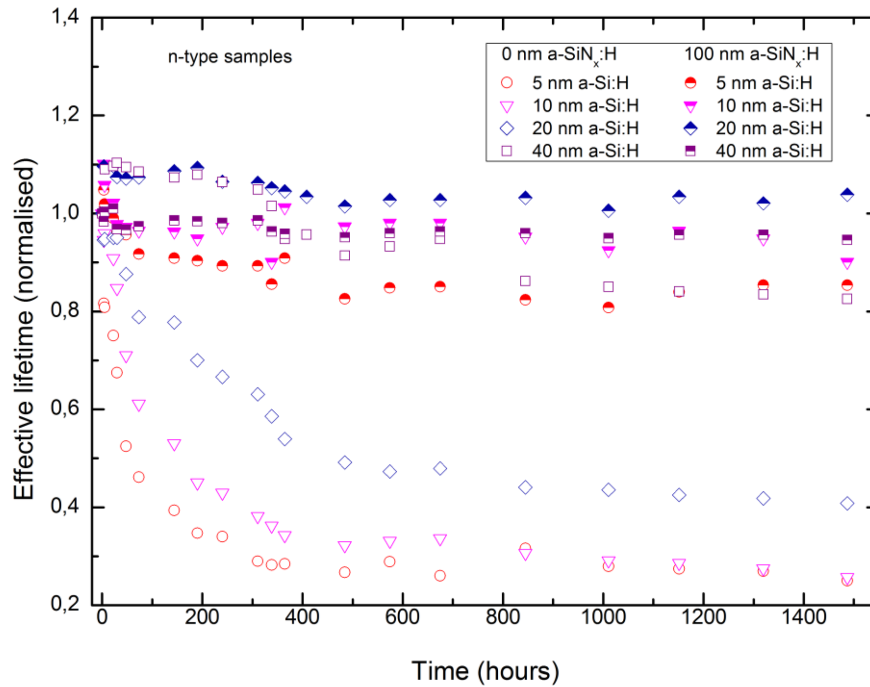

Figure 31 Normalised effective lifetimes of the *n*-type samples passivated with different stacks for an excess carrier concentration of 10^{15} cm^{-3} the first 9 weeks after deposition. The measured effective lifetimes are normalised with respect to the effective lifetimes measured one day after deposition.

Figure 31 shows the normalised effective lifetimes of the *n*-type samples for the first nine weeks after deposition. The normalisation is made with respect to the samples measured effective lifetimes one day after deposition. The relative degradation of the lifetimes becomes smaller with increasing a-Si:H layer thickness, both for the capped and the uncapped samples. The only exception from this is the capped 20 nm a-Si:H sample which degrades less than the capped 40 nm a-Si:H sample. The capped samples are quite stable whereas the uncapped samples with 5, 10 and 20 nm a-Si:H degrade to 27 - 50 % of their initial lifetime in less than three weeks. The behaviour of the 40 nm a-Si:H sample is more similar to the capped samples with thin a-Si:H layers. The lifetime of this sample degrades to 83 % of its initial value. For comparison the effective lifetime of the 5 nm a-Si:H sample degrades to 85 % of its initial value.

4.2.2.1. Temporal stability of the uncapped n-type samples

The effective lifetimes of the uncapped samples for the first nine weeks are shown in Figure 32. It can be seen that the lifetime of the uncapped samples degrade rapidly the first 500 hours and then stabilises during the following 6 weeks. The effective lifetime of the 5 nm a-Si:H sample degrades the most during the nine week period, from 4.1 to 1.0 ms, i.e. after 9 weeks it is only 25 % of what it was one day after deposition. The 40 nm and 20 nm a-Si:H samples stabilise at approximately the same value 2.6 -2.7 ms. The 10 nm a-Si:H sample has the highest effective lifetime of the uncapped samples, almost 8 ms one day after deposition, but after nine weeks the lifetime is reduced to 2 ms.

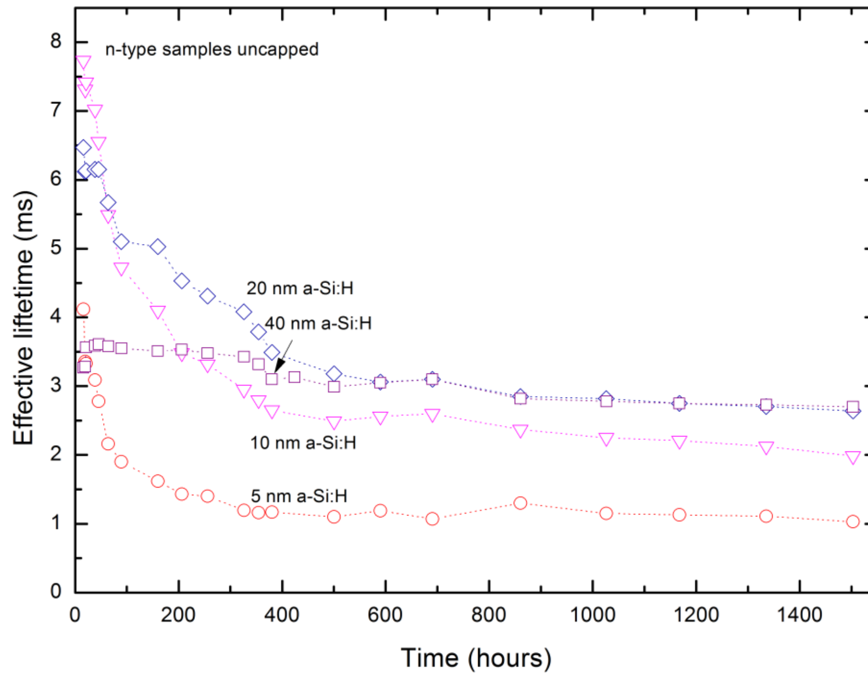

Figure 32 The measured effective lifetimes of the uncapped *n*-type samples for the 9 weeks after deposition for an excess carrier concentration of 10^{15} cm^{-3}. The dotted lines are guides to the eye.

4.2.2.2. Temporal stability of the n-type samples with 100 nm capping

The measured effective lifetimes of the capped *n*-type samples are shown in Figure 33. The capped samples with 20 and 40 nm a-Si:H thickness are quite stable with time. The lifetime of the 40 nm sample degrades to 95 % of its initial value one day after deposition. The 20 nm sample shows only very little degradation. The increase of the lifetime between the first and second measurement for this sample, shown as the first and second point in the graph, is most likely due to a small shift of the sample with respct to the QSSPC coil, resulting in a different area being measured. The samples with 5 and 10 nm a-Si:H thickness are degrading for the first 200 hours, then they are stable. Those might be less stable either because their lifetimes of are higher than the lifetimes of the other samples straight after depositon or because the a-Si:H layer is thinner and therefore the passivation it provides is less stable.

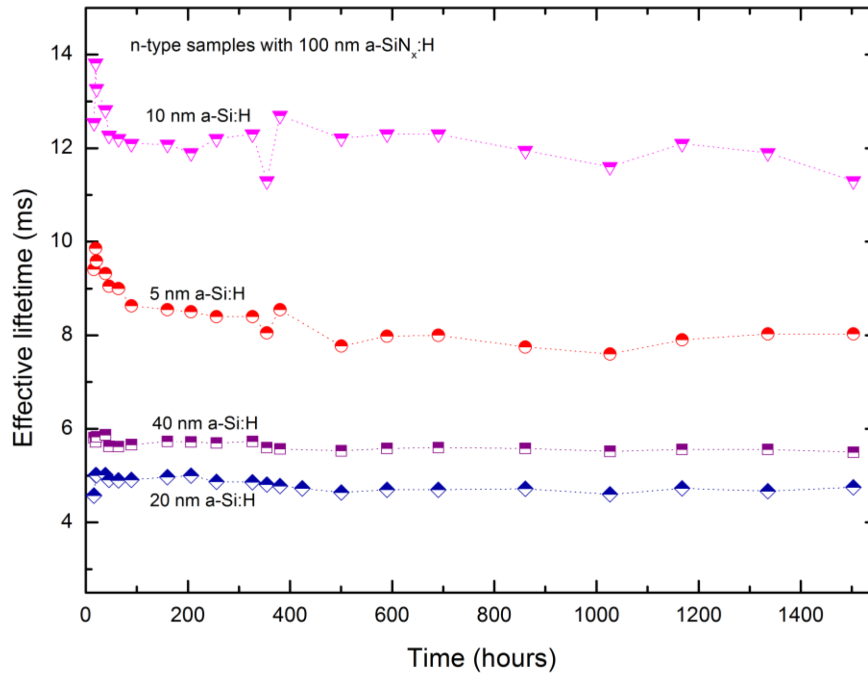

Figure 33 The measured effective lifetimes of the capped *n*-type samples for the 9 weeks after deposition for an excess carrier concentration of 10^{15} cm^{-3}. The dotted lines are guides to the eye.

4.2.2.3. *Effective lifetimes of the n-type samples nine weeks after deposition*

Figure 34 shows the effective lifetimes of the *n*-type samples nine weeks after deposition. The effective lifetimes of the uncapped samples increase with increasing thickness of a-Si:H. The increasing thickness does not seem to affect the effective lifetime much above 20 nm. For the capped samples there is no clear relationship between a-Si:H thickness and effective lifetime.

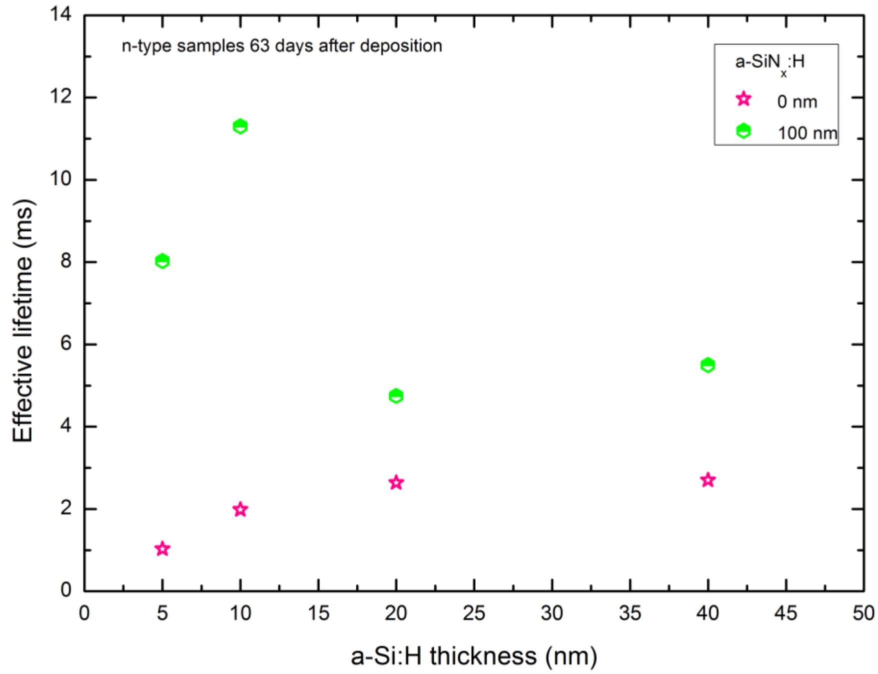

Figure 34 The effective lifetimes of the *n*-type samples 63 days after deposition for an excess carrier concentration of 10^{15} cm^{-3}.

Figure 35 shows the normalised effective lifetimes of the *n*-type samples 9 weeks after deposition. The samples are normalised with respect to the effective lifetime measured one day after deposition. The measurement points show that the lifetimes of the uncapped samples have degraded more the thinner the single a-Si:H layer is. For the capped samples the trend is not that clear but except for the sample with 40 nm a-Si:H the trend is the same as for the capped samples.

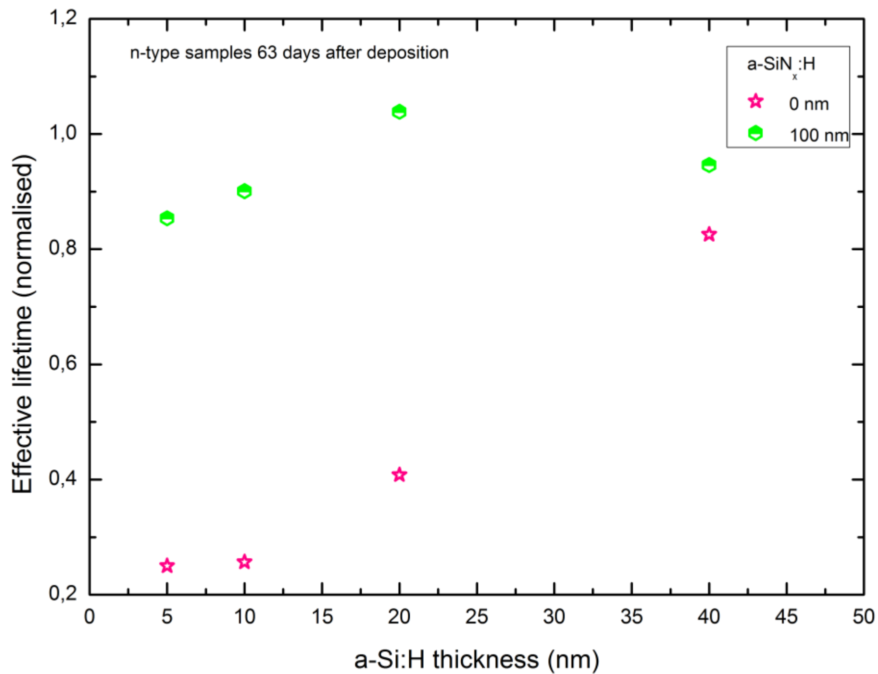

Figure 35 The normalised effective lifetimes of the *n*-type samples 63 days after deposition for an excess carrier concentration of 10^{15} cm^{-3} and normalised with respect to the effective lifetime measured one day after deposition.

4.2.2.4. *Surface recombination velocity of the n-type samples*

The SRVs of the samples were calculated from the measured effective lifetimes. An assumption of infinite bulk lifetime is used in the calculation resulting in an upper limit for the SRV for that particular effective lifetime. The SRVs in Figure 36 are given for an excess carrier concentration of 10^{15} cm/s.

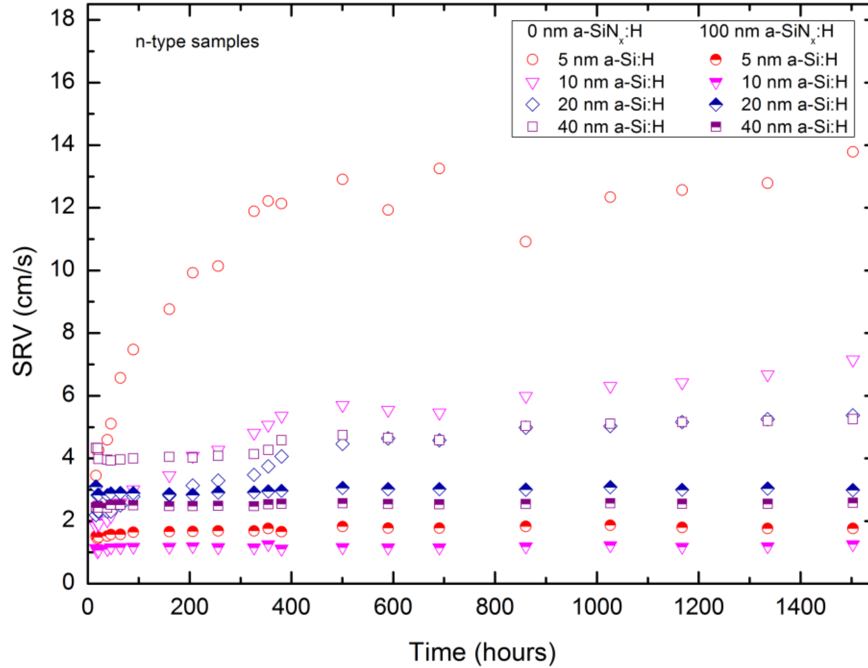

Figure 36 The surface recombination velocity (SRV) of all the *n*-type samples with different passivation layers. The SRVs for the first 9 weeks are shown in the graph. The SRVs are calculated from the measured effective lifetimes assuming infinite bulk lifetime and is therefore an upper limit of the SRV.

All the *n*-type samples have upper limits of the SRVs below 5 cm/s one day after deposition. The capped samples are quite stable. After nine weeks the highest upper limit of the SRVs of the capped samples is 3 cm/s. For the ideal cell model used for simulations in PC1D with parameter settings in Appendix 1 and a thickness of 200 µm, this corresponds to a conversion efficiency loss of 0.1 absolute per cent compared to a cell without surface recombination. For a similar cell, but with a thickness of 50 µm instead of 200 µm, the loss would be twice as large, i.e. 0.2 absolute per cent. The uncapped samples with thin layers of a-Si:H degrade the most. Nine weeks after deposition the upper limit of the SRV corresponding to the measured effective lifetime of the sample with a single layer of 5 nm a-Si:H is 13.8 cm/s. For the same PC1D model as described above the loss due to recombination would result in a conversion efficiency loss of 0.4 absolute per cent for a 200 µm cell and 0.7 absolute per cent for a 50 µm cell. The upper limits of the SRVs for the other uncapped samples are in the range from 5 to 8 cm/s. This corresponds to conversion efficiency losses of 0.2-0.3 absolute per cent for a 200 µm cell and 0.3-0.4 absolute per cent for a 50 µm cell. For higher bulk lifetimes the conversion efficiency losses due to these SRVs would be higher.

4.2.3. Summary of the results from the temporal stability measurements

The passivation quality of the single layers degraded rapidly for the first weeks or month, but the degradation decreased with increasing thickness of the a-Si:H layer. A month after deposition the passivation provided by the single layers seems stable with time. The stacks have a high temporal stability that seems to weakly depend on the thickness of the layer of amorphous silicon.

When the samples seem to have stabilised, nine weeks after deposition, the passivation quality of the *p*-type samples, both capped and uncapped, seem to improve with the a-Si:H thickness up to 20 nm. The effective lifetime of the samples of each a-Si:H thickness increase with increasing capping thickness. The *n*-type samples do not show a clear trend for the effective lifetime versus a-Si:H thickness after nine weeks.

4.2.4. Discussion of the temporal stability

Single layers of hydrogenated amorphous silicon provide very good passivation shortly after deposition, but degrades a lot more than the capped layers of the same thickness. Capping the a-Si:H layers with a-SiN_x:H provides good passivation quality with good temporal stability. The a-SiN_x:H capping layer is denser than the a-Si:H layer and may prevent the hydrogen from effusing out of the a-Si:H layer with time. There is not much difference between the temporal stability of the 100 and 200 nm capping layers. They are both stable with respect to time, which indicates that 100 nm is thick enough to prevent the hydrogen from being released with time and thus provide temporal stability of the stack.

The degradation of the a-Si:H single layers may have been influenced (increased) by the illumination of the samples during the measurements. It is known that illumination with UV light rapidly degrades the passivation quality of a-Si:H single layers [27]. The illumination used in the measurements have lower energy and is infrared light, but might still affect the passivation quality. Therefore it would have been useful to measure the effective lifetime of a reference sample from the same wafer or with the same single layer only twice the minimise the illumination of the sample. The measurements on the reference sample should only have been carried out once shortly after deposition and once after the frequently measured samples seem to have stabilised. The reference sample only measured twice and the more frequently measured sample should then be compared. In this way it would be possible to see if the degradation was larger for a sample that had been illuminated during about 20 measurements than the degradation of the sample which had been strored in the dark for the entire nine week period, except for the two measurements made. This was planned to be carried out in this thesis, but was not performed because the plans for cutting the wafers were changed when the non uniform passivation quality of the wafers was detected.

The measured lifetimes nine weeks after deposition indicate that the degradation of the samples depend both on the a-Si:H thickness and on the a-SiN_x:H thickness. The relative degradation is greater the thinner the a-Si:H layer is. This relationship between degradation and a-Si:H thickness

applies to all the samples without capping and to the capped samples with up to 20 nm a-Si:H thickness. This indicates that in a stack 20 nm of a-Si:H is enough to provide good passivation which is stable with time.

4.3. Thermal stability

The thermal stability of the passivation is important because firing is needed for the conventional metallisation processes of solar cells. In this section the results from the experiments investigating the thermal stability of the single layers and stacks are presented and discussed. The experiments carried out were rapid thermal annealings for one minute at different temperatures, one minute annealing at 450 °C in a belt furnace and a firing process normally used for metallisation with a peak temperature of 945 °C.

4.3.1. Rapid thermal annealing at different temperatures

The samples were annealed consecutively at different temperatures in the RTP. The effective lifetimes were measured straight before and six minutes after each annealing by PL imaging. The samples were at steady state at the particular temperature for one minute. The PL images taken before and after annealing were calibrated using a separate QSSPC measurement of a reference wafer with the same capping thickness as the investigated samples.

4.3.1.1. Rapid thermal annealing of the n-type samples

Figure 37 shows the PL images of the uncapped *n*-type samples before annealing and after annealing at 350, 450 and 500 °C. The calibrated effective lifetimes are given in the axis to the right. It can be seen that the measured effective lifetimes of the uncapped samples have improved after the annealing at 350 °C, degraded after the annealing at 450 °C and is too low to give an accurate value after the annealing at 500 °C. The sample with 40 nm a-Si:H is the only sample that is detectable in the PL image taken after the 500 °C annealing.

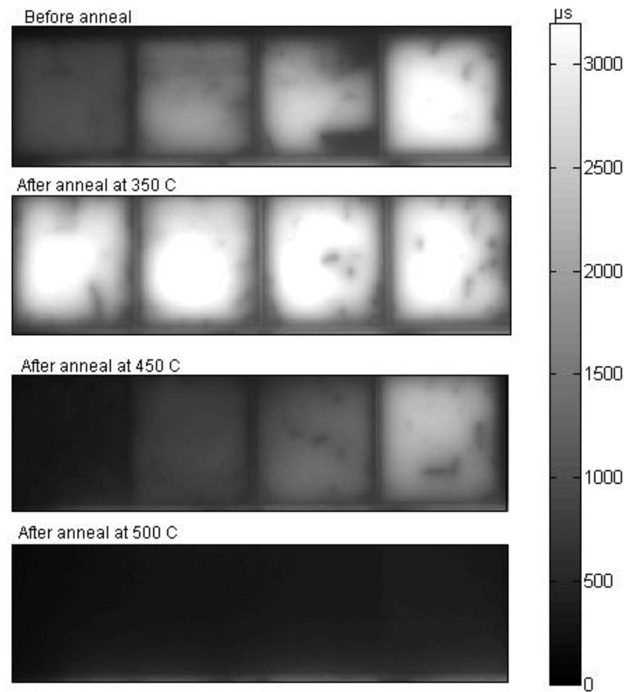

Figure 37 Photoluminescence images of the uncapped *n*-type samples before annealing and after annealing at 350, 450 and 500 °C. The scale on the right side shows the effective lifetime in µs. The effective lifetimes are calibrated using a QSSPC measurement of a reference sample placed next to the investigated samples in the PL images. From the left are the samples with 5, 10, 20 and 40 nm a-Si:H.

The emitted light detected from the investigated samples in the measurement after annealing at 500 °C does not give enough statistics to give valid values. Ideally, the calibration sample should have approximately the same lifetimes as the investigated samples for the calibration to be valid. In this case the reference cell has a lot higher lifetime than the investigated samples because the same reference sample is used both when the samples have improved and degraded. The light emitted from the reference sample, detected in the area around it, is considerable compared to the light emitted from the investigated samples. Therefore the accurate values of the investigated samples have not been determined, but it can be seen from the PL image that the lifetimes are very low and that some of the samples have higher lifetimes than the others after the 500 °C annealing. In Figure 37 the 40 nm a-Si:H sample can for example be seen to have higher lifetime than the other samples after annealing at 500 °C. The measured effective lifetimes after the annealings at 500 °C shown in the graphs below are therefore not accurate values.

The effective lifetimes, measured after the rapid thermal annealing experiments, are shown in Figure 38 and Figure 39, for uncapped and capped *n*-type samples, respectively. The effective lifetimes shown in these graphs are calculated from PL images such as the ones in Figure 37, for a small uniform area with high lifetime for each of the samples. The same area is used for calculating the lifetime after every annealing. All the samples reach a maximum lifetime after annealing at around 350 °C. This maximum value seems to be about 3.5 ms regardless of what the lifetimes before the annealing were. All samples are reduced to 0.1 ms or less after the one minute annealing at 500 °C.

Rapid thermal annealing of the *n*-type samples without capping

Annealing at 200- 400 °C improves the effective lifetimes of the uncapped samples. The 40 nm a-Si:H sample reaches its maximum lifetime during the annealing at 400 °C. The other samples reach their maximum lifetime during the annealing at 350 °C. How fast the lifetime of the uncapped samples decrease with increasing annealing temperature above 350 °C depends on the thickness of the amorphous silicon layer. The dependence on the thickness of the a-Si:H layer is stronger for the uncapped than for the capped samples.

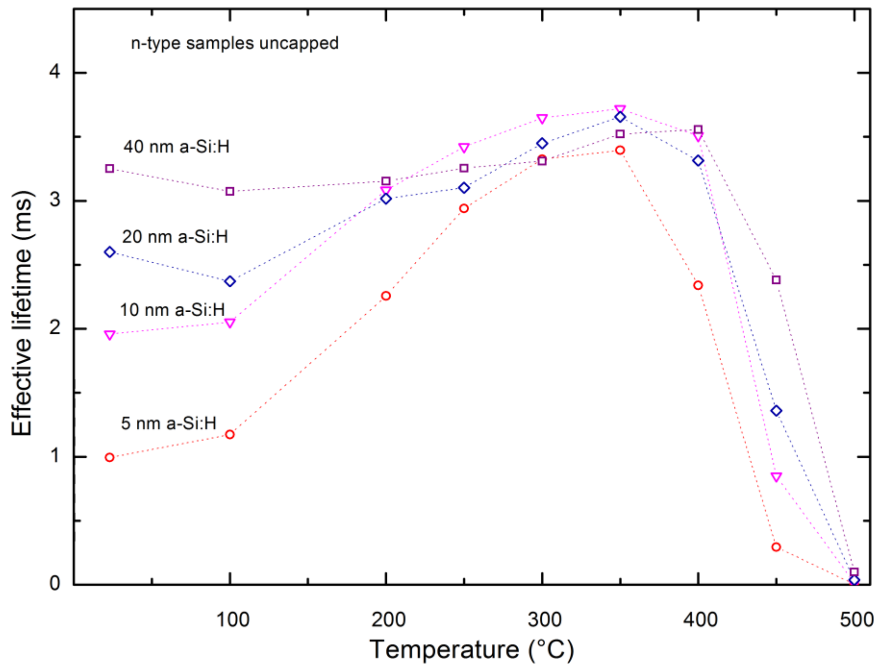

Figure 38 Lifetime stability of the *n*-type samples with respect to temperature. The graph shows the measured effective lifetimes of the *n*-type samples without capping after a 1 min annealing at different temperatures in a rapid thermal processing unit. The dotted lines are guides to the eye.

Rapid thermal annealing of the *n*-type samples with 100 nm capping

Annealing of the samples at 300-400 °C improves the effective lifetimes of the samples. All the capped *n*-type samples reach their maximum effective lifetime at the same temperature; 350 °C. A rapid decrease of the effective lifetime can be seen for temperatures above 400 °C. The improvement of these samples is not as large as for the uncapped samples. This might be because the effective lifetimes before the annealings are higher for the capped samples, than for the uncapped samples before annealing.

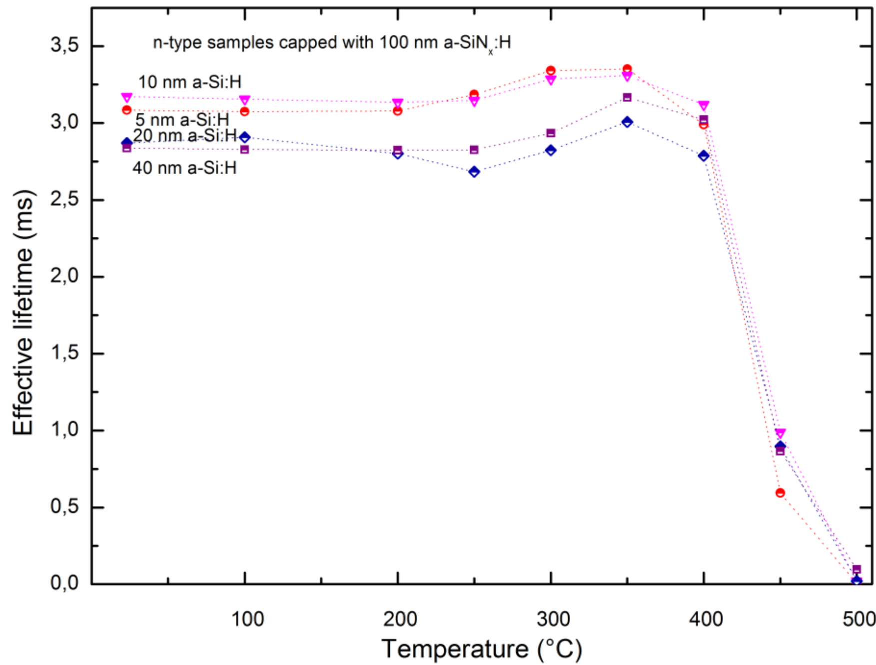

Figure 39 Lifetime stability of the *n*-type samples with respect to temperature. The graph shows the measured effective lifetimes of the *n*-type samples with 100 nm capping after a 1 min annealing at different temperatures in a rapid thermal processing unit. The dotted lines are guides to the eye.

4.3.1.2. Rapid thermal annealing of the p-type samples

All the effective lifetimes of the *p*-type samples are improved by annealing at temperatures between 250 and 350 °C. The effective lifetimes decrease fast for annealing at temperatures above 400 °C and are very low after annealing at 500 °C. The measured lifetimes before and after the annealing at the different temperatures are shown in Figure 40, Figure 41 and Figure 42 for the uncapped samples and the samples capped with 100 nm and 200 nm a-SiN_x:H, respectively.

Rapid thermal annealing of the *p*-type samples without capping

The measured effective lifetimes improve after the annealings up to 300 °C and are approximately the same after the annealings at 300 and 350 °C for all the uncapped samples. The maximum effective lifetimes of all the uncapped samples are reached for annealings at 300 and 350 °C and are between 2.0 and 3.1 ms. The sample with the thickest a-Si:H layer reaches the highest value. This is also the samples that have the highest effective lifetime before annealing. The thinner the a-Si:H layer is, the faster the effective lifetime decreases for temperatures above 350 °C. After annealing at 450 °C, the lifetimes of the samples are greatly reduced from the maximum lifetimes reached, and from the lifetimes before annealing too. The lifetimes after the 450 °C annealing are 60, 190 and 350 µs for the samples with 5, 10 and 20 nm a-Si:H, respectively.

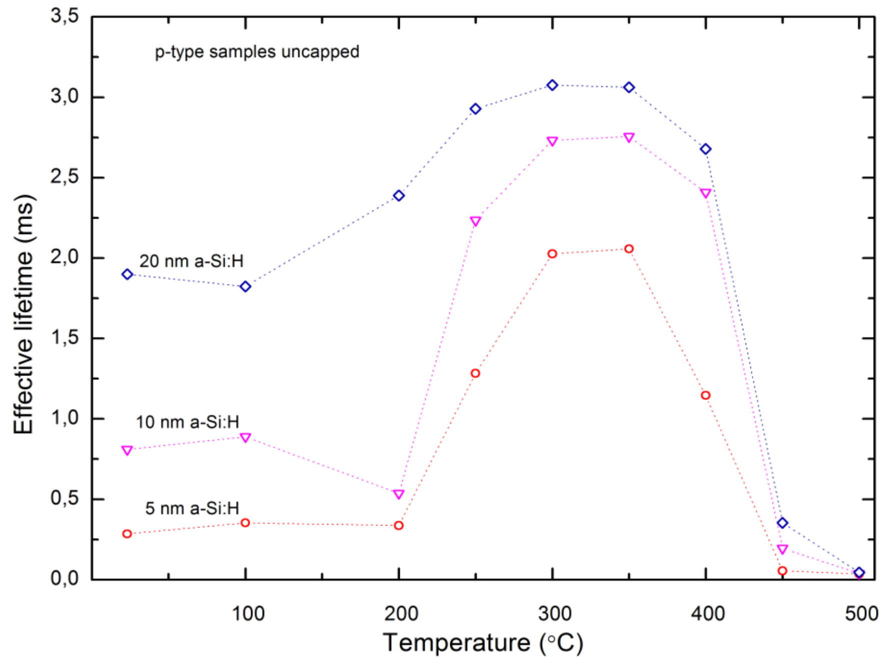

Figure 40 Measured effective lifetimes of the uncapped *p*-type samples with respect to annealing temperature. The lifetimes were measured 6 minutes after 1 min annealing in a rapid thermal processor. The annealings at different temperatures were consecutive. The dotted lines are guides to the eye.

Rapid thermal annealing of the *p*-type samples with 100 nm capping

The effective lifetimes of the samples with the thinnest a-Si:H layers decrease faster with the increasing annealing temperature for temperatures above 350 °C. The samples with the thinner a-Si:H layers of 5 and 10 nm reach maximum effective lifetimes after annealing at 300°C, while the samples with the thicker a-Si:H layers of 20 and 40 nm reach maximum effective lifetimes after the 350 and 400 °C annealing, respectively. The 5 nm a-Si:H sample decreases faster with higher temperatures and have started decreasing already after the 350 °C annealing. The 40 nm a-Si:H sample decreases slower with higher temperature, but after 500 °C this sample also has a very low lifetime (too low to measure exactly). The sample with 20 nm is different from the other samples, as the lifetime of this samples increase very little. All the other samples have a measured local minimum of the effective lifetime of around 1.2 ms regardless of the lifetime before the 200 °C annealing.

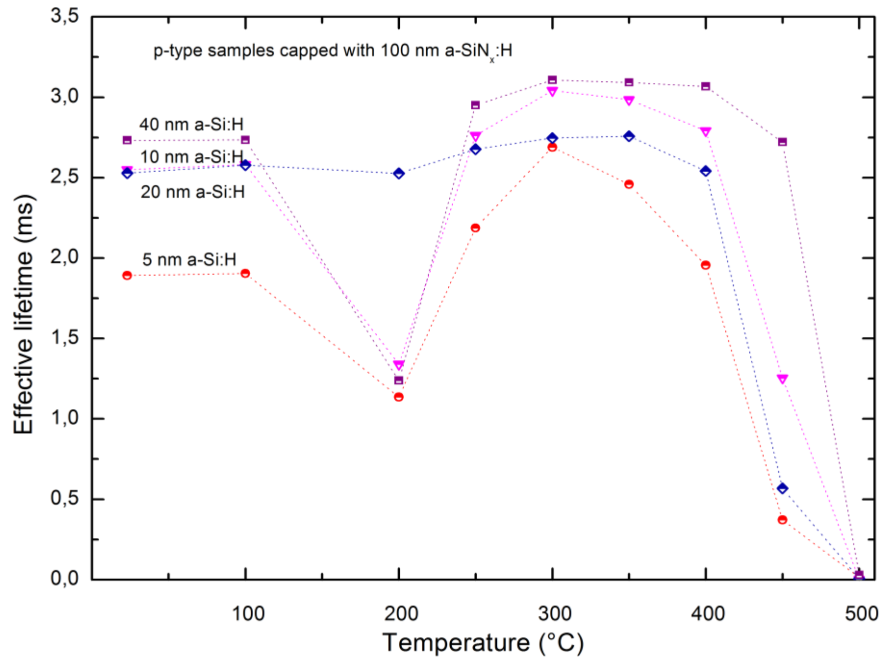

Figure 41 Measured effective lifetimes of the 100 nm a-SiN_x:H capped *p*-type samples with respect to annealing temperature. The lifetimes were measured 6 minutes after 1 minute annealing in a rapid thermal processor. The annealings at different temperatures were consecutive. The dotted lines are guides to the eye.

Rapid thermal annealing of the *p*-type samples with 200 nm capping

The sample with 40 nm a-Si:H and 200 nm a-SiN_x:H reaches its maximum effective lifetime after a higher annealing temperature; 400 °C, than the other samples. The sample with 20 nm a-Si:H reaches its maximum effective lifetime after an annealing at 350 °C. The samples with 5 and 10 nm a-Si:H reach their maximum lifetime at 300 °C. Hence the thicker the a-Si:H layer is, the higher is the annealing temperature resulting in the maximum effective lifetime. After the 450 °C annealing, the effective lifetime of the sample with 40 nm a-Si:H is a lot higher, above 2.5 ms, than that of the samples with thinner layers of a-Si:H, which are all below 0.5 ms. As for the samples capped with 100 nm, the samples reach local minimum effective lifetimes at 200 °C, except for the 20 nm a-Si:H sample.

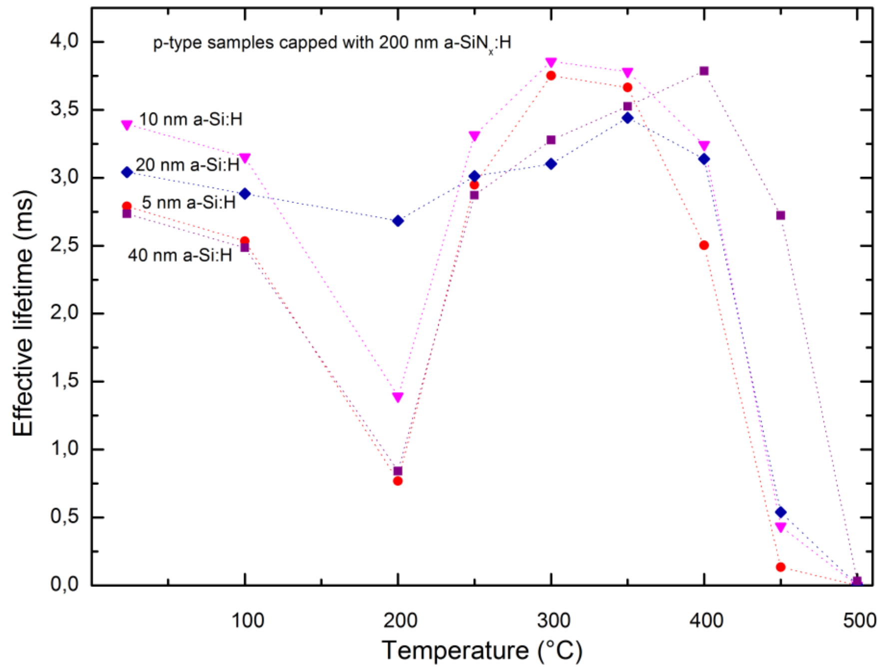

Figure 42 Measured effective lifetimes of the *p*-type samples capped with 200 nm a-SiN_x:H with respect to annealing temperature. The lifetimes were measured 6 minutes after one minute annealing in a rapid thermal processor. The annealings at different temperatures were consecutive. The dotted lines are guides to the eye.

4.3.2. Annealing in the belt furnace at 450 °C

The samples were annealed for one minute in an infrared belt furnace at 450 °C and were measured before and after the annealing. The measurements were carried out frequently for the first hour and day after the annealing, then about weekly for the following month. The annealing was carried out about a month after deposition. The effective lifetimes of the uncapped samples had already degraded quite a lot from the effective lifetimes measured one day after deposition when they were annealed in the belt furnace.

4.3.2.1. Annealing at 450 °C of the n-type samples

The effective lifetimes of the *n*-type samples, measured before the annealing and for the first month after the annealing are shown in Figure 43 and Figure 44 for the uncapped and capped samples, respectively.

Annealing at 450 °C of the *n*-type samples without capping

All the uncapped samples increase when they are annealed at 450 °C in the belt furnace. The samples with 20 and 5 nm a-Si:H have approximately the same effective lifetime before the annealing. The 5 nm a-Si:H sample increased more during the annealing, but seems to decrease more after the annealing as well. The 40 nm a-Si:H sample has the largest increase of measured effective lifetime and seems to be quite stable at the improved effective lifetime after annealing.

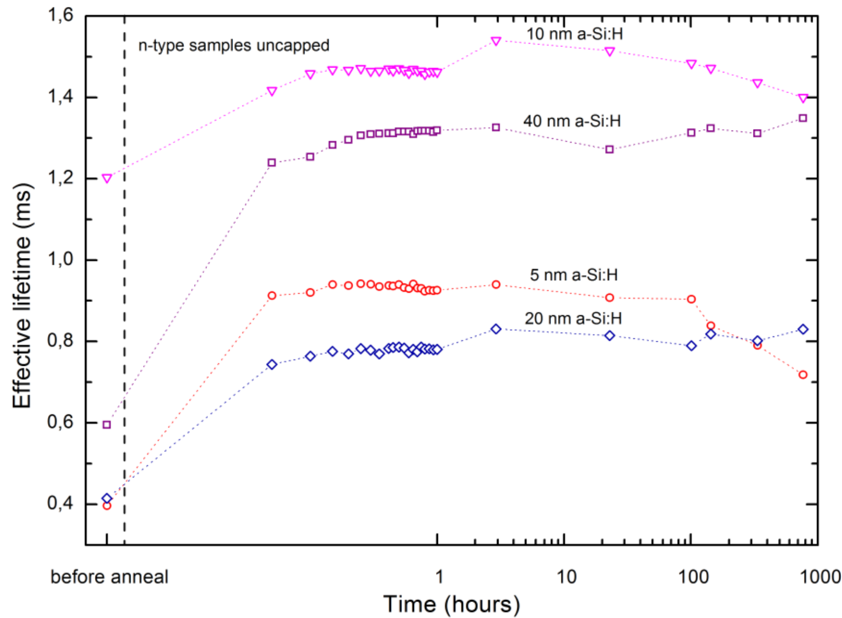

Figure 43 Effective lifetime stability of the uncapped *n*-type samples after a one minute annealing at 450 °C in a belt furnace. The lifetimes before the annealing are shown to the left and the lifetimes after the annealing are shown to the right of the vertical dashed lines. The dotted lines are guides to the eye.

Annealing at 450 °C of the *n*-type samples with 100 nm capping

The effective lifetimes of all the samples decrease during annealing except for the 40 nm a-Si:H sample. The 20 nm a-Si:H sample improves greatly during the first hour after the annealing when measurements are carried out every 3-5 minutes. The other capped samples also increase during this period, but not as much as the 20 nm a-Si:H sample. After one hour the lifetimes are quite stable for the following month. The second last measurement results in higher lifetimes than the other measurements for all the samples. It is likely that the high values are caused by a discrepancy in the calibration of the PL image and not a physical effect.

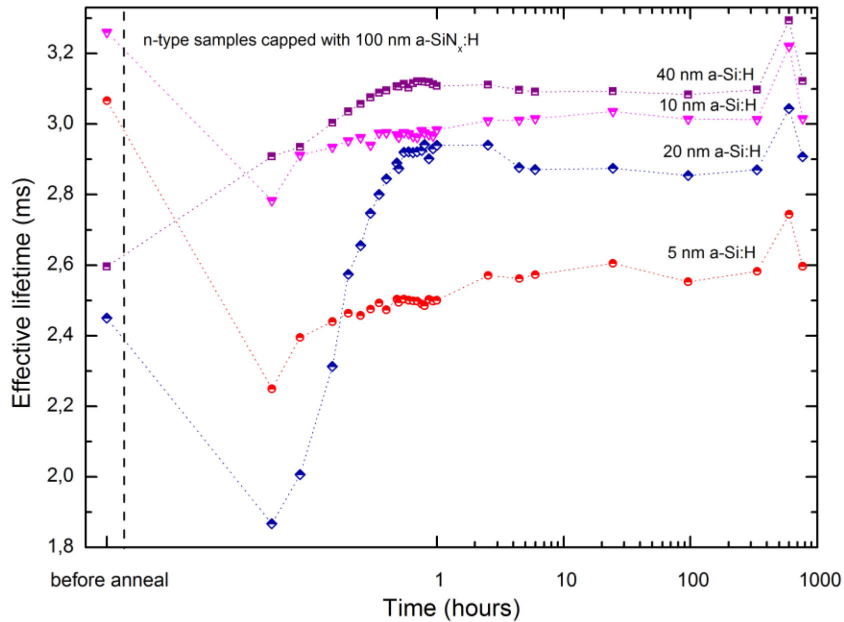

Figure 44 Effective lifetime stability of the capped *n*-type samples after one minute annealing at 450 °C in a belt furnace. The lifetimes before the annealing are shown to the left and the lifetimes after the annealing are shown to the right of the dashed vertical line. The dotted lines are guides to the eye.

4.3.2.2. *Annealing at 450 °C of the p-type samples*

The effective lifetimes of the *p*-type samples, measured before the annealing and for the first month after the annealing are shown in Figure 45, Figure 46 and Figure 47 for the samples with no, 100 and 200 nm capping, respectively.

Annealing at 450 °C of the *p*-type samples without capping

The effective lifetime of all the uncapped *p*-type samples increase during the annealing. The lifetime of the 20 nm a-Si:H sample keeps increasing within the first hour. Then it degrades slowly for the following month. The lifetimes of the two samples with the thinner a-Si:H layers decreases already 3 minutes after the annealing and has not yet stabilised one month later. The lifetime of the 5 nm a-Si:H sample is approximately the same as before the annealing, one month after the annealing, but seems it seems to keep degrading. The lifetimes of the samples with thicker a-Si:H layer are still higher than before the annealing one month after the annealing.

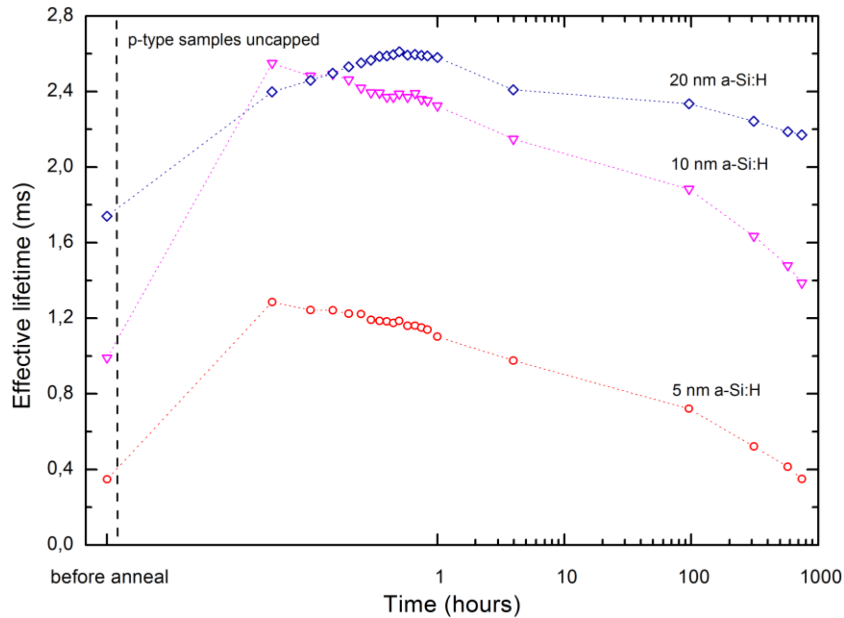

Figure 45 Effective lifetime stability of the uncapped *p*-type samples after 1 min annealing at 450 °C in a belt furnace. The lifetimes before the annealing are shown to the left ant the lifetimes after the annealing are shown to the right of the dashed vertical line. The dotted lines are guides to the eye.

Annealing at 450 °C of the *p*-type samples with 100 nm capping

The effective lifetime of the 5 nm a-Si:H sample decreases from 2.1 ms during the annealing and keeps decreasing for the following 100 hours, until it stabilises just below 1.4 ms. The effective lifetime of the 10 nm a-Si:H sample is approximately the same before and after annealing, about 2.3 ms and is only slightly lower one month later at 2.2 ms. The lifetimes of the samples with 20 and 40 nm increase during the annealing and are 2.7-2.8 ms after annealing. These samples remain quite stable at these values the month after the annealing. The thicker the a-Si:H layer is, the greater was the increase of the lifetime. Only the samples with the thinnest a-Si:H layer degrade considerably after the annealing.

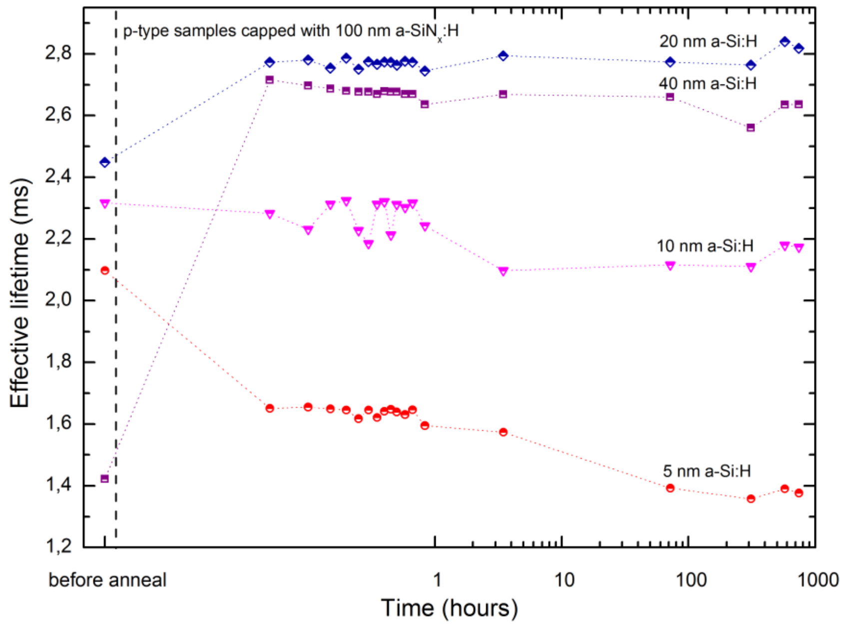

Figure 46 Effective lifetime stability of the *p*-type samples capped with 100 nm silicon nitride after 1 min annealing at 450 °C in a belt furnace. The lifetimes before the annealing are shown to the left and the lifetimes after the annealing are shown to the right of the vertical dashed line. The dotted lines are guides to the eye.

Annealing at 450 °C of the *p*-type samples with 200 nm capping

The samples with 20 and 40 nm a-Si:H have approximately the same effective lifetimes both before and after the annealing. Their lifetimes improved from 2.2 to 3.7 ms while the lifetime of the sample with 5 nm a-Si:H degraded from 2.9 to 2.3 ms during the annealing.

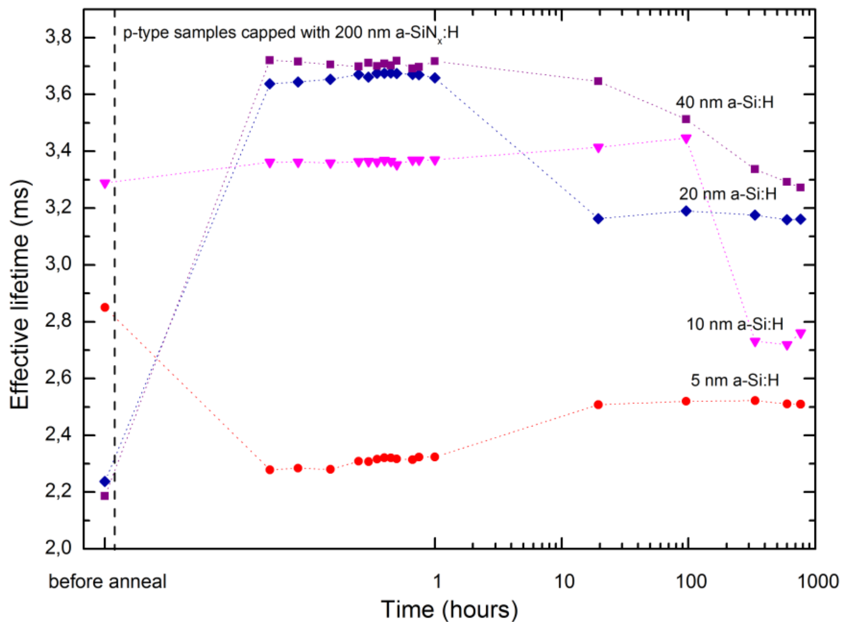

Figure 47 Effective lifetime stability of the *p*-type samples capped with 200 nm silicon nitride after 1 min annealing at 450 °C in a belt furnace. The lifetimes before the annealing are shown to the left and the lifetimes after the annealing are shown to the right of the vertical dashed line. The dotted lines are guides to the eye.

The effective lifetime of the 10 nm a-Si:H does not change much during the annealing or the following 4 days (96 hours). When the next measurement is made, 2 weeks (336 hours) after the annealing, the sample has decreased from 3.4 to 2.7 ms since the previous measurement was made. The PL images of these two measurements, presented in Figure 48, show that de decrease of the lifetime is caused by damage, which is probably a scratch in the surface passivation layers. It is not a uniform degradation of the entire sample as would be expected if it was caused by degradation of the passivation by effusion of hydrogen with time. The damage is probably caused by wafer handling.

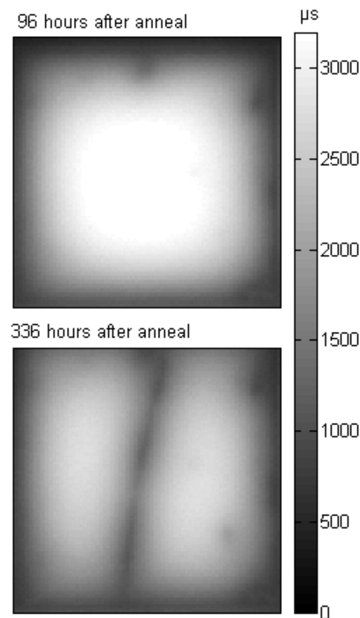

Figure 48 PL images of the sample with 10 nm a-Si:H and 200 nm a-SiN_x:H. The upper image is taken 96 hours after annealing and the lower image is taken 336 hours after annealing. A damage of the surface layers can be seen right across the sample in the lower image. The damage was probably caused by the wafer handling.

The sample with 20 nm a-Si:H which decreases from 3.7 to 3.2 ms between the measurements carried out 1 and 20 hours after annealing is probably also damaged by the wafer handling between the two measurements. The PL image shows areas with lower lifetimes looking like small scratches on the surface, and the degradation is not uniform.

The thicker the a-Si:H layer is, the greater was the increase of the normalised lifetime during the 450 °C anneal.

4.3.3. Normal firing process

All the *n*- and *p*-type samples were heat treated by a process similar to the firing that is normally applied for metallisation with standard screen printed pastes, using the LA-309 belt furnace as described in Section 3.1.4. The furnace has four heating zones at 780, 825, 870 and 945 °C and the total heating time was 8.8 s. The lifetimes of all the samples were severely degraded after going

through this normal firing process and were too low to be measured for all the samples. Hence the lifetimes were probably close to those of unpassivated samples.

4.3.4. Summary of the results from the thermal stability experiments

Annealing at 100 °C did not affect the effective lifetimes of the samples investigated. Annealing at 200 °C degraded some of the capped samples whereas the other samples were not affected. Between 250 and 450 °C all the samples first improved, then reached a maximum lifetime and finally started degrading. Bothe the stack and the single layers reached maxima at higher temperatures with increasing a-Si:H thickness. The samples reached their maximum lifetimes after annealing at temperatures between 300 and 400°C. All The *n*-type samples reached a maximum of about 3.5 ms. At 450 °C most samples with thicker a-Si:H layers have higher effective lifetimes than the samples with the thinner layers and most of the capped *p*-type samples have higher lifetimes than uncapped ones. After the annealing at 500 °C all the samples had degraded severely, having lifetimes below 0.1 ms but too low to measure exactly.

The one minute annealing in the belt furnace increased the lifetimes of all the uncapped samples. The relative improvement of the capped samples increased with increasing thickness of the a-Si:H layer. The samples with the stacks with the thinnest a-Si:H layers degraded during the annealing. Some of the capped samples degraded during the annealing and then improved during the one hour after the annealing when frequent measurements were carried out. Only one of the samples that decreased during the annealing had a lower effective lifetime than 1 ms one month later. None of the stacks or single layers could withstand a firing process used for metallisation with standard screen printing pastes (945 °C peak for 2.2 s).

4.3.5. Discussion of the thermal stability

The findings related to the thermal stability of the amorphous silicon single layers and amorphous silicon/silicon nitride stacks, corresponds quite well to previous results reported in the literature. Ulyashin et al. found that the passivation quality of amorphous silicon/silicon nitride stacks was improved after short annealing at temperatures from 350 to 500 °C [22]. For annealing at higher temperatures than 500 °C the passivation quality degraded [22]. They stated that the increased lifetime obtained by 4-5 minutes annealing in an infrared belt furnace below 500 °C was caused by redistribution of hydrogen at the a-Si:H/c-Si interface [22]. Above 600 °C the hydrogen was released from the interface, hence the number of defect states increased, resulting in degradation of the effective lifetime. [22]. The trends of the lifetimes with respect to annealing temperature described by Ulyashin et al. are quite similar to the trends found in this study. The difference between the findings of Ulyashin et al. and the findings of this study is that the degradation starts at lower temperatures for the samples investigated in this study. They degrade considerably during the 450 °C annealing, whereas the degradation is reported to start at 500 °C in Ulyashin et al.'s study [22]. The

samples were deposited at temperatures below 250 °C in both studies [22]. For some reason the stacks investigated in this study have lower thermal stability. The reason might be that the composition of the layers is different or that the film thicknesses of the stacks are different due to different deposition parameters. Even when the same deposition parameters are used, the composition and structure of the layers deposited, and hence their thermal properties, may be different, if different chambers are used.

Ulyashin et al. also investigated the hydrogen release and defect formation during heat treatment of a-Si:H, a-SiN_x:H and a-Si:H/a-SiN_x:H layers on crystalline silicon [22]. Even though the thermal stability of the stacks investigated in this study is lower, the trend is the same as for the stacks investigated by Ulyashin et al. Thus it is likely that the behaviour of the hydrogen in the single layers and stacks investigated in this study show the same trend as in Ulyashin et al.'s study. From neutron reaction analysis (NRA) Ulyashin et al. found that the uncapped amorphous silicon layer releases hydrogen at 400 °C [22]. Some of the hydrogen diffuses into the crystalline silicon [22]. NRA carried out on a layer of a-Si:H capped with a-SiN_x:H revealed that the hydrogen is better preserved in the amorphous silicon layer when it is capped than when it is not capped [22]. Hydrogen also diffused deeper into the crystalline silicon at 400 °C annealing for the capped than for the uncapped sample [22]. This could be the reason why the stacks investigated in this study have higher thermal stability than the single layers investigated. Ulyashin et al.'s NRA measurements also showed that the hydrogen concentration in the amorphous silicon layer after 600 °C annealing was less than one atomic per cent [22]. What happens to the amorphous silicon layer during annealing at 600 °C in Ulyashin et al.'s study, might be quite analogous to what happens to the amorphous silicon layer in the annealings at 500 °C carried out in the experiments for this thesis.

Gatz et al. investigated the thermal stability of hydrogenated amorphous silicon/silicon nitride stacks consisting of 10 nm a-Si:H and 60 nm a-SiN_x:H on 300 µm thick FZ wafers [6]. The a-SiN_x:H layers were deposited at 300 and 400 °C [6]. They found that the thermal stability of the stacks improves with higher deposition temperatures of the silicon nitride capping layer in the range from 300 to 450 °C [6]. The thermal stability of a stacks with a silicon nitride capping layer deposited at 230 °C is similar to that of the stack where the deposition temperature is 300 °C [6]. The improvement of the thermal stability achieved when increasing the deposition temperature from about 200 °C to 400 °C can therefore be expected to be about the same as the improvement seen when increasing the deposition temperature from 300 to 400 °C in Gatz el al.'s study. One way to improve the thermal stability of the stacks investigated in this study would therefore be to increase the deposition temperature of the silicon nitride capping layer to 400 °C. This would result in a denser layer preventing hydrogen from being released at higher temperatures [6]. One advantage of the stacks over other passivation techniques, like for examples silicon oxide, is the low temperature of the deposition process. Due to the low temperature, the bulk is not affected and the process is less energy demanding and more cost effective. Increasing the deposition temperature to 400 °C would still not affect the bulk, but would make the deposition more energy demanding and thus also more

expensive [17]. If the thermal stability is good enough to withstand the firing process because of improved stability of the stack, caused by higher deposition temperature, this may make up for the increased energy demand and expenses concerning the deposition. Being able to make contacts by screen printed pastes and firing instead of other solutions for metallisation which would be necessary with lower thermal stability would simplify the cell production.

The results indicate that 3.5 ms is a maximum value for the effective lifetime of the *n*-type wafers or the passivation layers. The specified minimum bulk lifetime of the wafers is 6.2 ms, but the corresponding excess carrier concentration is not known. The measured effective lifetimes are given for the excess carrier concentration used for calibration, $7.4 \cdot 10^{15}$ cm^{-3}. At this excess carrier concentration the effective lifetime of the reference wafer is 3.0 ms, whereas the highest effective lifetime of the calibration wafer is just below 5 ms, for an excess carrier concentration of about $1.5 \cdot 10^{15}$ cm^{-3}. This effective lifetime is relatively close to the specified minimum bulk lifetime. Hence the measured maximum effective lifetime of 3.5 ms could be common for all the samples because it is limited by the bulk lifetime.

The measured decrease of effective lifetimes after the annealing at 200 °C was an unexpected result. This is the same temperature as the deposition temperature for a-SiN_x:H and that might have something to do with it as this decrease has only been measured on the capped samples. This is an interesting effect which could be looked more into, but has not been investigated further in this thesis

None of the stacks investigated in this thesis have high enough thermal stability to withstand a normal firing process, needed for the metallisation process by screen printing with standard pastes. This is probably caused by the hydrogen being released from the a-Si:H layer and also by redistribution of the silicon atoms in the a-Si:H layer to a more crystalline like structure with many defects. The defects serve as recombination centres, thus increasing the high SRV. The metallisation therefore needs to be performed differently on these stacks or more thermally stable stacks need to be developed.

Deposition at higher temperatures, between 300 and 450 °C, have been found to increase the thermal stability of the stacks [6]. An alternative to the firing process at 900 °C for a few seconds used for standard screen printing pastes is firing processes at 400-500 °C for a few minutes which can be used for metallisation with low temperature screen printing pastes [6]. It has not been investigated whether the stacks in this thesis can withstand such a firing process. However, the experiment where the samples are annealed for one minute at 450 °C shows that some of the samples improve and some degrade during such a treatment. Only one of the samples that decrease during this annealing have got a lower effective lifetime than 1 ms one month after the annealing. This corresponds to an upper limit of the SRV of 14 cm/s.

The effective lifetimes of all the samples with single layers of a-Si:H on both *n*- and *p*-type wafers have increased after the annealing at 450 °C. However the effective lifetimes of these samples had

degraded since the deposition, so the increase is in fact entirely or partly a regeneration of the passivation quality they had right after deposition. The capped samples had not degraded much in the period after the deposition and therefore the annealing might have affected the passivation differently. The capped samples with 20 and 40 nm a-Si:H have higher effective lifetimes those with 5 and 10 nm a-Si:H one month after the annealing relative to the lifetimes before the annealing. It seems that at least 10 nm of a-Si:H is needed to avoid degradation of the effective lifetime of the capped *p*-type samples to below the value before annealing, either during the annealing or within the following month. On the *n*-type samples it seems that 20 nm of a-Si:H is needed to obtain the same properties as mentioned above.

4.4. Light induced improvement of the passivation from the stacks

An increase of the effective lifetime of the *p*-type samples with 40 nm a-Si:H and 200 and 100 nm a-SiN_x:H after was observed after 642 hours. This increase occurred while these samples were used as references for calibration of PL images. In detail the following observations were made

- The effective lifetime of the *p*-type sample with 40 nm a-Si:H and 200 nm a-SiN_x:H increased from 3.45 to 3.65 ms during the 80 minutes when 16 measurements were made. The sample had not been moved or touched within the 1 hour period when 15 of these measurements were carried out and the effective lifetime increased by 6 %. The lifetime of this sample increased when it was used as a reference for the RTA experiment as well, but between each of those seven measurements it might have been moved slightly. Therefore the results from the RTA experiment are not plotted in Figure 49.
- The *p*-type sample with 40 nm a-Si:H and 100 nm a-SiN_x:H increased from 2.66 to 2.72 ms during the 50 minutes when 13 measurements were carried out. The sample was not moved or touched within this period when the effective lifetime increased by 4 %.
- The *p*-type sample with 10 nm a-Si:H and no capping was also used as a reference for 15 measurements within one hour, but did not improve as much as the capped samples, only 0.7 % from 739 to 734 µs.

The measurements made on the samples while they were used as references without being touched or moved between the measurements are plotted versus time in Figure 49.

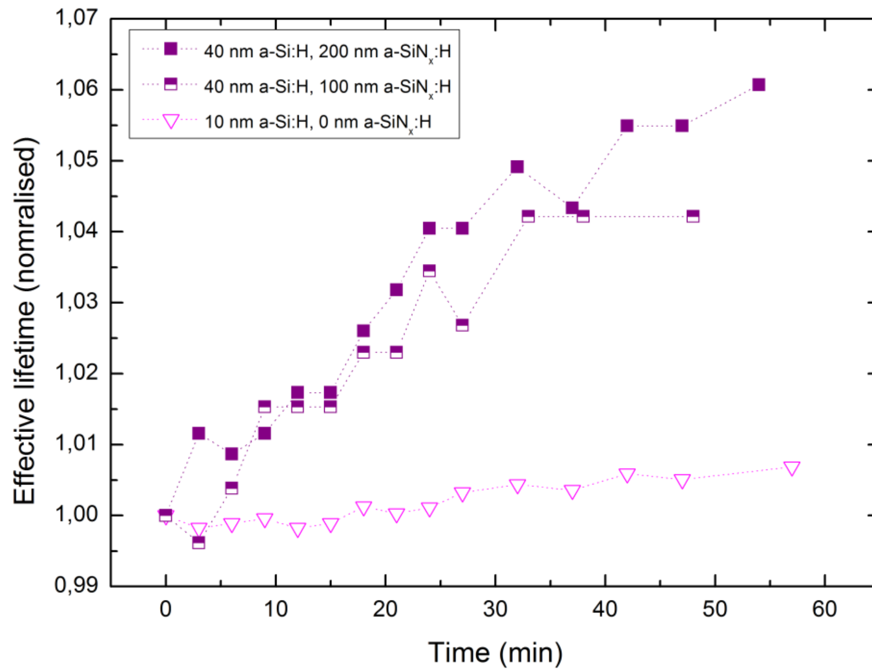

Figure 49 Normalised measured lifetimes of the samples with 40 nm a-Si:H and 200 or 100 nm a-SiN_x:H capping and the sample with a 10 nm a-Si:H single layer. The lifetimes of each sample are normalised with respect to the lifetime obtained from the first measurement of that sample shown in the graph. These samples were used as reference samples to be able to calibrate the *p*-type samples with 200, 100 and 0 nm capping used in the annealing experiments.

These observations indicate that repeated illuminations with light pulses of wavelength 808 nm improve the effective lifetime of the capped samples. The illumination with long wavelength light might function like an annealing, giving the hydrogen atoms enough energy to redistribute and reducing the number of recombination active states at the surface. As it is only observed for the capped samples it might also have something to do with field effect passivation. It would be interesting to know whether this increase of the passivation quality is reproducible with similar stacks and for what range of wavelength the passivation improves and degrades. It is also very relevant to find out whether this effect can be observed in stacks with different a-Si:H thicknesses. This observed effect could be utilised to improve the passivation quality and thus the conversion efficiency of solar cells.

5. Conclusions

5.1. Passivation provided shortly after deposition

All the stacks and single layers investigated provided very good surface passivation resulting in high effective lifetimes and low SRVs one day after deposition. The best effective lifetime was measured on an *n*-type sample one day after deposition and was 12.5 ms for an excess carrier concentration of 10^{15} cm^{-3}. The upper limit of the surface recombination velocity (SRV) was calculated to be 1.0 cm/s for this sample. The highest effective lifetime of a passivated *p*-type sample was measured to be 5.3 ms for an excess carrier concentration of 10^{15} cm^{-3} shortly after deposition of a single layer of 20 nm a-Si:H. The corresponding upper limit of the SRV was calculated to be 2.7 cm/s. It seems to be a trend, for both the *n*- and *p*-type samples, that the samples with capping have higher effective lifetimes than the uncapped samples one day after deposition. This may be due to field effect passivation provided by fixed charges in the silicon nitride layer. Another reason for the higher lifetimes may be the extra time that the capped samples are at 200 °C. This is likely to function as an annealing, reducing the number of recombination active states at the a-Si:H/c-Si interface.

5.2. Temporal Stability

The stacks have a high temporal stability that might weakly depend on the thickness of the layer of amorphous silicon. The passivation provided by the single layers of a-Si:H degrades rapidly with time and the degradation seem to decrease with increasing thickness of the a-Si:H layer. After nine weeks, the effective lifetimes of the *p*-type samples with 5, 10 and 20 nm a-Si:H films were reduced to about 30 % of their value one day after deposition. The effective lifetimes of the *n*-type samples with 5 and 10 nm a-Si:H layers, had decreased to 25 % of their value one day after deposition. One month after deposition the passivation provided by the single layers seems quite stable. After nine weeks the best measured lifetime was 11.3 ms corresponding to upper limits of the SRV of 1.3 cm/s on *n*-type and 4.0 ms corresponding to an upper limit of the SRV of 3.6 cm/s on *p*-type. The thickest a-Si:H layer of 40 nm was almost as stable as the stacks. The stacks are probably more stable because the silicon nitride prevents the hydrogen from effusing out from the interface with time. The passivation quality of the *p*-type samples, both capped and uncapped, nine weeks after deposition seem to improve with the a-Si:H thickness up to 20 nm. This indicates that 20 nm of a-Si:H is enough for temporal stability of a stack.

5.3. Thermal stability

The thermal stability of the passivation is important because of the metallisation processes of solar cells and has therefore been investigated. After rapid thermal annealings at temperatures between 250 and 450 °C the effective lifetimes of all the samples investigated first improved, then reached a maximum and finally started degrading. A maximum lifetime occurred at 300-400 °C, probably

because of redistribution of hydrogen, thus lower defect density at the surface and lower SRV. Rapid degradation was observed from 450 °C and after annealing at 500 °C the effective lifetimes were below 0.1 ms. This was probably caused by effusion of hydrogen, resulting in higher defect density at the surface and higher SRV. In general the thicker a-Si:H layers reach their maximum lifetimes and start degrading at higher temperatures than the thinner a-Si:H layers, indicating that they are more thermally stable. It seems to be a trend that the stacks degrade less than the single layers for annealing temperatures above 400 °C, most likely because the capping prevents the hydrogen from effusing out from the interface.

Firing at 945 °C peak degrades the effective lifetimes of all the investigated samples to about the same as an unpassivated sample, thus the stacks and single layers cannot withstand a firing process for metallisation with standard pastes, but low temperatures pasted might be possible to use . A one minute annealing in a belt furnace at 450 °C improved the effective lifetime of some samples and degraded others. The lifetimes of all the uncapped samples improved. The capped *p*-type samples with the thinnest a-Si:H layers degraded, whereas the samples with thicker a-Si:H layers were stable or improved during the anneal. Higher deposition temperatures of the silicon nitride may increase the thermal stability of the stacks.

5.4. Light induced improvement of the passivation from the stacks

The measured effective lifetimes of two *p*-type samples with stacks were observed to increase during frequent measurements, i.e. repeated illumination with infrared light of 808 nm wavelength. This indicates that the illumination may improve the passivation provided by the stacks. This possible effect needs to be investigated further, to determine whether it can be reproduced. If the effect is real, it is interesting to find out for what wavelengths and what stacks this effect occurs. This possible effect could be utilised to further improve the conversion efficiency of silicon solar cells passivated with stacks.

5.5. Suggestions for further work

Stacks consisting of amorphous silicon and silicon nitride double layers provide very good passivation as deposited and therefore are promising surface treatments for high efficiency solar cells. However the thermal stability should be improved to be able to implement this passivation in cell fabrication with metallisation processes using screen printed pastes. Therefore further investigations of the passivation quality provided by amorphous silicon/silicon nitride stacks should be carried out to get a more thorough understanding of the passivation provided as deposited, the temporal and thermal stability and effects of illumination.

A very interesting observation in this study was that illumination seems to improve the effective lifetime of the capped samples. This potential effect could be utilised to improve the passivation

quality and thus the conversion efficiency of solar cells. Therefore further investigation of any light induced degradation and improvement of the stacks would be very interesting. Which range of wavelengths that potentially degrade and improve the passivation quality is very relevant for applications of the passivating stacks in solar cells.

When stacks and single layers are deposited, all the samples should ideally be in the same temperature for the same length of time. Then the effect of the added capping layer can be isolated, excluding the possible effect of the extended time at 200°C, which function like an annealing for the a-Si:H layer.

If the bulk lifetime is known one could calculate the SRV from the measured effective lifetimes more accurately, thus the comparison of the different stacks and single layers can be done with more certainty and it is possible to directly compare the SRV of each layer. Investigating different stacks on for example four quarter pieces from the same wafer could also exclude the potentially different bulk lifetimes influencing the effective lifetimes. These samples are large enough for QSSPC measurements on a uniform area without edge effects and the possible contribution to the effective lifetime of potentially different limiting bulk lifetimes are excluded.

The rapid thermal annealings at different temperatures should be carried out on different samples for each temperature instead of consecutive annealings of the same piece as was done in this study. This would require more samples and therefore be more expensive. Successive one minute annealing at the same temperature could be carried out to investigate the influence of the time at each temperature. Annealing in forming gas could also be carried out to see if this can increase the thermal stability.

In the rapid thermal annealing experiments it was seen that some of the capped samples degraded at 200 °C and then improved at 250 °C. There was not enough time to investigate why the annealing at 200°C degraded the uncapped samples and whether this had something to do with the deposition temperature of the silicon nitride which was also 200 °C.

Neutron reflectometry can be used to gain further understanding of the behaviour of the hydrogen in the stacks and single layers. From neutron reflectometry measurements carried out on as deposited, annealed and illuminated samples the position of the hydrogen in the passivating layers could be determined in the different cases. Thus it could among others give an insight into why the passivation improves at certain temperatures and degrades at others.

References

1. Nelson, J., *The Physics of Solar Cells*. 2004, London, UK: Imperial College Press.
2. Boyle, G., *Renewable energy, Power for a sustainable future*. 2nd ed. 2004, Oxford, UK: Oxford University Press.
3. Chen, C.J., *Physics of Solar Energy*. 2011, New Jersey, USA: John Wiley & Sons Inc.
4. Sherwani, A.F., Usmani, J.A., and Varun, *Life cycle assesment of solar PV based electricity generation systems: A review.* Renewable and Sustainable Energy Reviews, 2010. **14**(1): p. 540-544.
5. Saint-Cast, P., Hofmann, M., Dimitrova, T., Wagenmann, D., Rentsch, J., and Preu, R., *Firing stable passivation with a-Si/SiNx stack layers for crystalline silicon solar cells*, in *European Photovoltaic Solar Energy Conference and Exhibition (EU PVSEC)*2009: Hamburg, Germany. p. 5.
6. Gatz, S., Plagwitz, H., Altermatt, P.P., Terheiden, B., and Brendel, R., *Thermal stability of amorphous silicon/silicon nitride stacks for passivating crystalline silicon solar cells.* Applied Physics Letters, 2008. **93**(17): p. 173502-173502-3.
7. Cham Thi, T., Koyama, K., Ohdaira, K., and Matsumura, H., *Passivation characteristics of SiNx/a-Si and SiNx/Si-rich-SiNx stacked layers on crystalline silicon.* Solar Energy Materials and Solar Cells, 2012. **100**(0): p. 169-173.
8. Koyama, K., Ohdaira, K., and Matsumura, H., *Excellent passivation effect of Cat-CVD SiNx/i-a-Si stack films on Si substrates.* Thin Solid Films, 2011. **519**(14): p. 4473-4475.
9. Tucci, M. and Serenelli, L., *Metastability of SiNx/a-Si:H crystalline silicon surface passivation for PV application.* Thin Solid Films, 2008. **516**(20): p. 6939-6942.
10. Green, M.A., *Solar Cells, Operating Principles, Technology and System Applications*. 1998, Sydney, Australia: The University of New South Wales.
11. Streetman, B.G. and Banerjee, S., *Solid State Electronic Devices*. 5th ed. 2000, New Jersey, USA: Prentice Hall.
12. Freiburg Insruments Inline Metrology. *Minority carrier lifetime*. [cited 2013 25.04]; Available from: http://www.freiberginstruments.com/technology/electrical-characterization/minority-carrier-lifetime.html.
13. Rein, S., *Lifetime spectroscopy: a method of defect characterization in silicon for photovoltaic applications*. 2005, Berlin: Springer. 1 online resource (xxvi, 489 s.) : ill. (some col.).
14. Neamen, D.A., *Semiconductor Physics and Devices, Basic Principles*. Second ed. 1997.
15. Honsberg, C. and Bowden, S. *Surface Recombination*. [cited 2013 24.01]; Available from: http://www.pveducation.org/pvcdrom/characterisation/surface-recombination.
16. Marstein, E.S., *Recombination, Lecture notes distributed in the course UNIK4450 at University of Oslo*, Hasle, I., Editor 2012.
17. Aberle, A.G., *Crystalline Silicon Solar Cells, Advanced Surface Passivation and Analysis*. 2004, Sydney, Australia: Centre for Photovoltaic Engineering, University of New South Wales.
18. Honsberg, C. and Bowden, S. *PC1D*. [cited 2013 06.05]; Available from: http://www.pveducation.org/pvcdrom/characterisation/pc1d.
19. University of New South Wales. *PC1D*. [cited 2012 06.05]; Available from: http://www.pv.unsw.edu.au/info-about/our-school/products-services/pc1d.
20. Rahman, M. and Khan, S., *Advances in surface passivation of c-Si solar cells.* Materials for Renewable and Sustainable Energy, 2012. **1**(1): p. 1-11.
21. Lelièvre, J.F., Fourmond, E., Kaminski, A., Palais, O., Ballutaud, D., and Lemiti, M., *Study of the composition of hydrogenated silicon nitride SiNx:H for efficient surface and bulk passivation of silicon.* Solar Energy Materials and Solar Cells, 2009. **93**(8): p. 1281-1289.
22. Ulyashin, A.G., Bentzen, A., Diplas, S., Suphellen, A., Gunnaes, A.E., Olsen, A., et al. *Hydrogen Release and Defect Formation During Heat Treatments of SiNx:H/a-Si:H Double Passivation*

Layer on c-Si Substrate. in *Photovoltaic Energy Conversion, Conference Record of the 2006 IEEE 4th World Conference on*. 2006.

23. Helland, S., *Electrical Characterization of Amorphous Silicon Nitride Passivation Layers for Crystalline Silicon Solar Cells*, in *Department of Materials Science and Engineering*2011, Norwegian University of Science and Technology. p. 113.
24. De Wolf, S., Agostinelli, G., Beaucarne, G., and Vitanov, P., *Influence of stoichiometry of direct plasma-enhanced chemical vapor deposited SiNx films and silicon substrate surface roughness on surface passivation.* Journal of Applied Physics, 2005. **97**(6): p. 063303-063303-8.
25. Cuevas, A., Kerr, M.J., and Schmidt, J. *Passivation of crystalline silicon using silicon nitride*. in *Photovoltaic Energy Conversion, 2003. Proceedings of 3rd World Conference on*. 2003.
26. Lauinger, T., Moschner, J., Aberle, A.G., and Hezel, R., *Optimization and characterization of remote plasma-enhanced chemical vapor deposition silicon nitride for the passivation of p-type crystalline silicon surfaces.* Journal of Vacuum Science & Technology A: Vacuum, Surfaces, and Films, 1998. **16**(2): p. 530-543.
27. De Wolf, S., Demaurex, B., Descoeudres, A., and Ballif, C., *Very fast light-induced degradation of a-Si:H/c-Si(100) interfaces.* Physical Review B, 2011. **83**(23): p. 233301.
28. Li, H. and Wenham, S. *Passivating property and thermal stability of amorphous silicon/silicon nitride double passivating layer on CZ crystalline Si substrate*. in *European Photovoltaic Solar Energy Conference and Exhibition*. 2011. Hamburg, Germany.
29. De Wolf, S. and Kondo, M., *Nature of doped a-Si:H/c-Si interface recombination.* Journal of Applied Physics, 2009. **105**(10): p. 103707-103707-6.
30. Pankove, J.I. and Tarng, M.L., *Amorphous silicon as a passivant for crystalline silicon.* Applied Physics Letters, 1979. **34**(2): p. 156-157.
31. Sinton Consulting Inc., *User Manual, WCT-120 Photoconductance Lifetime Tester*, 2006: Colorado, USA.
32. Nagel, H., Berge, C., and Aberle, A.G., *Generalized analysis of quasi-steady-state and quasi-transient measurements of carrier lifetimes in semiconductors.* Journal of Applied Physics, 1999. **86**(11): p. 6218-6221.
33. Herlufsen, S., Schmidt, J., Hinken, D., Both, K., and Brendel, R., *Camera-based Photoluminescence Lifetime Imaging of Crystalline Silicon Wafers*, in *24th European Photovoltaic Solar Energy Conference*2009: Hamburg, Germany.
34. Clark, J., Macias, T., and Roode, C., eds. *Continuous belt IR furnace, Reference Manual*. 2.6a ed. 2008, FurnacePros: Orange, USA.
35. Allwin21 Corp. *AccuThermo AW 610*. [cited 2013 21.04]; Available from: http://www.allwin21.com/Item.asp?catid=34&id=75.
36. Focsa, A., Slaoui, A., Charifi, H., Stoquert, J.P., and Roques, S., *Surface passivation at low temperature of p- and n-type silicon wafers using a double layer a-Si:H/SiNx:H.* Materials Science and Engineering: B, 2009. **159–160**(0): p. 242-247.

Appendix 1, PC1D model parameter settings

The parameters used in the PC1D simulations in this thesis are given in Table 8.

Table 8 Parameter setting of the PC1D model used for simulations of the conversion efficiency of a cell for different SRVs.

Parameter	Setting
Dielectric constant	11.9
Band gap	1.124 eV
Temperature	300 K
Intrinsic carrier density	10^{10} cm^{-3}
Refractive index	3.58
Doping concentration *n*-type emitter	10^{20} cm^{-3}
Doping concentration *p*-type base	10^{16} cm^{-3}
Incident spectrum	Air mass 1.5 (AM1.5)
Intensity	0.1 W cm^{-1}
Bulk lifetime of electrons and holes ($\tau_n = \tau_p$)	1 ms
Cell area	1 cm^2
Exterior reflectance	0
Internal reflectance	0
Surface charge	0
Carrier mobilities	Internal model
Material settings	Program default
Free carrier absorption	enabled
Texturing	none